Next-to-simplified dark matter models

Memoria de tesis doctoral realizada por
Javier Quilis Sancho
presentada ante el Departamento de Física Teórica
de la Universidad Autónoma de Madrid
para optar al Título de Doctor en Física

Trabajo dirigido por el
Dr. J. Alberto Casas González
Profesor de investigación del CSIC
Instituto de Física Teórica
Universidad Autónoma de Madrid
y el
Dr. Roberto Ruiz de Austri Bazán
Profesor del Instituto de Física Corpuscular
Universidad de Valencia

Instituto de Física Teórica
UAM-CSIC

Madrid, Febrero de 2019

A José Vicente i Carmen per haver-me portat fins ací.
I a Cristina per haver-me acompanyat.

LIST OF PUBLICATIONS

This thesis is based on the following scientific articles:

- **Reopening the Higgs portal for singlet scalar dark matter**
  J.A. Casas, D.G. Cerdeño, J.M. Moreno, J. Quilis
  DOI:10.1007/JHEP05(2017)036 [**arXiv:1701.08134**].

- **Extended Higgs-portal dark matter and the Fermi-LAT Galactic Center Excess**
  J.A. Casas, G.A. Gómez Vargas, J.M. Moreno, J. Quilis, R. Ruiz de Austri
  DOI:10.1088/JCAP/1475-7516/2018/06/031 [**arXiv:1711.10957**].

- **Anomaly-free Dark Matter with Harmless Direct Detection Constraints**
  S. Caron, J.A. Casas, J. Quilis, R. Ruiz de Austri
  DOI:10.1007/JHEP12(2018)126 [**arXiv:1807.07921**].

Abstract

Dark matter constitutes the 27% of the energy content of the universe. However, the nature of dark matter is still a mystery. The Standard Model does not have any reasonable explanation to solve this problem, so the need for a theory beyond Standard Model is evident. In this context, simplified dark matter models are a good first attempt to solve this problem. But simplified models are limited by their simplicity and in many cases experimental searches put several bounds on them, constraining severely the parameter space. For these reasons, a step forward is needed. One way to do that is to enlarge the particle content of this kind of models, looking for more realistic configurations.

In this thesis we adopt this idea of going next to simplified models and study two relevant models in the context of dark matter portals. In the first one we re-visit the well known singlet-scalar Higgs portal, one of the simplest dark matter models, consisting of a singlet-scalar coupled to the Higgs boson. This model is of great interest since, with just an extra particle, it can reproduce the dark matter density and has a rich phenomenology. However, since its postulation, experimental searches have tested the model putting severe bounds on its parameter space and nowadays is close to be excluded. A simple way to relax these constraints is to extend the dark sector. In this thesis we study the case of the simplest extension, adding an extra singlet-scalar. We analyze the new phenomenology due to this new scalar, specially coannihilation effects. Also, we impose the experimental constraints in the extended model to see how the new parameter space is restricted. Finally, we test how well this model can explain the galactic center excess.

On the other hand, we study another kind of dark matter portal, called Z' portal. This scenario implies the existence of an extra $U(1)$ symmetry in the gauge group. In this kind of framework the strongest constraints come from di-lepton searches at colliders and bounds from direct detection experiments. A simple way to relax these constraints is to choose a leptophobic mediator, i.e. with no direct couplings to leptons, and interacting axially to the dark matter particle, so that the coupling between the dark matter and quarks is spin-dependent. Taking this considerations into account, we look for the simplest possible configuration that fulfill these requirements and cancels the anomalies of the new gauge group, and we study the phenomenology of a representative model of this kind.

Resumen

La materia oscura constituye el 27% del contenido de energía del universo. Sin embargo, la naturaleza de la materia oscura es un misterio. El Modelo Estándar no contiene ninguna respuesta razonable para resolver este problema, por tanto es necesario una teoría más allá del Modelo Estándar. En este contexto, los modelos simplificados de materia oscura son una buena primera aproximación para resolver este problema. No obstante, los modelos simplificados están limitados por su simplicidad y en muchos casos las búsquedas experimentales ponen varios límites en ellos, restringiendo considerablemente el espacio de parámetros. Por estas razones, un paso más allá es necesario. Una manera de darlo es aumentar el número de partículas del modelo, buscando configuraciones más realistas.

En esta tesis adoptamos esta idea de ir más allá de los modelos simplificados y estudiamos dos modelos relevantes en el contexto de portales de materia oscura. En el primero revisamos el conocido portal de Higgs con un escalar singlete, uno de los modelos de materia oscura más simple, que consiste en un escalar singlete acoplado al bosón de Higgs. Este modelo tiene un gran interés debido a que, con solo una partícula extra, es capaz de reproducir la densidad de materia oscura y tiene una rica fenomenología. Sin embargo, desde que se postuló, búsquedas experimentales han testado el modelo poniendo límites fuertes en el espacio de parámetros y a día de hoy está cerca de ser excluido. Una sencilla manera de relajar estas restricciones es extender el sector oscuro. En esta tesis estudiamos el caso de la extensión más simple, añadiendo un escalar singlete extra. Analizamos la nueva fenomenología debido a este escalar, especialmente efectos de coaniquilación. Además, imponemos todos los límites experimentales en este modelo extendido para ver como queda el nuevo espacio de parámetros. Finalmente, testamos cómo de bien es capaz de explicar el exceso del centro galáctico.

Por otro lado, estudiamos otro tipo de portal de materia oscura, el llamado portal Z'. Este escenario implica la existencia de una simetría $U(1)$ extra en el grupo gauge. En este tipo de situaciones los límites mas fuertes vienen de las búsquedas de di-leptones y de experimentos de detección directa. Una manera fácil de relajar estas restricciones es eligiendo un mediador leptofóbico, es decir, sin acoplamientos directos con los leptones, y que interactúe axialmente con la materia oscura, de manera que el acoplamiento entre la materia oscura y los quarks sea dependiente del spin. Teniendo estas consideraciones en mente, buscamos el modelo más simple que cumpla estos requisitos y que cancele las anomalías del nuevo grupo de simetrías gauge, y estudiamos la fenomenología de un modelo representativo de este tipo.

Contents

1 Introduction **1**

2 Dark matter **5**

2.1 Evidences 6

2.2 Candidates for non-baryonic dark matter 12

3 Weakly Interacting Massive Particles **19**

3.1 Thermal production 20

3.2 Experimental searches 26

4 Higgs Portal. Minimal extension of the singlet-scalar Higgs Portal **33**

4.1 Estatus of the singlet-scalar Higgs portal 34

4.2 The extended singlet-scalar Higgs portal (ESHP) 37

4.2.1 The relic density 37

4.2.2 Observational and experimental constraints 40

4.3 Results 43

4.4 Effective-theory description 47

4.5 Applying the ESHP to the Galactic Center Excess 50

4.5.1 The Galactic Center Excess 50

4.5.2 Fitting the Galactic-Center Excess in the ESHP model 53

4.5.3 Results 55

5 Z' Portal. Minimal leptophobic anomaly free Z' model **59**

5.1 Anomaly-free leptophobic Z's 60

5.2 Anomaly-free leptophobic Z', with axial coupling to DM 62

5.3 Phenomenology of the Model 66

5.3.1 Kinetic mixing . . . 66
5.3.2 Dark Matter Constraints . . . 67
5.3.3 Bounds from EW observables and LHC . . . 69
5.4 Results . . . 71

6 Conclusions **75**

Appendix A Radiative contributions to the $S_1 S_1 h$ vertex **83**

Appendix B Anomaly-free completions of $U(1)_B$ **87**
B.1 Classification of solutions . . . 87
B.2 Special Choices of Y_ψ, Y_η . . . 89
B.3 Axial coupling of the dark matter . . . 90

Appendix C $Z - Z'$ mixing **93**
C.1 Kinetic mixing . . . 93
C.2 Scalar sector and spontaneous symmetry breaking . . . 95

Bibliography **103**

Chapter 1

Introduction

The goal of every physicist has always been the understanding of what surrounds them, how the world works. Particle physicists, in particular, have focused on the basic elements that constitute the universe and how they interact. The Standard Model of particle physics (SM) is probably, together with Albert Einstein's General Relativity, the most remarkable theory so far postulated. With just twelve matter fields and four interactions among them the SM is able to explain a huge number of phenomena observed in nature with an outstanding precision. Besides, the theory, i.e. the Lagrangian, is so "simple" that can be printed in a mug or a t-shirt.

The SM is a quantum field theory in four dimensions based on a gauge symmetry group $SU(3)_C \times SU(2)_L \times U(1)_Y$ and it is renormalizable and invariant under the Poincaré group. The matter content is divided in three families with the same quantum numbers, differing only in the masses. Every family has two quarks, one with positive charge and one with negative charge, and two leptons, one charged and one neutral and (nearly) massless. The interactions between the particles are driven by three forces: electromagnetic, weak and strong. These forces are mediated by vector bosons: the photon, γ, in the case of the electromagnetic force, the W and Z bosons for the weak force and the gluon for the strong force. The discovery of the last piece of the puzzle was announced the 4th of July of 2012, when CERN proclaimed the detection of the Higgs boson, responsible for the electroweak symmetry breaking and for the masses of all the other SM particles. The particle content of the SM is summarized in Fig. 1.1

The interactions of the SM particles are given by the symmetries of the model with the following Lagrangian

$$\mathcal{L}_{SM} = \mathcal{L}_{YM} + \mathcal{L}_{\psi} + \mathcal{L}_{\text{Yuk}} + \mathcal{L}_{\text{Higgs}}. \tag{1.1}$$

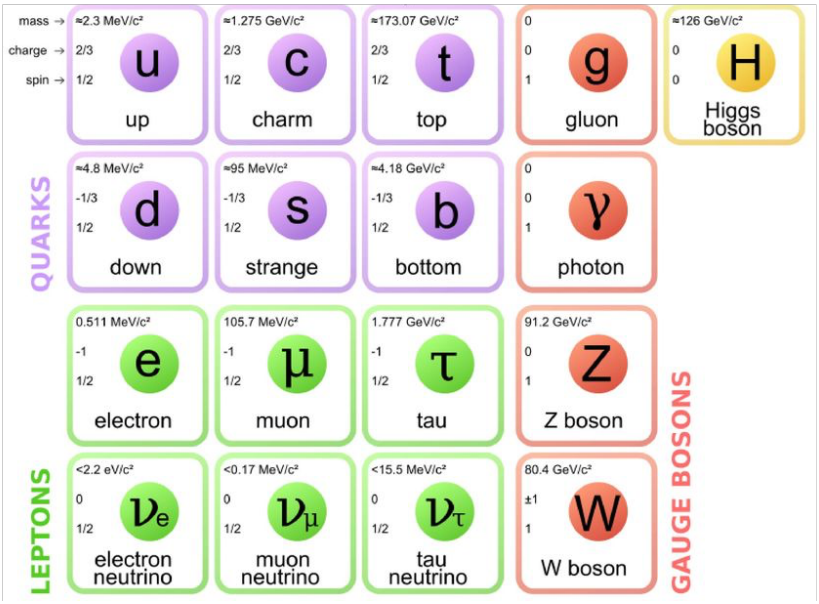

Figure 1.1: Summary of the Standard Model particle content.

The Yang-Mills part is given by

$$\mathcal{L}_{YM} = -\frac{1}{4}G^a_{\mu\nu}G^{\mu\nu a} - \frac{1}{4}W^a_{\mu\nu}W^{\mu\nu a} - \frac{1}{4}B_{\mu\nu}B^{\mu\nu}, \tag{1.2}$$

where $G^a_{\mu\nu}$, $W^a_{\mu\nu}$ and $B_{\mu\nu}$ are the gauge boson field strengths, normalized the corresponding gauge coupling, g_s, g and g', respectively. The fermionic kinetic terms are

$$\mathcal{L}_\psi = i\overline{Q}_L \not{D} Q_L + i\overline{L}\not{D}L + i\overline{u}_R\not{D}u_R + i\overline{d}_R\not{D}d_R + i\overline{e}_R\not{D}e_R, \tag{1.3}$$

with $\not{D} = \gamma_\mu D^\mu$ and D_μ the covariant derivative, $D_\mu = \partial_\mu - i\frac{g_s}{2}\lambda_a G^a_\mu - i\frac{g}{2}\tau_a W^a_\mu - i\frac{g'}{2}B_\mu$, Q_L; L are the $SU(2)_L$ quark and fermion doublets; u_R, d_R and e_R the up and down right handed quark and the right handed charged lepton. The Yukawa part of the Lagrangian is

$$\mathcal{L}_{\text{Yuk}} = -Y_u\overline{Q}_L\tilde{\Phi}u_R - Y_d\overline{Q}_L\Phi d_R - Y_e\overline{L}\Phi e_R + h.c., \tag{1.4}$$

where Y_u, Y_d and Y_e are the Yukawa matrices and Φ is the Higgs boson doublet. Finally, the part of the Lagrangian related to the Higgs boson is

$$\begin{aligned} \mathcal{L}_{\text{Higgs}} &= (D_\mu\Phi)^\dagger(D^\mu\Phi) - V(\Phi), \\ V(\Phi) &= -\mu^2\Phi^\dagger\Phi + \lambda(\Phi^\dagger\Phi)^2, \end{aligned} \tag{1.5}$$

The only freedom in the previous Lagrangian is the choice of the three gauge couplings, g_s, g and g', the Yukawa matrices, Y_u, Y_d and Y_e, which induce the masses and mixings of the particles, and the two parameters of the Higgs sector, μ and λ, the mass term and the quartic coupling. These parameters are well measured experimentally and allow for calculations of different phenomena with oustanding precision and agreement with the observations.

One illustrative example is the anomalous magnetic moment of the electron, a_e, with an extraordinary agreement between the SM prediction and the experimental measurement [1]

$$\begin{aligned} a_{e,SMpred.} &= (115965214.0 \pm 2.8) \times 10^{-11}, \\ a_{e,measure.} &= (115965219.3 \pm 1.0) \times 10^{-11}. \end{aligned} \tag{1.6}$$

This example and others show the predictive power of the SM theory.

Despite of the incredible results of the theory, the SM is not the ultimate theory for nature. There are several problems from both theoretical and experimental point of view that cannot be explained within the SM. Now we list the most relevants of them:

- Neutrino masses. In the tradicional SM Lagrangian, neutrinos are exactly masses. Due to the representations of the matter fields in the gauge group, a mass term for neutrinos is forbidden. However, neutrino oscillations are a clear indication that neutrinos have masses. Neutrino masses can be accommodated with a dimension-5 operator of the kind $(\bar{L}\Phi)(\bar{\Phi}L)/\Lambda$, but the explanation of this operator would imply physics ata higher scale.

- Hierarchy problem. If the SM is an effective theory, the Higgs mass should receive quantum corrections proportional to the cut-off scale of the theory. In the absence of an intermediate scale, the next scale to the electroweak scale is the Planck mass, $M_P \simeq 10^{19}$. This would imply corrections proportional to this scale. Thus, either there is a fine tuned cancellation of the various contributions, or the mass of the Higgs boson should not be of the order of the EW scale. This issue would also affect the rest of the SM particle masses. A new scale at the order of the TeV could alleviate this problem.

- Fermionic masses. The Higgs mechanism explains how fermions get masses, nevertheless the differences in the masses of the fermions, i.e. the structure of the Yukawa matrices, is still a mystery. There is no explanation for the difference among the particles of a single family or why the masses are different for each family, despite the fact that they share the same quantum numbers.

- Strong CP problem. Although Quantum Chromodynamics (QCD) allows a CP-violating term in the Lagrangian, i.e. $\mathcal{L}_{QCD} \supset \theta \frac{g_s^2}{32\pi^2} G^{a\mu\nu}\tilde{G}_{a\mu\nu}$, CP violation is very constrained in the QCD context by the experiments. Hence, this θ parameter should be smaller

than 10^{-9}. Again, this can be interpreted as fine tuning; however, it might be an indication of physics beyond the standard model (BSM).

- Gravity. The SM successfully describes electroweak and strong interactions. However a quantum description for gravity, and an ultimate theory englobing all the forces in nature, has not been achieved so far.

- Dark matter (DM). There are undisputed astrophysical and cosmological evidences that indicate that SM matter particles conform only around the 15% of the matter of the universe and 4% of the total energy content. The other 80% of matter (around 25% of the total energy content) is in form of what is called dark matter. The nature of this matter is unknown and finding the solution implies going BSM.

This thesis is dedicated to the last problem of the list, the nature of dark matter. In Chapter 2 we present the main evidences that indicate the existence of dark matter and the most remarkable candidates for dark matter particles. In Chapter 3 we will focus on one of the candidates, the weakly interacting massive particles, and we will review its production in the early universe and the different searches aimed to detect them. Chapter 4 is dedicated to explore one of the most popular models, the Higgs portal, and study an extension of it. In Chapter 5 we will focus on another kind of model, the Z' portal, looking for a leptophobic and axially coupled version. Finally, in Chapter 6, we will summarize the results and conclusions.

Chapter 2

Dark matter

Dark matter plays a fundamental role in the understanding of cosmology. But the nature of this invisible and hard to catch component of the universe remains unknown. Searching for DM has always been searching for what cannot be seen. After the publication of Isaac Newton's treatise *PhilosphiæNaturalis Principia Mathematica* in 1687, the understanding of motion and Universal Gravity provided astronomers and cosmologists with a remarkable tool to study the dynamics of the cosmos. In this context, the study and interpretation of the motion of the astronomical objects became a way to predict the existence of undiscovered and invisible (at least with the observational tools of the time) entities.

The first person in doing so was maybe the german mathematician Friedrich Bessel, which in 1844 claimed that the motion of the stars Procyon and Sirius indicated the existence of invisible companion stars affecting gravitationally these two visible ones [2].

Two years later the astronomers Urbain Le Verrier and John Couch Adams postulated the existence of a new planet to explain the motion of Uranus. The calculations of Le Verrier were so accurate that the german astronomer John Galle discovered Neptune the same evening he received the letter within 1 degree of the predicted position by Le Verrier.

In the last part of the 19th century, the invention of astronomical photography opened a way for a better observation of the distribution of the visible matter of the cosmos and its motion and, therefore, the study of unseen matter. During the first decade of the 20th century, Lord Kelvin was one of the first in estimating the amount of DM [3], although at the beginning it was thought of as faint stars. He described the stars of the Milky Way as gas particles interacting through gravity and related the size of the galaxy with the velocity dispersion of the stars. Similar studies were made by Henri Poincaré [4] and Ernst Öpik [5], among others. Nevertheless, the first estimations of the amount of DM were of the same order of magnitude of the visible matter.

The astronomer Fritz Zwicky, considered probably the most famous pioneer in the field of DM, took a big step in the estimations of the DM amount in 1933. Studying the redshifts

of several galaxy clusters, published by Edwin Hubble and Milton Humason two years before [6], he noticed a strange behavior in the velocities of some galaxies within the Coma Cluster [7].

The velocity expected for these galaxies was around one order of magnitud lower than the observed value. Hence, Zwicky concluded that the DM was present in much greater amount than luminous matter. Nevertheless, this idea did not really permeate in the scientific community.

In the following decades the study of the rotation curves of galaxies helped to reach a better understanding of them. However, it was not until the 70s, when the results from the measurement of the galaxy rotation curves became relevant. In 1970, the astronomers Vera Rubin and Kent Ford published their observations of the Andromeda Galaxy [8]. The conclusion of these studies was that an extra amount of matter, electromagnetically invisible, was needed at the outer part of the galaxy to explain the rotation curves. These discrepancies in the masses of the galaxies were the first strong evidences for the existence of dark matter.

The nature of this extra matter became a mystery. And the mystery remains nowadays. As we have seen, at the beginning DM was thought of as faint stars and other cosmological objects less luminous than ordinary stars. This is the so-called *baryonic dark matter* and is referred to non-luminous gas or Massive Astrophysical Compact Halo Objects (MACHOs). Nevertheless, currently we know that cosmological searches have determined that this baryonic dark matter cannot constitute a large fraction of the DM of the universe without being in disagreement with Big-Bang Nucleosynthesis (BBN) and the small Cosmic Microwave Background (CMB) anisotropies. Thus, the possibility of *non-baryonic dark matter* arises and many possible candidates come from this idea.

In this chapter we will go through the different evidences observed for the existence of DM in the universe. Afterwards, we will discuss briefly some of the most studied candidates for non-baryonic dark matter.

2.1 Evidences

The pioneer work from Zwicky, Rubin and Ford was the seed of a large amount of observations that confirm that there is more matter than we observe. Evidences for DM are found in astrophysical and cosmological contexts. In this section we show the most relevant evidences at different scales: galaxies, clusters of galaxies and the structure of the universe.

Rotation curves of spiral galaxies

Probably the strongest evidence for DM comes from the rotation curves of spiral galaxies. The visible matter of these galaxies is composed of stars, interestelar gas and cosmic dust.

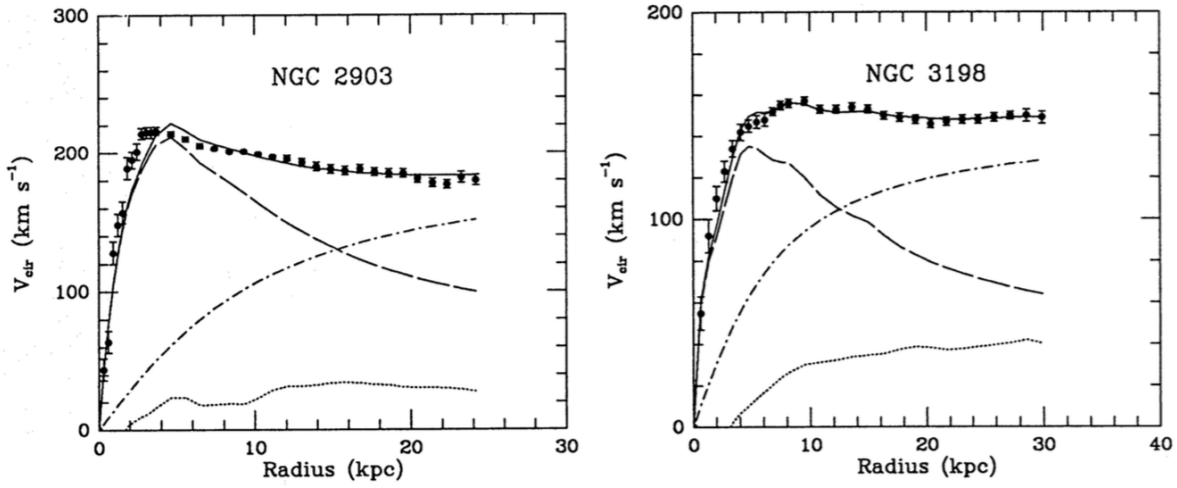

Figure 2.1: Dark-halo fits (solid curves) to the rotation curves of two galaxies, NGC 2903 and NGC 3198. The different components are also shown: the dashed curves correspond to visible matter, the dotted curves for the gas and the dash-dot curves for the dark halo. Images taken from [9].

Most of this matter is around the center of the galaxy in a rotating disc. The rest is in the arms that come out from the disk and rotate, as well, giving to the galaxy the characteristic form of a spiral. Now, since the matter in the arms is in orbit and does not collapse into the center or scape the galaxy, the centrifugate force due to the rotation and the gravitational force must compensate. Using Newton's law, one can relate the velocity of the matter, v, in terms of the distance of the matter from the center, r, and the total mass of matter inside the sphere of radius r, $M(r)$. In average,

$$v = \sqrt{\frac{GM(r)}{r}}, \tag{2.1}$$

where G is the gravitational constant. If, like we said, most of the mass is in the center of the galaxy, we should expect that the velocity of the matter in the arms decreases with the distance, roughly like $v \propto 1/\sqrt{r}$.

Nonetheless, the observations from Ford and Rubin of the Andromeda galaxy were in disagreement with this [8]. In Fig. 2.1 we can see the velocity curves of spiral galaxies NGC 2903 and NGC 3198 [9]. As we can see, at about 5 kpc from the center, the approximate extension of the luminous disk, the velocity curves (solid lines) arrive to their maximum. After that, the curves remain approximately constant with the distance unlike we would expect if the luminous matter (dashed curves) was the main contribution to the mass of the

galaxy. Therefore, this is not the case. If we add an extra source of matter with a profile that grows proportional to the distance with the galaxy center, $M(r) \propto r$, in the region where this source dominates, i.e. far from de disk, the velocity curves become approximately constant, reproducing the observations. This invisible extra source is the dark halo (dash-dot lines).

These two examples are not extraordinary cases. In every spiral galaxy studied happens this situation, which reinforces the idea that the dark halo dominates the mass distribution of the galaxies.

Velocity dispersion of galaxies

Clusters of galaxies also provide very strong evidences for DM. A galaxy cluster is a system formed by galaxies (from hundreds to thousands) bounded gravitationally, with a mass between $10^{14} - 10^{15}$ solar masses, $M_\odot$, and an extension between $2 - 10$ Mpc. The study of the velocity of the galaxies in the cluster is crucial to inquire the composition of the cluster. The first in doing this kind of study, as we mention, was Zwicky[7, 10]. He studied the Coma Cluster (that contains roughly a thousand of galaxies) and used the virial theorem to infer the mass of a galaxy cluster.

The virial theorem treats clusters as statistical steady, spherical, self gravitational systems of N objects of average mass m and average velocity v, separated by an average distance r. The average kinetic energy of a galaxy is just $E_{kin} = mv^2/2$, while the virial energy of a galaxy comes from Newton's law, $E_{vir} = -G(N-1)m^2/2r \simeq GNm^2/2r$. The virial theorem estipulates that kinetic and virial energies are related as $2E_{kin} = -E_{vir}$. With this relation we can derive the total mass of the system, M, in terms of the average velocity and distance

$$mv^2 = \frac{GNm^2}{2r} \rightarrow M = Nm = \frac{2rv^2}{G}. \tag{2.2}$$

The average velocity and distance are quantities that can be measured by astronomers. Zwicky used this method to estimate the mass of the Coma cluster, obtaining a mass of $M \sim 4.5 \times 10^{10} M_\odot$. However, the measured luminosity of the cluster was $L \sim 8.5 \times 10^7 L_\odot$, and the mass to light ratio for the galaxies is of order one, therefore, the prediction for the mass of the cluster was $M \sim 8.5 \times 10^7 M_\odot$. The discrepancy was huge and Zwicky was the first in pointing out that this difference could be due to the existence of some dark matter in the clusters. Nowadays we know that visible galaxies constitute only 1% of the matter in a cluster while the rest is gas and dark matter, being the dark matter the dominant component (constituting even up to the 90% in some cases).

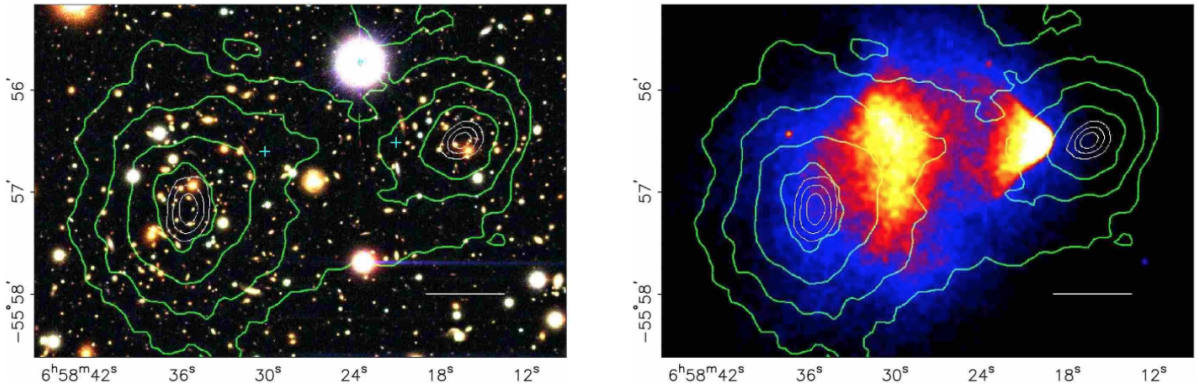

Figure 2.2: The merging cluster 1E0657-558. The left panel shows the luminous matter. The right panel shows the hot gas. The temperature of the hot gas is represented in colors, being blue the coolest temperature and white the hottest. In both panels the green contours represent the gravitational contours. Images taken from [12].

Bullet cluster

Although the issues about the rotation curves of spiral galaxies and the velocity of galaxies inside clusters are easily explained by assuming extra invisible matter in addition to the visible stars and galaxies, many physicists have tried to explain them revising Newton's law of gravity. This kind of theories are called Modified Newtonian Dynamics (MOND) and work quite well for the cases of galaxy rotation and velocity dispersion [11]. These theories could invite to reject the idea of the existence of invisible matter. However, they fail to explain the Bullet cluster.

The Bullet cluster (1E 0657-558) consists on a collision of two clusters of galaxies [12]. As we mentioned in the previous subsection, clusters are composed by galaxies, hot gas and dark matter, being dark matter the dominant component. During the collision, galaxies barely interacted and ended up in two splitted groups. On the other hand, the hot gas was detected, using X-ray techniques, at the center of the collision. A possible interpretation is that during the collision the hot gas particles interacted changing their trajectories. The majority of the baryonic mass is in form of hot gas, hence, the peak of the gravitational field would be expected at the center of the collision if clusters were formed just by baryonic matter. However, using gravitational lensing techniques, the mass density peaks after the collision coincide with the two new groups of galaxies formed. The explanation to this is that DM, that englobes the majority of the mass, is made of weakly coupled particles that did not interact during the collision, like the galaxies. In Fig. 2.2 we can have a look at this event. In the left panel we can see a picture of the luminous matter and in green the

gravitational contours. It can be appreciated that the contours coincide with the luminous matter. However in the right panel we see the distribution of the hot gas, measured by its X-ray emission, superposed to the gravitational contours. The color distribution is the temperature of the hot gas, increasing the temperature from blue to white. We can see that the gas is situated in between the two final clusters of galaxies.

MOND theories are not successful explaining the Bullet cluster, easily understood with the existence of DM.

Gravitational lensing

General relativity taught us that gravity not only affects matter. The trajectory of light is also modified by strong gravitational fields. This effect is called *gravitational lensing*. Studying the distortion of the light coming from background galaxies we are able to determine the mass distribution of the object bending the light, a cluster of galaxies for example. Now, this gravitational field is produced by both dark and visible matter, without distinction. Besides, we have tools to measure the baryonic matter. In the case of a cluster of galaxies for example, X-ray emission of hot gas or measuring the light emitted by luminous galaxies, are techniques to analyze the baryonic matter of the cluster. Confronting the results from the measurements of baryonic matter and gravitational lensing can show the amount and distribution of DM in the universe [13].

An example of this comes from the Bullet cluster, just mentioned, were the comparison between the baryonic matter distribution and the gravitational field measured by gravitational lensing offers a clear evidence for DM [14].

X-ray emission from hot gas

The existence of hot gas clouds in clusters can also indicate the existence of DM. The gas is at high temperature and radiates X-rays that can be measured, providing a profile of the density and the temperature of the gas. Now, the gas is expected to be in hydrostatic equilibrium, meaning that the pressure of the gas is compensated by the gravitational force of the system. By comparing the pressure of the gas with the mass of the baryonic matter, it is straightforward to deduce that an extra source of mass (much larger than the baryonic matter) is needed in order for the gas to hold on. In Fig. 2.3 we can see the example of the COMA cluster [15]. The right panel shows the optical image while in the left panel we can see the gas temperature. Without an extra source of matter, coming from the dark halo, the gas would evaporate.

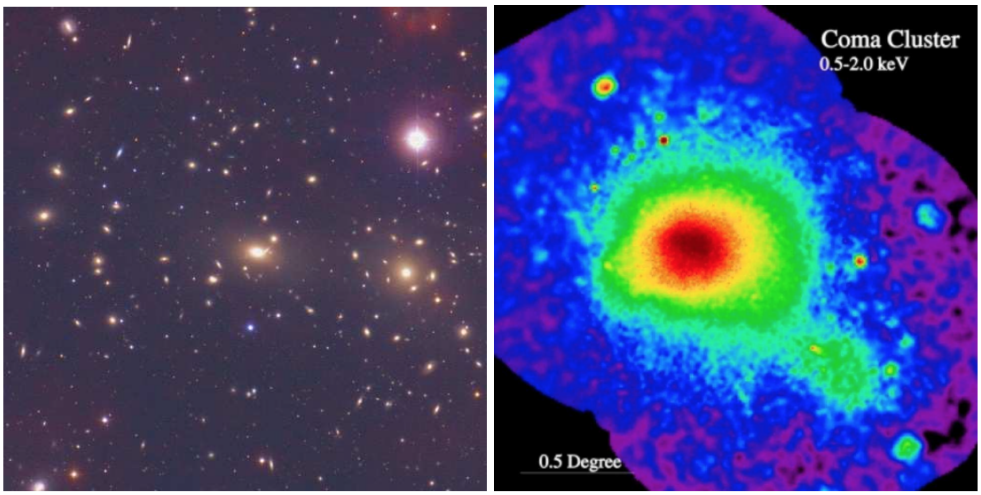

Figure 2.3: The hot gas from the COMA cluster. The left panel shows the luminous matter. The right panel is an X-ray image from ROSAT satellite. Images taken from [15].

CMB

The Cosmic Microwave Background (CMB) is called, very accurately, the oldest picture of the universe. At the early universe, when the temperature was very high, matter and radiation were in thermal equilibrium forming a plasma. While the universe was expanding, the temperature decreased and, at around 3000 K ($\sim$ 380000 years after the Big Bang), the energy was low enough and allowed protons and electrons to form hydrogen atoms (the energy at that temperature is about 0.26 eV while the ionization energy of hydrogen is 13.6 eV). This epoch is called *recombination time*. With electrons confined in hydrogen atoms, photons did not longer scatter with free electrons and escaped through the universe. This radiation traveled almost unalterable until today, when experiments like WMAP (Wilkinson Microwave Anisotropy Probe) [16] or Planck [**?**] measured their energy.

The measurement of the CMB revealed that it is remarkably uniform, with a temperature of 2.73 K across the universe and is a nearly a perfect blackbody. However, precision measurements spotted fundamental anisotropies within the CMB. These fluctuations can be seen in Fig. 2.4. The fluctuations are very small, though. Only about 30 ± 5 μK.

The origin of these anisotropies comes from two effects. At large scales, they are attributed to gravitational effects, called Sachs-Wolfe effects [18]. In more dense areas photons needed more energy to escape the gravitational field, leaving with less energy than photons from regions with less density. At low scales the fluctuations are due to what is called acoustic oscillations [19]. Before photon decoupling, baryons and photons formed a plasma. This

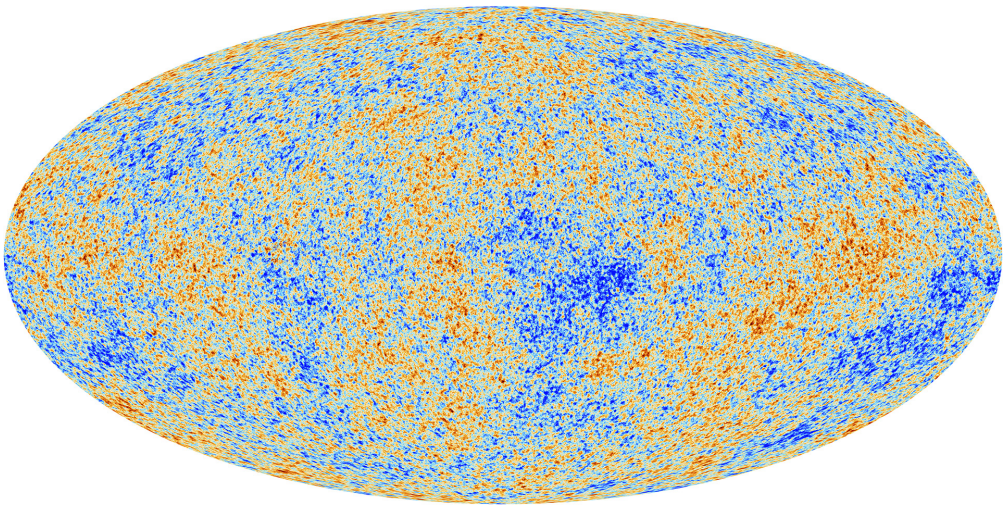

Figure 2.4: Map of the anisotropies of the CMB. The blue points correspond to the lowest temperatures while the red points are the highest. The difference between them of of the order of 30 μK. Image taken from [17].

plasma, due to gravitational forces and its own pressure, oscillates. First it collapses because of gravity, and when the pressure is too high expands, and repeats the process over and over until photons decouple. Depending on the moment of the decoupling in the oscillation the temperature of the photons vary.

The problem (or the advantage) with these explanations for the origin of the fluctuations is that baryonic matter cannot be responsible for the large scale differences. Matter became electrically neutral only at the epoch of recombination. Before that, electromagnetic forces prevented matter from creating gravitational formations. Hence, the existence of some neutral matter before the recombination time is needed to form the large scale structures. At the same time, dark matter did not form part of the baryon-photon oscillating fluid. This difference in the behavior between the two kinds of matter makes possible to measure the density of both dark and visible matter. The last result obtained by the Planck satellite [20] determines the density of the DM and the baryonic matter,

$$\Omega_{DM}h^2 = 0.1199 \pm 0.0022. \qquad \Omega_b h^2 = 0.02214 \pm 0.00024. \tag{2.3}$$

2.2 Candidates for non-baryonic dark matter

As we mentioned at the beginning of this chapter, DM was originally thought of as faint stars and other cosmological objects less luminous than visible stars. In other words, it was

thought of as baryonic dark matter. But, as we pointed out, the existence of such a large amount of baryonic matter is in disagreement with BBN and CMB. Therefore, the idea of the existence of non-baryonic dark matter grew up and nowadays is the most extended one. There are many candidates for non-baryonic dark matter. Below, we list the most relevant ones.

Neutrinos

Looking for a DM candidate, the first particles that came to particle physicists' minds were the only non-charged particles of the SM: neutrinos. Neutrinos only interact weakly (they do not have electromagnetic or strong interactions) and are stable, or at least long lived. So, they are, *a priori*, a suitable candidate for DM. Due to its small mass, neutrinos are predicted to emerge from the early universe with relativistic velocity. Hence, they represent an example of *hot dark matter* (HDM).

By the end of the 1970s SM neutrinos were considered as a possible candidate for DM [21–25]. In the mid 1980s, thanks to the improvement of numerical simulations, it became possible to test the predictions of neutrinos and other candidates for DM related to large scale structure in the universe. Numerical simulations showed how particles evolve under gravity in an expanding universe, for different kinds of DM. In the case of hot dark matter, simulations showed that relativistic particles tend to collapse into very large structures first and later break into galaxy-sized halos. The patterns of the structures formed by HDM were incompatible with galaxy surveys[26]. Therefore, HDM particles, and SM neutrinos in particular, were excluded as the main DM particles of the universe.

In contrast, if DM particles are non relativistic, also known as *cold dark matter* (CDM), the process of structure formation is somehow opposite to the one for HDM. In this case, the particles form small halos that merge into larger structures. This is in a better agreement with observations, so CDM candidates get, nowadays, much of the attention.

Having in mind that DM should be non-relativistic, Scott Dodelson and Lawrence Widrow proposed in 1993 a scenario where a new kind of neutrino, neutral under the SM gauge group (no electromagnetic, weak or strong interactions), could be a realistic DM candidate [27]. These new neutrinos, called *sterile neutrinos* (to differenciate them from SM neutrinos, also called *active neutrinos*), would interact with SM particles through gravity and the small mixing with SM neutrinos.

There are several production mechanisms of sterile neutrinos discussed in the literature, many of them based on non-thermal production. The two most relevant ones are production through the active-sterile mixing and production by particle decays. The first one is based on the fact that any reaction able to produce active neutrinos can produce also sterile neutrinos [27–30]. While the second mechanism relies on the existence of a heavy scalar coupled to SM particles that decays into the sterile neutrinos [31–34]. Both mechanisms are in agreement

with observations.

Another interesting feature of these sterile neutrinos is the possibility of solving the neutrino mass problem. In the SM, neutrinos are exactly massless as a consequence of gauge invariance and renormalizability [35–37]. However, experiments have proven that neutrinos have non-zero masses [38].

A possible origin for neutrino mass can come from effective field theory. Starting with a five-dimensional operator of the kind [39]

$$\mathcal{L} \supset \frac{1}{\Lambda} A_{\alpha\beta} (\tilde{L}_\alpha \tilde{\Phi})(\Phi^\dagger L^c_\beta), \tag{2.4}$$

where L_α are the leptonic doublets, with α the three leptonic flavors (e, μ, τ), Φ is the Higgs field doublet, $A_{\alpha\beta}$ is a complex dimensionless matrix and Λ is a scale. Once the Higgs field takes a vacuum expectation value (VEV), the neutrino mass matrix is

$$m_\nu = A_{\alpha\beta} \frac{v^2}{\Lambda}, \tag{2.5}$$

where $v \simeq 174$ GeV is the Higgs VEV. One possible origin for this non-renormalizable operator are sterile neutrinos: an extension of the SM with sterile neutrinos, singlets under the gauge symmetry group, would imply new lagrangian terms as

$$\mathcal{L} \supset -F_{\alpha I} \tilde{L}_\alpha N_I \tilde{\Phi} - \frac{M_I}{2} \tilde{N}^c_I N_I + h.c., \tag{2.6}$$

where N_I are the sterile neutrinos, $F_{\alpha I}$ is a dimensionless complex matrix, and M_I are the Majorana masses of the sterile neutrinos. If the Majorana masses are big enough the sterile neutrinos can be integrated out and the result is a five-dimensional operator as the one in Eq. 2.4, triggering small masses for the SM neutrinos. This is the so-called (type I) seesaw mechanism. In a particular case of this see-saw mechanism [40–43], the sterile neutrino can have masses of order keV o MeV and could be a CDM candidate.

Sterile neutrinos, then, are a suitable solution for both DM and neutrino masses. For this reason they have been extensively studied in the literature.

Axions

QCD is an extraordinarily successful theory able to describe the strong force experienced by quarks and gluons with remarkable precision. However, the QCD Lagrangian allows for a term

$$\mathcal{L}_{QCD} \supset \theta \frac{g_s^2}{32\pi^2} G^{a\mu\nu} \tilde{G}_{a\mu\nu}, \tag{2.7}$$

where $G^{a\mu\nu}$ is the gluon field strength and θ is related to the phase of the QCD vacuum. If θ is of order unity, as we could expect, this term would imply a strong P and CP violation.

However, there is no P or CP violation observed in strong interactions. This interactions impose an upper limit in the parameter θ, that must be smaller than $\sim 10^{-9}$ [44]. This constraint could be understood as just an unlikely condition of the theory, but it has been interpreted as a sign of new physics by many theorists. The explanation of the smallness of this value is the strong-CP problem.

Probably, the most interesting solution was proposed by Roberto Peccei and Helen Quinn in 1977 [45, 46]. They introduced a global $U_{PQ}(1)$ symmetry, spontaneously broken, that dinamically shifts θ to zero, in agreement with the observations, thus solving the strong-CP problem. Since this new symmetry is broken, it implies the existence of a Nambu-Goldstone boson, which was called the *axion* [47, 48].

The axion acquires a mass of order $m_a \sim \Lambda^2_{QCD}/f_{PQ}$, where $f_{PQ} = v_a/N$ is called the axion decay constant; v_a is the VEV of the field that breaks the $U_{PQ}(1)$ symmetry and N is an integer related to the color anomaly of the PQ symmetry [47]. Depending on the value of the axion decay constant, the axion can have masses of the order of the weak scale.

However, experimental results constrain the mass of the axion. Since the axion mixes with the neutral pion, π^0, an axion of a mass larger than 1 MeV would decay quickly into e^+e^-, implying a lifetime smaller than 10^{-11} s. But searches for decays like $\pi^+ \to a(e^+e^-)e^+\nu_e$, exclude this scenario [49]. For lower masses the axion is long-lived, with a lifetime over 10^{-11} s, and is safe from these searches, although extra constraints come into play. Axions may be produced in beam dumps due to their mixing with π or η and their couplings to photons, gluons and quarks, which would mean the existence of processes such as $p + N \to a + X$, $e + N \to a + X$ or $a + N \to X$. This kind of interactions have been tested experimentally and they rule out axions with masses over 50 keV.

Other restrictions come from astrophysical results [50, 51]. Axions are produced and emitted by stars in processes like Compton-like scattering ($\gamma + e \to a + e$), axion bremsstrahlung ($e + N \to N + e + a$) or the Primakoff process ($\gamma + N \to N + a$). Since axions are light and weakly coupled, they scape the star once they are produced. So, an excessive axion production would accelerate the energy radiation of the star and hence, its evolution. Red giant evolution excludes axions with masses between 200 keV and 0.5 eV for hadronic axions [52–54]. And for axions with a large coupling to electrons the lower limit becomes stronger, ruling out axions with masses between 200 keV and 10^{-2} eV [55]. Finally, Supernova 1987a excludes axions with masses between 2 eV and 3×10^{-3} eV [56–60]. Once both astrophysical and laboratory constraints are combined, we end up with an upper limit for the axion mass of 3×10^{-3} eV.

To avoid these constraints, axions must be weakly interacting and very light. An axion with these features might be stable and, if it is sufficiently produced, could be a candidate for DM.

WIMPs

As we have seen, solutions to fundamental problems like neutrino masses, or the strong-CP problem could provide us as well with a DM candidate. However, the fact that none of these cases have been proven, despite their attractiveness, pushed physicists to explore other alternatives to the nature of DM.

A long list of exotic ideas appeared, but all of them shared some similarities, besides being electrically neutral and non-strongly interacting. The DM production is thermal and in order to be CDM, DM particles should not be very light, heavier than 1-100 keV depending on the model. Furthermore, the self-annihilation cross section needed to provide the observed relic density is of the order of $\sigma v \sim 10^{-26}$ cm^3/s, where v is the velocity of the DM particles. Interestingly, this number is of the order of the cross section that arises from the weak force. Thus, this kind of candidates received a common name: *weakly interacting massive particles* (WIMPs).

In this framework, DM lives in a hidden sector, that can have its own gauge symmetry group and matter content within the dark sector. There must be, though, a connection between the two sectors that allows the DM to annihilate into SM particles and get the correct relic density at the early universe. This mechanism is usually called a portal [61–73]. Different portals have been proposed in the literature. Depending on the nature of the particle that acts as mediator. The most relevant types are scalar and vector portals.

If we think about scalar portals, the first possibility that comes to mind is the only scalar of the SM: the Higgs boson. The Higgs portal [61] is probably the most popular portal in the literature due to its simplicity and rich phenomenology. With a single scalar in the dark sector coupled to the Higgs, one can reproduce the correct relic density. Besides, the coupling with the Higgs makes this model testable. Dark matter searches have constrained this model, leaving only a few areas of its parameter space allowed, which are expected to be explored in future experiments [74]. The mediator, however, might be a new scalar. Then, the connection between sectors is through the mixing of the new scalar and the Higgs. The problem with this construction is that all the couplings of the SM particles with the Higgs have to be re-escaled with this mixing. Experimental observations, such as electroweak precision observables (EWPO) or Higgs measurements, impose an upper bound on the mixing angle $\sin^2\alpha < 0.1$ [75–78]. With this consideration, models safe from experiments that provide the correct DM density have been proposed in the literature.

The other possibility is a vector boson mediator. In the SM the Z boson could play a role between the dark sector and the SM [73]. But, as it happens with the Higgs portal, the parameter space is very constrained (even more than the Higgs case) [79]. Therefore the possibility of new vector bosons naturally arises. The existence of a new gauge boson implies the enlargement of the gauge symmetry group with an extra $U(1)$ symmetry. If both sectors have particles charged under this new symmetry, we expect DM annihilation into SM

particles through the new Z' boson. Also the Z and the Z' bosons generically mix, opening new annihilation channels. However, like in the scalar case, this mixing can not be very large. The mixing is restricted by EWPO, which put an upper limit of $\sin\theta < 10^{-3}$ [80]. This kind of mediators has been explored experimentally in colliders.

Supersymmetric dark matter

A particular case of WIMP arises from another fundamental problem of the SM: the well known hierarchy problem [81–85]. The SM, complemented with some mechanism for neutrino masses, constitutes a theory that describes remarkably well all the observed phenomenology. The SM heaviest particles have masses around the electroweak (EW) scale. In the absence of new physics at higher energies, the theory should work up to the next fundamental scale, namely the Planck scale. However, the Higgs mass receives enormous quantum corrections from the effects of virtual particles coupled to it, being the largest the one from the top quark $\delta m_H^2 \sim -y_t \Lambda_{UV}^2/8\pi^2$, where y_t is the top Yukawa, $\mathcal{O}(1)$, and Λ_{UV} is an ultraviolet momentum cutoff, which is at least the energy scale at which new physics enters. If there is no new physics at any scale this cutoff would be the Planck scale and the Higgs mass would receive gigantic corrections. These corrections not only affect the Higgs boson. Since all the SM particles get their masses through the Higgs mechanism (except, maybe, for neutrinos), the corrections would be transferred to fermions and gauge bosons and all the masses would be way larger. This is not what we observe in nature, though. Hence, this inconsistency is a sign of need of new physics at an intermediate scale.

In the early 1970s, Supersymmetry (SUSY) was proposed as a solution of the hierarchy problem [86–88]. The theory introduces a symmetry where for every particle of the standard model there exists a partner with the same mass and quantum numbers except for the spin. If the SM particle is a boson the partner would be a fermion and the other way around. Since the quantum corrections coming from a boson and a fermion have opposite signs these would cancel one to one. However, these extra particles have not been discovered yet. Therefore SUSY must be broken at some scale, so that the extra particles become more massive than the SM ones.

A consequence of this theory is that introduces several particles which are neutral under electromagnetic and strong interactions; e.g. the superpartners of the neutrinos, photon, Z boson, Higgs boson and the graviton. If somehow any of them is stable and abundant enough could also be a solution for DM.

In supersymmetric extensions of the SM, there may exist interactions that violate baryon and lepton number, which would lead to proton decay in a timescale of years or less. Being this in disagreement with observations regarding proton stability [89], an extra symmetry called R-Parity is imposed [90–93]. The main consequence of this discrete symmetry is that SUSY particles are produced or annihilate in pairs and, then, a SUSY particle could

only decay into another SUSY particle (and SM). Hence, the lightest SUSY particle (LSP) becomes stable.

Coming back to the possible DM candidates, in the Minimal Supersymmetric Standard Model (MSSM) and extensions of it, the superpartners of the B boson, the neutral W boson and the two Higgses mix into four neutralinos. The lightest neutralino [94–97] and the sneutrino (superpartner of the neutrino) [98, 99] are the two possible candidates in this minimal extension of the SM[1]. Although the sneutrinos fulfill the features required for DM, the coupling to the Z boson gives rise to a large annihilation cross section, which implies a small relic density. Hence the sneutrino is not a viable DM candidate. On the other hand, the lightest neutralino can reproduce the observed DM density and has been extensively studied in the literature.

[1] In extensions of the MSSM that include gravity, the superparner of the graviton, called gravitino, could also be a DM candidate.

Chapter 3

Weakly Interacting Massive Particles

In section 2.2 we discussed about different dark matter candidates. Initially, dark matter was thought ofas non-luminous baryonic matter. However, as already mentioned, cosmological evidences exclude the possibility that all the dark matter of the universe is baryonic. At that point, the search for a neutral particle that could play the role of DM intensified and the first option was the neutrino, the only neutral particle of the SM. But neutrinos were soon excluded since they would be HDM. Hence, finding a suitable cold dark matter particle became the goal for particle theorists. Sterile neutrinos, axions and supersymmetric dark matter appeared as natural DM candidates, although as they had been introduced to solve other fundamental problems.

Generally speaking, a good DM candidate should present a number of properties:

- Electrically neutral. The new particle can not interact with photons. Astrophysical observations indicate that DM does not produce electromagnetic radiation of any kind. Also, colored particles are not a good DM possibility since colored object hadronize and can be observed. So, it must be neutral under both interactions.

- Stable. To account for the dark matter density, the new particle must be stable. The lifetime of this particle, if it decays at all, must be greater that the lifetime of the universe.

- Cold. The particle should not be relativistic. As mentioned in Section 2.2, numerical simulations show that HDM form large structures incompatibles with the observations.

Taking this properties into account, the concept of *weakly interacting massive particle* arose. WIMPs are stable and quite massive particles which interact weakly with SM particles, usually through the exchange of a mediator known as a portal. The variety of WIMP models is huge but all of them coincide in some basic aspects.

Since WIMPs are expected to (slightly) couple to SM, this allows for the search of these hypothetical particles. Different techniques have been employed. Trying to measure collisions of DM particles with SM particles (direct detection), the results of DM annihilation (indirect detection) or the production of DM particles in colliders are the different possible approaches that experimentalists have explored in the hunt for DM. So far no positive detection has been registered, which is translated in different constraints for WIMP models.

In this chapter we will discuss first the production mechanism for WIMPs to provide the observed relic density and then we will present the different experiment techniques used to detect DM.

3.1 Thermal production

WIMPs are normally assumed to be produced thermally[1]. This means that, in the early universe, particles in the dark sector and the SM were in equilibrium in the thermal bath. While the universe expands the temperature decreases and particles loose energy. At a certain point, the processes between the DM and the SM sectors become inefficient and the dark matter density becomes approximately constant. This decoupling is called *freeze-out* and the temperature when it happens is around $T_{fo} \simeq m_\chi/20$, where m_χ is the mass of the WIMP.

BBN occurs at a temperature $T_{BBN} \simeq 0.8$ MeV. This is important as it implies that a WIMP with a mass of 100 MeV or larger would decouple before BBN, when there are no data. Then, some assumptions have to be made to do the relic density calculations. The entropy of matter and radiation is assumed to be conserved and the freeze-out occurs while the universe is radiation dominated.

Starting with the different species in the thermal plasma where particles are in thermal and chemical equilibrium, the distribution function of a species i at energy E_i, $f_i(E_i)$, is given by the Fermi-Dirac of Bose-Einstein distributions, for fermions and bosons respectively,

$$f_i(t, E_i) = \frac{1}{\exp((E_i - \mu_i)/T) \pm 1}, \tag{3.1}$$

where the $-$ $(+)$ sign refers to fermions (bosons), μ_i is the chemical potential of the species and the time evolution is parametrized by the temperature of the universe, T. These calculations are for non-relativistic particles (we are studying the case of CDM), hence, it is legitimate to use the Boltzmann distribution for both fermions and bosons,

$$f_i(t, E_i) = \exp(-(E_i - \mu_i)/T). \tag{3.2}$$

[1]Non-thermal production mechanisms are also possible, i.e. a decay from a heavier particle whose density was thermally fixed, or mechanisms that involve quantum-mehcanical oscillations.

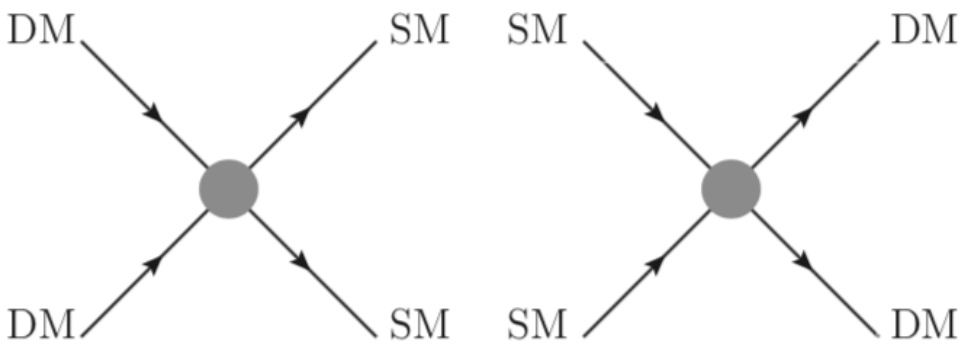

Figure 3.1: Processes that take place in the plasma, keeping species from dark sector and SM in equilibrium

At temperatures much higher than m_χ, the production of WIMPs by the collision of SM particles was in equilibrium with the annihilation of WIMP pairs into SM particles. The rate for both processes, illustrated in Fig. 3.1, is given by

$$\Gamma_{ann} = \langle \sigma_{ann} v \rangle n_{eq}, \tag{3.3}$$

where σ_{ann} is the annihilation cross-section of WIMPs into SM particles, v is the relative velocity of DM particles and n_{eq} is the number density of WIMPs in thermal equilibrium, which for non-relativistic WIMPs is given by

$$n_{eq} = g_\chi \left(\frac{m_\chi T}{2\pi} \right)^{3/2} \exp(-(m_\chi - \mu_\chi)/T), \tag{3.4}$$

where g_χ are the degrees of freedom of the WIMP.

As the universe expands the temperature decreases. Once it falls below m_χ SM particles do not have enough kinetic energy to produce DM particles and the number density of WIMPs drops exponentially with the temperature, as shown in Eq. 3.4. At a certain point the annihilation rate, Γ_{ann}, becomes smaller than the expansion rate of the universe and the annihilation of WIMPs ceases. After that, the number of WIMPs remains constant for a comoving volume.

In more detail, [100], the evolution of the number density of a particle χ, $n(t)$, is related to the distribution function of the particle, $f(t, E_\chi)$,

$$n(t) = \frac{g_\chi}{(2\pi)^3} \int d^3\vec{p} f(t, E_\chi). \tag{3.5}$$

The temporal evolution of the number density is given by the Liouville operator, $\hat{L}[f]$, which, written in a covariant way, reads

$$\hat{L}[f] = \frac{df}{d\tau} = \frac{\partial f}{\partial x^\mu}\frac{dx^\mu}{d\tau} + \frac{\partial f}{\partial p^\mu}\frac{dp^\mu}{d\tau} = p^\mu \frac{\partial f}{\partial x^\mu} - \Gamma^\mu_{\sigma\rho} p^\sigma p^\rho \frac{\partial f}{\partial p^\mu}, \tag{3.6}$$

where $\Gamma^\mu_{\sigma\rho}$ is the affine connection.

For a Friedmann-Robertson-Walker (FRW) universe, the distribution function does not depend on position or momentum. Hence, the Liouville operator becomes

$$\hat{L}[f] = E\frac{\partial f}{\partial t} - \Gamma^0_{\sigma\rho} p^\sigma p^\rho \frac{\partial f}{\partial E} = E\frac{\partial f}{\partial t} - H|\vec{p}|^2 \frac{\partial f}{\partial E}, \tag{3.7}$$

where H is the Hubble constant. Then, the number density evolution reads

$$\frac{g_\chi}{(2\pi)^3}\int \frac{d^3\vec{p}}{E}\hat{L}[f(t, E_\chi)] = \frac{dn}{dt} + 3nH. \tag{3.8}$$

On the other hand, the evolution of the distribution function is directly connected to the particle collisions produced in the plasma. We can define a collisional operator, $C[f]$, that encodes the dependence on number-changing processes and that is related to the Liouville operator as follows,

$$\hat{L}[f(t, E_\chi)] = C[f(t, E_\chi)], \tag{3.9}$$

where $C[f(t, E_\chi)]$ is defined for reactions of the type $\chi_i\bar{\chi}_j \leftrightarrow AB$ (shown in Fig. 3.1). For these $2 \leftrightarrow 2$ reactions, the collisional operator reads

$$\begin{aligned}\frac{g_\chi}{(2\pi)^3}\int \frac{d^3\vec{p}}{E}C[f(t, E_\chi)] = \int d\Pi_i d\Pi_j d\Pi_a d\Pi_b (2\pi)^4\delta^4(p_i + p_j - p_a - p_b)\times \\ [f_i f_j(1 \pm f_a)(1 \pm f_b)|\mathcal{M}_{ij\to ab}|^2 - f_a f_b(1 \pm f_i)(1 \pm f_j)|\mathcal{M}_{ab\to ij}|^2],\end{aligned} \tag{3.10}$$

where the $-$ $(+)$ sign, again, refers to fermions (bosons), $\mathcal{M}$ is the invariant polarized amplitude, summed over the final states and averaged over the initial states, and $d\Pi_i$ is the Lorentz invariant phase space,

$$d\Pi_i \equiv \frac{g_i}{(2\pi)^3}\frac{d^3\vec{p}}{2E_i}. \tag{3.11}$$

This equation is valid both when the particles $\chi_i\bar{\chi}_j$ are identical (Majorana fermions) or when they are not.

To simplify the calculations we make several assumptions. First, we assume that the SM particles A and B, once produced by the annihilation, enter quickly into thermal equilibrium. This implies that we can replace their distribution factors, $f_{a,b}$, with the equilibrium distributions, $f^{eq}_{a,b} \simeq \exp(-E_{a,b}/T)$, where we have neglected the chemical potencial for simplicity and taken Boltzmann distribution functions (Eq. 3.2) for both fermions and bosons.

For the same reason, the $(1 \pm f_\alpha)$ factors can be approximated by 1. Now, from energy conservation, in a $\chi_i \bar{\chi}_j \leftrightarrow AB$ reaction $E_i + E_j = E_a + E_b$. This obvious equality is translated into a useful relation between the product of distribution functions in equilibrium, which reads

$$f_i^{eq} f_j^{eq} = \exp(-(E_i + E_j)/T = \exp(-(E_a + E_b)/T) = f_a^{eq} f_b^{eq}. \tag{3.12}$$

Finally, the annihilation and creation processes are assumed to conserve CP, implying that $|\mathcal{M}_{ij\to ab}|^2 = |\mathcal{M}_{ab\to ij}|^2 = |\mathcal{M}|^2$.

Under these assumptions, Eq. 3.10 simplifies to

$$\begin{aligned} \frac{g_\chi}{(2\pi)^3} \int \frac{d^3\vec{p}}{E} C[f(t, E_\chi)] = \int d\Pi_i d\Pi_j d\Pi_a d\Pi_b (2\pi)^4 \times \\ \delta^4(p_i + p_j - p_a - p_b)[f_i f_j - f_i^{eq} f_j^{eq}]|\mathcal{M}|^2. \end{aligned} \tag{3.13}$$

On the other hand, the annihilation cross-section reads,

$$\sigma \equiv \sigma_{ij\to ab} = \int (2\pi)^4 \delta^4(p_i + p_j - p_a - p_b)|\mathcal{M}|^2 \frac{d^3\vec{p}_a}{(2\pi)^3 E_a} \frac{d^3\vec{p}_b}{(2\pi)^3 E_b} \times \frac{1}{F}, \tag{3.14}$$

where $F = [(p_i \cdot p_j)^2 - m_i^2 m_j^2] = 2vE_iE_j$, with v the relative velocity between the particles i and j. Then, using the thermal average cross-section times velocity,

$$\langle \sigma v \rangle = \frac{\int \sigma v \frac{f_i}{(2\pi)^3} d^3\vec{p}_i \frac{f_j}{(2\pi)^3} d^3\vec{p}_j}{\int \frac{f_i}{(2\pi)^3} d^3\vec{p}_i \frac{f_j}{(2\pi)^3} d^3\vec{p}_j}, \tag{3.15}$$

Eq. 3.10 becomes

$$\frac{g_\chi}{(2\pi)^3} \int \frac{d^3\vec{p}}{E} C[f(t, E_\chi)] = -\langle \sigma v \rangle (n^2 - n_{eq}^2). \tag{3.16}$$

Comparing Eq. 3.8 and Eq. 3.16 we get the Boltzmann equation for the number density evolution:

$$\frac{dn}{dt} + 3nH = -\langle \sigma v \rangle (n^2 - n_{eq}^2). \tag{3.17}$$

A useful definition is the ratio of number of particles to entropy, called yield, $Y \equiv n/s$, where s is the total entropy of the universe. In the absence of entropy production, the total entropy per comoving volume is constant. And the time evolution of the yield goes like

$$\frac{dY}{dt} = \frac{1}{s}\left(\frac{dn}{dt} + 3Hn\right). \tag{3.18}$$

Hence, we can express the Boltzmann equation in terms of the yield as follows,

$$\frac{dY}{dt} = -s\langle \sigma v \rangle (Y^2 - Y_{eq}^2). \tag{3.19}$$

The evolution of the universe is related to the temperature of the system, thus it is convenient to define a new variable $x \equiv m_\chi/T$. Then, the evolution of the yield can be expressed as

$$\frac{dY}{dx} = -\frac{s}{H(T)x}\langle\sigma v\rangle(Y^2 - Y_{eq}^2). \tag{3.20}$$

Using the definitions for the Hubble constant and the entropy for a FRW cosmology the yield evolution is

$$\frac{dY}{dx} = -\left(\frac{45}{\pi M_P^2}\right)^{-1/2} \frac{g_\star^{1/2} m_\chi}{x^2}\langle\sigma v\rangle(Y^2 - Y_{eq}^2), \tag{3.21}$$

where $g_\star^{1/2}$ is the degree of freedom parameter and M_P is the Planck mass.

As explained at the beginning of the section, at early times, when the temperature is higher than m_χ, creation and annihilation processes are balanced and the number density of the species in the thermal bath remains constant. But, when the temperature decreases below m_χ, the kinetic energy is not enough to produce WIMP pairs and the number density (and, hence, the yield) decreases exponentially with the temperature because of WIMP annihilation, following Eq. 3.4. However, when the expansion rate of the universe becomes larger than the annihilation rate, $H > \Gamma_{ann}$, WIMPs cannot annihilate and the yield remains approximately constant up to now. This is called the freeze-out. We can see the yield evolution in Fig. 3.2. The solid line represents the yield at the equilibrium, decreasing exponentially as expected, and the dashed lines are the yield evolution. As we can see, the yield follows the equilibrium until the moment of the freeze-out, when it stabilizes. The moment of the freeze-out depends on the value of $\langle\sigma v\rangle$. For larger values of $\langle\sigma v\rangle$ WIMPs are able to stay longer in equilibrium at the plasma and the freeze-out occurs later, thus leading a smaller yield at present times.

More precisely, the yield after the freeze-out goes as

$$Y_\infty \simeq \left(\frac{45}{\pi M_P^2 g_\star}\right)^{1/2} \frac{x_{fo}}{m_\chi\langle\sigma v\rangle}, \tag{3.22}$$

where $x_{fo} \equiv m_\chi/T_{fo}$, with T_{fo} the temperature at the freeze-out. The typical temperature of the decoupling for WIMPs of masses between 1-100 GeV is $T_{fo} \simeq m_\chi/20$, as can be seen in Fig. 3.2. Eq. 3.22 shows the dependence of the Yield on $\langle\sigma v\rangle$. As we mentioned, for larger values of $\langle\sigma v\rangle$ we get lower values for the yield at present times.

Finally we can compute the DM relic abundance in terms of the yield after the freeze-out

$$\Omega_\chi h^2 = \frac{\rho_\chi h^2}{\rho_c} = \frac{m_\chi n h^2}{\rho_c} = \frac{m_\chi s_\infty Y_\infty h^2}{\rho_c}, \tag{3.23}$$

where s_∞ is the entropy density and ρ_c is the present critical density. For the case of a DM

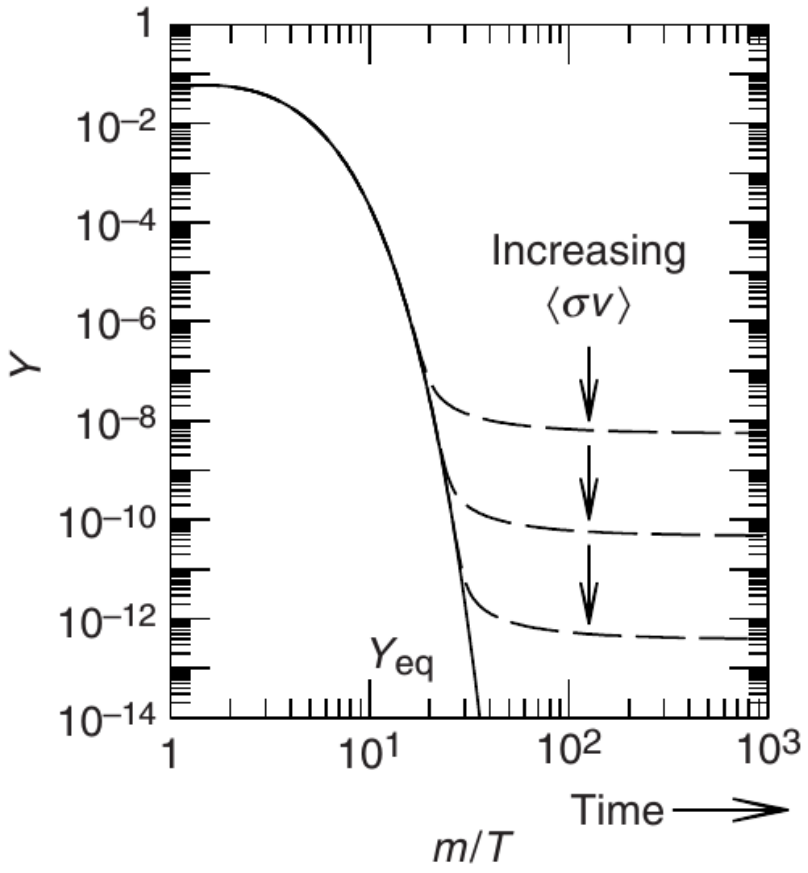

Figure 3.2: Yield evolution. The solid line represents the yield in equilibrium while the dashed lines represent the yield evolution. The yield evolution follows the equilibrium until the moment of the freeze-out, when it becomes approximately constant. The moment of freeze-out depends on the value of $\langle \sigma v \rangle$, happening later for larger values of the cross-section.

mass of EW size, $m_\chi \sim 100$ GeV, the relic density is

$$\Omega_\chi h^2 \sim \frac{10^{-27} cm^3/s}{\langle \sigma v \rangle}. \tag{3.24}$$

Since the observed relic abundance is $\Omega_\chi h^2 \sim 10^{-1}$, a cross-section $\langle \sigma v \rangle \sim 10^{-26}$ is required to obtain the correct relic density. This is an interesting result, since for a EW WIMP mass, such cross section is achieved with couplings of weak-interaction magnitude. This remarkable coincidence is called the WIMP miracle.

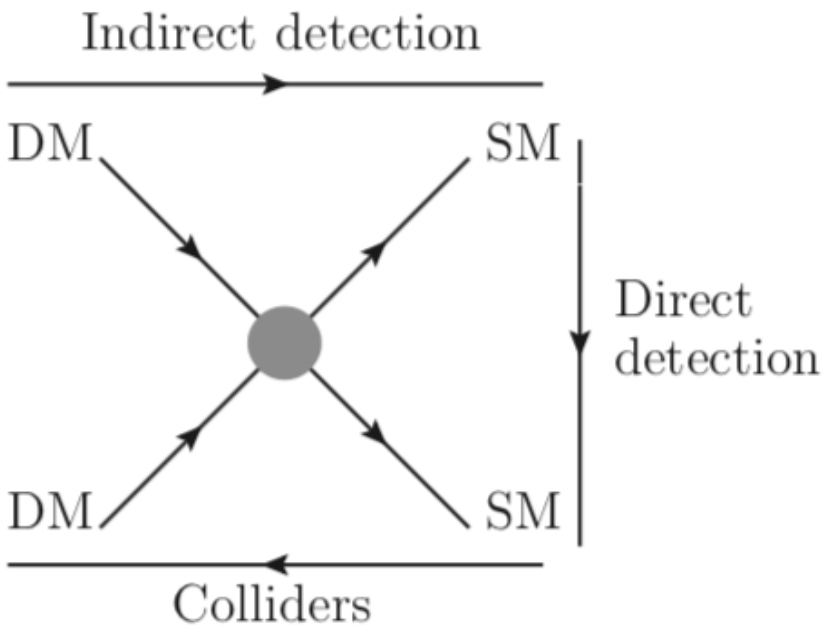

Figure 3.3: Diagram containing the different DM searches.

3.2 Experimental searches

If dark matter is connected with the SM, as it is demanded for WIMPs to be produced thermally, the interactions between dark matter and SM can be exploited to try to prove the existence of DM and study its nature. Different techniques have been and are used for this search. Fig. 3.3 shows a diagram displaying of the different searching techniques. One way of detecting DM is by measuring the energy transferred to SM particles by elastic collisions between the DM floating in the halo and a target in a detector. This is known as *direct detection* (DD). Another way for testing DM is by observing the particles produced by the annihilation of WIMPs in the universe. Notice that, although the relic ensity has remained approximately constant since the freeze-out, collisions of WIMP pairs in the halo can produce SM particles that can be detected. This technique is called *indirect detection* (ID). Finally, DM can be produced in *colliders*. Collisions of SM particles at high energy can produce DM particles. However, since they are neutral, they are invisible for the detectors. Nevertheless, there can be other observable particles produced in the collision. A way of probing DM in colliders is by looking for the SM companions and missing energy in the collision that would correspond to the DM particle produced. In this Subsection we take a closer look on these three mechanisms to search for DM and their actual status.

Direct detection

Assuming that DM is composed by WIMPs, the flux of WIMPs on Earth is around $10^5(100\ \mathrm{GeV}/m_\chi)cm^{-2}s^{-1}$. The flux is large enough to expect that, even with such a low cross section, a detectable fraction of particles could collide elastically and produce a measurable recoil in a nucleus. There are three detection signals to observe the energy transferred in the collision: heat production (phonons), excitation of a nucleus that de-excites emitting scintillation photons, or indirect ionisation of atoms. Experiments focus their detection strategy on one or two of these signals. A detailed review on the subject can be found in reference [101].

From DD experiments we can obtain bounds on the event rate and the recoil energy, which translates into bounds on the DM mass and the DM coupling with quarks. The differential event rate is given by

$$\frac{\mathrm{d}R}{\mathrm{d}E_R} = \frac{\rho_0}{m_N m_\chi}\int_{v_{min}}^{\infty} v f(v)\frac{\mathrm{d}\sigma_{WN}}{\mathrm{d}E_R}(v, E_R)dv, \tag{3.25}$$

where ρ_0 is the local DM density, m_N is the nucleus mass, $f(v)$ is the velocity distribution of DM in the detector normalized to one and $\frac{\mathrm{d}\sigma_{WN}}{\mathrm{d}E_R}(v, E_R)$ is the differential cross-section for the WIMP-nucleus scattering. The velocity distribution is Gaussian, with a dispersion, σ, related to the local circular speed, $v_c = (220 \pm 20)$ km s^{-1}, $\sigma = \sqrt{3/2}v_c \simeq 270$ km s^{-1}. The recoil energy reads

$$E_R = \frac{\mu_N^2 v^2(1-\cos\theta^\star)}{m_N}, \tag{3.26}$$

where μ_N is the WIMP-nucleus reduced mass and $\theta^\star$ is the scattering angle in the center-of-mass frame.

The WIMP-nucleus cross-section includes the information about the interactions between DM and ordinary matter. It basically depends on the coupling between DM and quarks, and can be separated into a spin-dependent (SD) and a spin-independent (SI) part. The spin-dependent contribution comes from the axial-axial coupling between WIMP and quark currents. In the case of a WIMP fermion the corresponding Lagrangian goes as

$$\mathcal{L} \supset \alpha_q^A(\bar{\chi}\gamma_\mu\gamma_5\chi)(\bar{q}\gamma^\mu\gamma_5 q), \tag{3.27}$$

and in the case of a WIMP spin-1 field as

$$\mathcal{L} \supset \alpha_q^A\epsilon^{\mu\nu\rho\sigma}(B_\rho \overleftrightarrow{\partial}_\mu B_n u)(\bar{q}\gamma^\sigma\gamma_5 q). \tag{3.28}$$

On the other hand, the spin-independent contribution is produced by scalar-scalar and vector-vector couplings,

$$\mathcal{L} \supset \alpha_q^S(\bar{\chi}\chi)(\bar{q}q) + \alpha_q^V(\bar{\chi}\gamma_\mu\chi)(\bar{q}\gamma^\mu q). \tag{3.29}$$

With this distinction, the differential cross-section can be expressed as

$$\frac{\mathrm{d}\sigma_{WN}}{\mathrm{d}E_R} = \frac{m_N}{2\mu_N^2 v^2}(\sigma_0^{SI} F_{SI}^2(E_R) + \sigma_0^{SD} F_{SD}^2(E_R)), \tag{3.30}$$

where $\sigma_0^{SI,SD}$ are the WIMP-nucleus spin-dependent and -independent cross-section at zero momentum transfer and $F_{SI,SD}$ are form factors that encode the dependence on the momentum transfer.

The spin-independent cross section is proportional to the square of the number of nucleons, A^2, while the spin-dependent contribution is proportional to $(J+1)/J$, where J is the nuclear angular momentum. For experiments with heavy targets, $A > 20$, the SI component dominates. Although there are experiments dedicated to SD couplings using targets with a large nuclear angular momentum, the majority of experiments are based on targets with heavy nuclei. Therefore, the strongest limits come from the spin-independent WIMP-nucleus cross-section and, except in the models where this SI cross-section is suppressed, are the most stringent restriction in DM models.

As mentioned, most of DD experiments use targets with heavy nuclei. Silicon, germanium, iodine or xenon are the usual targets. They measure the energy recoil and the collision rate to determine the mass and the cross-section of the DM. However, the experiments have a lower limit in the energy recoil sensitivity. Due to the absence of conclusive DM detection, the experiments impose an upper limit in the WIMP-nucleus SI cross-section as a function of the mass. In Fig.3.4 we can see the limits for the SI WIMP-nucleon cross section imposed by different DD experiments. For low masses, the two most relevant collaborations are CDMS and CRESST. Limits from the CDMS collaboration are provided by the SuperCDMS [102] (already completed) and CDMSlite [103] (still active) experiments. The CRESST collaboration provides bounds from the experiments CRESST-II [104] (completed) and CRESST-III [105] (active) experiments. These low mass experiments are based on germanium. In the case of high masses, LUX, Xenon, and PandaX are the relevant collaborations. The LUX experiment [106] has already finished while PandaX-II [107] and Xenon1T [108] are still taking data. These experiments for large masses are based on xenon, heavier than germanium. The sensitivity is lower at smaller masses. The reason is that for lower masses the energy recoil is smaller and the collisions can not reach the energy threshold. Using lighter targets would increase the sensitivity at lower WIMP masses, as well as the background. Fig. 3.4 explicitly shows the sensitivity prospects of future DD experiments as well. The CDMS collaboration is preparing four detectors for the SuperCDMS SNOLAB experiment [109]: Si HV and Si iZIP based on silicon and Ge HV and Ge iZIP based on germanium, to explore the low mass regime. For large masses, the LUX-ZEPLIN collaboration is working on the LZ experiment [110], based on germanium.

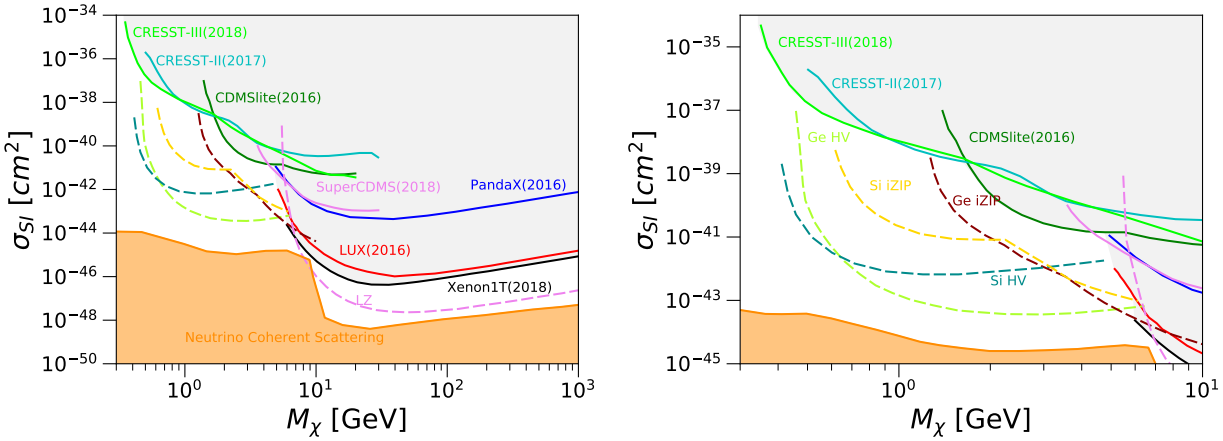

Figure 3.4: Spin independent WIMP-nucleon cross section constraints from different direct detection experiments. The solid lines are bounds coming from experimental data while the dashed lines are future prospects. The strongest bounds for low WIMP masses come from SuperCDMS [102] (violet) CDMSlite [103] (dark green), CRESST-II [104] (cyan) and CRESST-III [105] (green). At large masses LUX [106] (red), PandaX-II [107] (blue) and Xenon1T [108] (black) provide the most restrictive limits in the cross section. Future prospects are shown from LZ [110] (pink) and the four detectors of SuperCDMS SNOLAB [109], Si HV (dark cyan), SI iZIP (dark yellow), Ge HV (light green) and Ge iZIP (dark red). The orange line shows when the cross section becomes comparable with the neutrino coherent scattering [111].

Indirect detection

Even if DM is stable and does not decay, WIMPs can self-annihilate through collisions in the halo, producing SM particles. These products can be detected and provide information about the coupling of WIMPs and SM. For detailed lectures on indirect detection searches see reference [112]. WIMP annihilation could in principle produce any particle of the SM, depending on the coupling between the two sectors. However, the detection products are the stable particles at the end of the decay chains. These particles can be neutral, like photons or neutrinos, or charged, as electrons, positrons, protons or antiprotons.

In the case of photons, we have to distinguish between the different final states of the annihilation process. Specifically for the photon case, we can have three spectral categories: hadronic continuum, leptonic or lines. In the hadronic case, if DM annihilates to τ leptons, gauge bosons or quarks, neutral and charged pions will be produced in their decays and then neutral pions decay into photon pairs, giving rise to a continuum spectrum. If DM annihilation occurs mostly to electrons and muons (leptonic case) photons are produced as a part of the 3-body final states, by internal bremsstrahlung or final state radiation. In this case the spectrum is quite hard, peaked around the WIMP mass. Finally, if DM annihilates into two photons or a monoenergetic photon plus another particle, the spectrum contains a gamma-ray spectral line. This last case, if possible, is suppressed, since DM can not couple to photons directly, so the coupling should occur at loop level. On the other hand, the background would be very low.

For neutrinos the situation is similar for hadronic and line spectra (although line searches would be a challenge) but in the leptonic case it can differ, since muons would produce an unsuppressed neutrino spectrum while in direct annihilation to electrons the neutrino signal would be very small.

Charged particles differ from neutrinos and photons in the fact that they have interactions with other particles in their cosmic paths which change their spectrum and trajectories, unlike photons or neutrinos that travel in straight lines. For that reason the signal and the background are more challenging to model.

Many experiments are exploring these final products of DM annihilation. In experiments of gamma-rays searches, such as Fermi-LAT, H.E.S.S. or MAGIC, they measure gamma-rays coming from Dwarf Spheroidal Galaxies [113, 114] and the Galactic Center [115]. Their results are translated into limits in the DM annihilation cross section times velocity for different channels, such as e^+e^-, $\mu^+\mu^-, \tau^+\tau^-$, W^+W^-, $u\bar{u}$ or $b\bar{b}$.

For neutrino searches, the most relevant bounds come from IceCube [116] and ANTARES [117]. These experiments analyze the astrophysical neutrino flux by looking for an excess produced by dark matter annihilation. The absence of it imposes limits also in the DM annihilation cross section times velocity.

Finally, experiments as AMS [118], AMS-02 [119] or PAMELA [120] study cosmic

rays. Antimatter fluxes, positrons and antiprotons, are the most important source of DM information when we consider charged particles. However, as mentioned, these searches imply large uncertainties.

Colliders

Another way to probe the DM existence is production in colliders. The coupling between the DM and the SM allows for the production of WIMP pairs through the collision of SM particles, if it is kinematically allowed. Obviously, since DM particles are electrically neutral and weakly interacting, they will leave the detector without trace. However the WIMP pairs can be produced along with other SM particles that could be detected. This information together with the missing transverse energy, $\not{E}_T$ of the process, gives hints about DM. If the WIMP pair was produced alone no signal in the detector would be seen. The main searches of this kind are the production of a DM pair plus an extra SM particle, called *mono-X searches*, being X the SM particle to be detected. For a good review on collider searches for DM see [121].

In proton-proton collisions, one possibility is the production of a QCD jet from initial state radiation, along with the WIMP pair. In these *mono-jet searches*, the main object is a jet with high transverse momentum, p_T, plus missing transverse energy. The probability of finding an event with just one jet is very small [122], usually these processes involve events with several energetic jets. The SM background is sizable, although can be estimated using data-driven methods. Processes like $pp \to Z(\nu\bar{\nu})+$ jets can be estimated from analogous events with the Z boson decaying leptonically, or processes like $pp \to W(l\nu)+$ jets, with an undetected lepton, can be inferred from events where the lepton is identified. Also events with mismeasured jets can provide an unbalanced transverse momentum. However these events can be detected rejecting cases where $\not{p}_T$ does not point into the direction of the leading jet. With these considerations, the background can be quite well estimated.

Another particle that can be radiated from the initial state is a vector boson (γ, Z or W). *Mono-V searches* look for a vector boson and missing transverse momentum. A difference whit the mono-jet is that, although the cross section might be quite smaller, the process is much cleaner. Mono-photon searches are the simplest ones, requiring just a high transverse momentum photon and no isolated leptons [123, 124]. The background levels are typically low, and coming only from misidentification of an electron or a jet. Leptonic Z decays are also a clean signal. They require a large missing transverse momentum in the opposite direction of the di-lepton system, and a di-lepton invariant mass close to the Z mass, to reduce the background [125, 126]. The last possibility is the production of W boson along with the WIMP pair. If it decays leptonically, the neutrino contributes to the missing momentum and we observe an event with a single lepton [127, 128]. In this case the background is significant coming mainly from processes where an off-shell W decays

leptonically, producing an identical signature.

Mono-Higgs searches focus mainly on $\gamma\gamma$[129–131] and $b\bar{b}$[132–134] in the final states. For $\gamma\gamma$ the background is very small while for $b\bar{b}$ is quite the opposite, so techniques to identify a Higgs boson with high transverse momentum are needed. The main problem with these Higgs searches is that they are limited by statistics.

If DM couples dominantly to heavy quarks, another interesting search is to look for top quark pairs with missing transverse momentum [135, 136]. An example is the search for a W, from a top decay $t \to Wb$, decaying hadronically [123, 137], or semi-leptonically [138] as well as fully leptonic channels [139], which are only limited by statistics. Another possibility is the production of just one top quark in addition with DM [140].

There has not been seen any relevant excess in any of this mono-X searches. Therefore, as in the cases of DD and ID, we get exclusion limits for the coupling between sectors.

Finally, if DM is lighter than half of the Higgs mass, it could be possible for a Higgs to decay into a WIMP pair. Measuring the visible decays is possible to estimate the Higgs invisible cross section, which would put un upper bound on the Higgs decay to DM. Another possibility is to search for particles produced along with the Higgs boson, which decay into DM, such as vector bosons [125, 141, 142]. Combining the different searches, the present bound for the invisible branching ratio of the Higgs is $\mathrm{BR}_{inv} < 0.25$ [141, 143].

Chapter 4

Higgs Portal. Minimal extension of the singlet-scalar Higgs Portal

As mentioned in Sec. 2.2, the simplest WIMP model that reproduces the correct relic density is the well known *singlet-scalar Higgs portal* (SHP). The model consists in the addition of just one extra particle, a singlet scalar, S, coupled to the Higgs boson, as the name of the model indicates. The uniqueness of this model is that, despite its simplicity, it presents a remarkable phenomenology, being able to reproduce the DM density. For this reason, it has been studied extensively since its proposal [144–150].

To ensure the stability of the DM, an extra Z_2 symmetry is imposed, affecting only the new scalar, $S \to -S$. Including all the possible renormalizable terms and assuming the Z_2 symmetry, the Lagrangian of this model reads

$$\mathcal{L}_{\text{SHP}} = \mathcal{L}_{\text{SM}} + \frac{1}{2}\partial_\mu S \partial^\mu S - \frac{1}{2}m_0^2 S^2 - \frac{1}{2}\lambda_S |H|^2 S^2 - \frac{1}{4!}\lambda_4 S^4. \tag{4.1}$$

In the previous equation S has been assumed to be a real field, but the modification for the complex case is trivial.

After EW symmetry breaking, the Higgs field acquires a vacuum expectation value, $H^0 = (v+h)/\sqrt{2}$, and new terms appear, including a trilinear coupling between S and the Higgs boson, $(\lambda_S v/2)hS^2$.

Assuming that the $S-$particles are in thermal equilibrium in the early universe, the final DM relic density is determined by their primordial annihilation rate into SM-particles. The relevant processes, illustrated in Fig. 4.1, are usually dominated by the $s-$channel annihilation through a Higgs boson (leftmost diagram of the figure).

The efficiency of the annihilation depends on just two parameters, $\{m_0, \lambda_S\}$ or, equivalently, $\{m_S, \lambda_S\}$, where $m_S^2 = m_0^2 + \lambda_S v^2/2$ is the physical $S-$mass after EW symmetry breaking. Fig. 4.2 shows the (black) line in the $\{m_S, \lambda_S\}$ plane along which the relic abun-

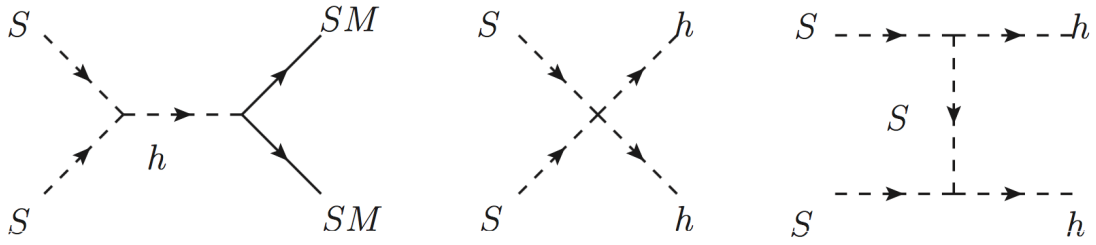

Figure 4.1: Singlet-scalar Higgs portal scenario (SHP): annihilation processes of the DM candidate, S.

dance of S, $\Omega_S h^2$, coincides with the Planck result $\Omega_{CDM} h^2 = 0.1198 \pm 0.003$ at 2σ [20]. The (gray) region below is in principle excluded, as it corresponds to a higher relic density.

4.1 Estatus of the singlet-scalar Higgs portal

As exposed in Sec. 3.2, experimental searches test DM models. Since, so far, there is no positive detection in any experiment, they typically impose bounds on the couplings and masses of the particles of DM models. And the Higgs portal model is not an exception.

Different limits from all kinds of experiments constrain the parameter space of the model, excluding significant areas of it. These include limits from direct detection experiments [111, 151–162], indirect searches [163–189], as well as collider bounds [141, 190–197]. We illustrate the effects of these limits in Fig. 4.2. In deriving direct and indirect detection bounds, we are assuming by default (left panel) that the density of S scales up in the same way as its cosmological relic abundance. Thus, we consider a scale factor $\xi \equiv \Omega_S/\Omega_{CDM}$ for direct detection and ξ^2 for indirect detection. In the region where $\xi < 1$, S cannot be the only DM component, so contributions from other particles (e.g., axions) are needed. The region where $\xi > 1$ (gray area) is obviously excluded (though perhaps could be rescued if some non-standard cosmology is invoked, see below). For this reason, we have not showed the shadowed regions inside this gray area. It is worth noting that the excluded areas are extremely sensitive to astrophysical uncertainties in the DM halo parameters [198] and nuclear uncertainties in the hadronic matrix elements [188].

Current bounds from direct DM detection, most notably from the new results from LUX [106], PandaX-II [199] and Xenon1T [108], set an upper bound on the DM-nucleon elastic scattering cross section (and hence on the DM coupling to the Higgs). Nowadays the strongest DD bounds come from Xenon1T and they constrain a larger area of the parameter space, althought during most of this chapter we will impose the bounds from LUX, which do not differ much with the present bounds from Xenon1T. The LUX bound rules out the red

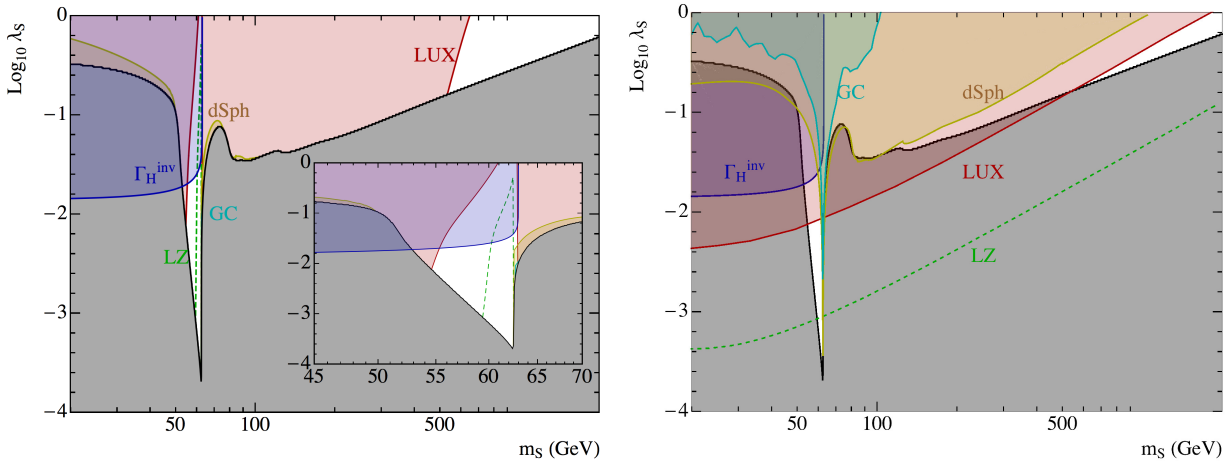

Figure 4.2: Excluded regions on the parameter space of the SHP model from different experimental constraints. The gray area (below the black line) is excluded since the relic density exceeds the Planck result. The blue area (labeled Γ_H^{inv}) is ruled out from the invisible Higgs width. The red area (LUX) is excluded by direct DM detection limits. Yellow (dSph) and cyan (GC) areas are excluded by indirect detection constraints on the continuum spectrum of gamma-rays (from dwarf Spheroidal galaxies) and monochromatic gamma-ray lines (from the Galactic Centre), respectively. The dashed green line represents the predicted reach of the future LZ detector. The left panel includes a scale factor, ξ, in the calculations while in the right plot it is assumed that some extra non-thermal effects amend the prediction for the relic density, so that $\xi = 1$.

area in Fig. 4.2. Next-generation experiments, with larger targets and improved sensitivity are going to further explore this parameter space. We indicate in the figure the expected reach of the LZ detector by means of a green dashed line. Similarly, Fermi-LAT data on the continuum gamma-ray flux from dwarf spheroidal galaxies (dSPh) and monochromatic gamma-ray lines from the Galactic Center set upper bounds on the DM annihilation cross section which also rule out some areas of the parameter space, mainly for DM masses below 100 GeV (light brown and cyan areas respectively). It should be noticed that, as λ_S decreases, the $\xi-$factor increases, so that the indirect detection rate increases as well. Consequently, the excluded areas from indirect detection extend downwards in the plot. Finally, for masses below $\sim$ 63 GeV, the DM can contribute to the invisible decay of the SM Higgs boson. Current LHC constraints on this quantity set an upper bound on the DM-Higgs coupling [141]. The blue region in Fig. 4.2 is excluded for this reason.

For comparison, the right panel of Fig. 4.2 shows the direct and indirect detection constraints when the local DM density is assumed to take the canonical value, $\rho_0 = 0.3$ GeV cm^{-3}, regardless of the computed thermal relic abundance; in other words, we have set $\xi = 1$. This

would apply if non-thermal effects modified the final relic abundance, reconciling it with the observed one (see, e.g., Ref. [200]). Note that, since the value of ξ has been fixed, the areas excluded by indirect detection bounds now extend upwards.

In either case, the conclusion is that the combination of experimental constraints and the requirement of obtaining the correct relic abundance rules out a big and interesting portion of the viable parameter space of the Higgs portal (see Ref. [79] for a recent comprehensive study), leaving only the white areas in Fig. 4.2. Interestingly, as previous analyses have shown [201–204] there still remains a narrow window of $S-$masses in the Higgs-funnel region ($m_S \simeq m_h/2$) and, besides, there is a large allowed range for higher masses, $m_S \gtrsim 500$ GeV. Next generation experiments such as XENON1T [205], already taking data, and, especially, LZ [206] (shown explicitly) will test completely the region of large DM masses and a large part of the narrow window at the Higgs-resonance. In particular, LZ could exclude the Higgs-portal scenario almost completely, or, hopefully, get a positive detection. The possibility of totally closing the Higgs-portal windows in the near future using complementary constraints from indirect detection has been analyzed in refs. [79, 201, 203].

Various solutions have been proposed in order to avoid experimental constraints in the SHP model. In general, in order to break the correlation between the relic abundance and direct detection predictions, the model has to be extended. For example, the mediator (Higgs) sector can be enlarged with new scalars [207–209]. Non-linear Higgs portals [210] and high-dimensional operators in models with composite Higgs [211] have been considered as well. One can also extend the dark sector to include new particles charged under the SM gauge group, such as a doublet, a triplet, or a top-partner (see, e.g., [212–215]), or even consider multicomponent dark matter scenarios [209, 216–219]. More complex scenarios have also been analysed, where both the dark matter and mediator sectors are enlarged [220], for example, adding new portals related to neutrino physics [221–224]. There is also the possibility that the dark matter is a singlet-fermion, in which case the Higgs-portal interactions occur at the non-renormalizable level. Finally, one can consider changing the nature of the DM candidate, see for example Refs. [225, 226].

The goal of this chapter is to consider and examine the most economical modification of the conventional SHP model that could escape the present and future searches, thus offering a viable (slightly modified) Higgs-portal scenario if a positive detection does not occur. The model consists of the addition of a second singlet scalar in the dark sector, which opens up new annihilation and coannihilation channels (previous work in this line has been carried out in Ref. [227]). We should stress that our solution is not unique: for example, this model has a simplicity similar to the secluded-dark-matter scenario [228], but it works in a different way.

The results of this chapter have been published in Refs. [74, 229].

4.2 The extended singlet-scalar Higgs portal (ESHP)

The modification of the conventional SHP model that we consider consists simply of extending the DM sector with the addition of a second scalar. Denoting S_1, S_2 the two scalar particles, and imposing a global Z_2 symmetry ($S_1 \to -S_1$, $S_2 \to -S_2$) in order to guarantee the stability of the lightest one, the most general renormalizable Lagrangian reads

$$\begin{aligned}\mathcal{L}_{\rm ESHP} &= \mathcal{L}_{\rm SM} + \frac{1}{2}\sum_{i=1,2}\left[(\partial_\mu S_i)^2 - m_i^2 S_i^2 - \frac{1}{12}\lambda_{i4} S_i^4\right] - \frac{1}{6}\lambda_{13} S_1 S_2^3 - \frac{1}{6}\lambda_{31} S_1^3 S_2 - \frac{1}{4}\lambda_{22} S_1^2 S_2^2 \\ &\quad -\frac{1}{2}\lambda_1 S_1^2|H|^2 - \frac{1}{2}\lambda_2 S_2^2|H|^2 - \lambda_{12} S_1 S_2\left(|H|^2 - \frac{v^2}{2}\right) \ , \end{aligned} \tag{4.2}$$

where the subscript ESHP stands for "extended singlet-scalar Higgs portal". The terms in the second line describe the DM/SM interactions, which occur through the Higgs sector. After EW breaking, $H^0 = (v+h)/\sqrt{2}$, there appear new terms, including trilinear terms between $S_{1,2}$ and the Higgs boson, such as $(\lambda_{12} v)\, h S_1 S_2$. Stability constraints in this type of models have been studied in Ref. [230]. We have chosen S_1, S_2 to be the final mass eigenstates (after EW breaking), with physical masses, $m_{S_i}^2 = m_i^2 + \lambda_i v^2/2$, thus the form of the last term in Eq. (4.2). From now on, S_1 will represent the lightest mass eigenstate of the dark sector, and thus the DM particle.

4.2.1 The relic density

The extra terms in the Lagrangian open up new ways of DM annihilation, illustrated in Fig. 4.3. These include processes mediated by S_2 (in $t-$channel) and co-annihilation processes. Besides, if S_1 and S_2 are in thermal equilibrium between them (thanks to the interaction terms in the first line of Eq. (4.2)), the processes driving S_2-annihilation contribute to the DM annihilation as well.

We are interested in the possibility that S_1 plays the role of DM, and that it reproduces the observed relic density while evading the bounds discussed in the previous section for the usual SHP model. Hence we will mainly focus in the regime where λ_1 (the equivalent to λ_S in the ordinary Higgs-portal) is small. As a matter of fact, λ_1 might be even vanishing, and the processes of Fig. 4.3 could still produce the necessary annihilation. However, this is not a natural choice from the point of view of quantum field theory. Since 1-loop diagrams with two λ_{12} vertices generate $S_1^2|H|^2$ interactions, a conservative attitude is to assume that λ_1 is not smaller than $\sim \lambda_{12}^2/(4\pi)^2$. The same argument holds for λ_2. Actually, for the sake of definiteness we will set $\lambda_2 = \lambda_{12}^2/(4\pi)^2$ through the chapter.

Moreover, all the processes where a λ_1-vertex is involved get new radiative corrections. In particular, the trilinear vertex (after EW breaking) $S_1 S_1 h$, which appears in DM

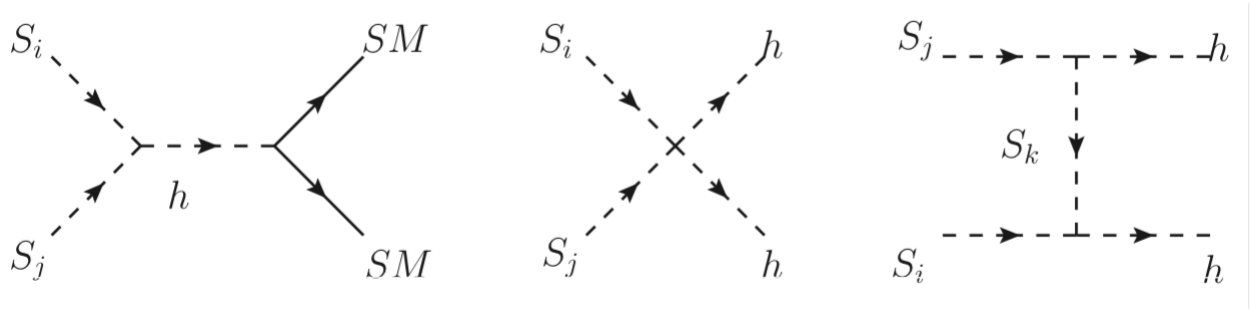

Figure 4.3: Extended Higgs-portal scenario (ESHP): annihilation processes involving particles of the dark sector, S_i, $i = 1, 2$.

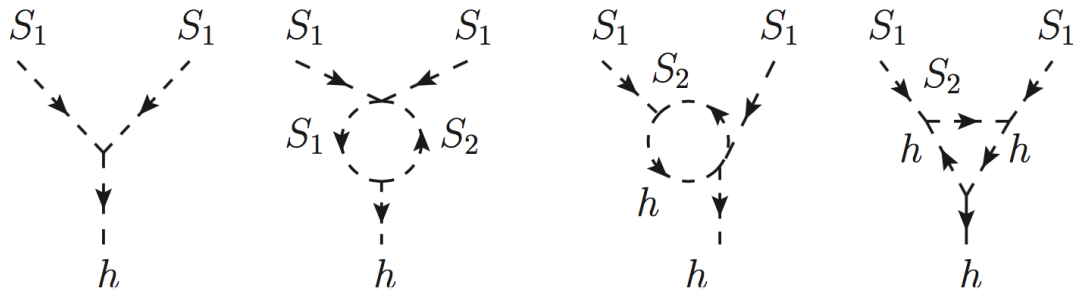

Figure 4.4: Tree-level $S_1 S_1 h$ vertex and main 1-loop corrections.

annihilation and scattering processes (relevant for indirect and direct detection), has to be corrected by 1-loop diagrams, such as the ones depicted in Fig. 4.4. Due to the adopted smallness of λ_2, other 1-loop diagrams are subdominant. Assuming for simplicity that λ_{31} (involved in the second diagram of Fig. 4.4) is of the same order as λ_{12}, all these contributions are $\mathcal{O}(\lambda_{12}^2/(4\pi)^2)$, which is precisely the smallest natural value for λ_1. This means that only when λ_1 is close to this lower limit the contributions of these diagrams may be significant[1]. Nevertheless, for consistency, we have included the contribution of the 1-loop diagrams in all cases. A detailed discussion of these radiative corrections is given in the Appendix A.

Let us now turn our attention to the computation of the relic density. We will start by considering a scenario in which λ_1 is as small as possible ($\lambda_1 = \lambda_{12}^2/(4\pi)^2$). Then, λ_1 can be neglected for all the relevant physical processes in most cases, so the only significant parameters to describe the DM physics are m_{S_1}, m_{S_2}, and λ_{12}. For each value of the DM mass, m_{S_1}, we are interested in finding out which combinations of m_{S_2} and λ_{12} lead to the

[1]In that case, there may be accidental cancellations between the tree-level and the radiative corrections, as can be checked from the explicit expressions given in the Appendix A. Moreover these cancellations can be more or less significant depending on the external momenta entering the vertex. This opens the possibility of blind spots for direct or indirect detection, while keeping a sizable annihilation in the early universe.

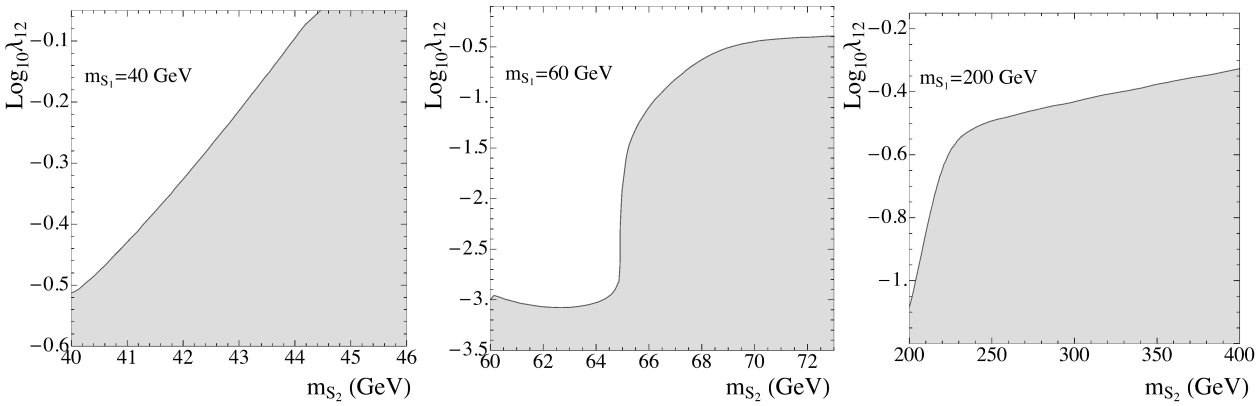

Figure 4.5: Range of values in the $\{\lambda_{12}, m_{S_2}\}$ plane leading to the correct DM relic density for three illustrative values of the DM mass: (from left to right) $m_{S_1} = 40$ GeV, 60 GeV, and 200 GeV. The DM-Higgs coupling has been fixed to $\lambda_1 = \lambda_{12}^2/(4\pi)^2$. The solid black line represents the Planck result. The grey area below this line is excluded since $\Omega_{S_1} > \Omega_{CDM}$.

correct relic density.

Fig. 4.5 shows the line along which the correct DM relic abundance is obtained for three representative cases, namely $m_{S_1} = 40$, 60, and 200 GeV, i.e., below, around and above the Higgs resonance (left, middle and right panels, respectively). Let us discuss each case separately.

For small DM masses (left panel), the correct relic density can be obtained through coannihilation effects with S_2 for a wide range of values of λ_{12} when $m_{S_2} - m_{S_1} \lesssim 5$ GeV. As m_{S_2} grows and departs from m_{S_1}, the required value of λ_{12} is larger and, at some point, it becomes non-perturbative.

When m_{S_1} is not far from the Higgs resonance (middle panel), we observe two different regimes. If $m_{S_1} + m_{S_2}$ is smaller than m_h, but such that $m_{S_1} + m_{S_2} \approx m_h$, the resonant condition for the s-channel $S_1 S_2 \to h \to SM\ SM$ can still be satisfied (S_1 and S_2 can have the correct energy due to their kinetic energy in the thermal bath) and the required value of λ_{12} is small. [2] On the other hand, when $m_{S_1} + m_{S_2} > m_h$ the resonant effect is not possible. Consequently λ_{12} has to increase to reproduce the correct relic density. For sufficiently large m_{S_2} and λ_{12}, the corresponding value of the λ_1 coupling (which in this example is set to $\lambda_1 = (\lambda_{12}/4\pi)^2$) and the size of the 1-loop diagrams of Fig. 4.4 become large enough for the DM to be efficiently annihilated through the usual SHP process, $S_1 S_1 \to h \to$ SM SM.

[2] Actually, it is quite independent of m_{S_2}, for the following reason. The amount of DM annihilated in this way is proportional to the product of two Boltzman factors: the one that suppresses the S_2-density and the one that kinematically suppresses the $S_1 S_2 \to h$ process. As m_{S_2} increases, the first Boltzman factor decreases and the second one increases, keeping the product almost constant.

In this regime, the model works essentially as the conventional SHP and the S_2 particle is irrelevant. Then the line in the plot becomes horizontal since the required value of λ_1 is related to that of λ_{12} through the above identification. However, the model could also work with essentially the same λ_1 and a smaller λ_{12}.

Finally, for $m_{S_1} > m_h/2$ (right panel), we can distinguish two regimes. When $m_{S_2} \sim m_{S_1}$, coannihilation effects are still present and the dependence with λ_{12} resembles that of the left panel. However, for large m_{S_2} coannihilation effects are not effective and the relic density becomes less sensitive to m_{S_2}. In that case, if $m_{S_1} > m_h$ (as in the example of the figure), the t-channel diagram of Fig. 4.5, with S_1 in the external legs annihilating through S_2-exchange into a pair of Higgs bosons, is kinematically accessible and it becomes the main contribution to the annihilation cross section.

4.2.2 Observational and experimental constraints

From the discussion in the previous subsection, it seems that for any value of m_{S_1}, we can suitably choose $\{m_{S_2}, \lambda_{12}\}$ to reproduce the correct relic density. Since λ_1 can be very small, one might expect that the ESHP model can evade easily the usual constraints on the singlet-scalar Higgs-portal.

However, this is not so straightforward. First, a sizable λ_{12} has potential impact on several observables, as we are about to see. Also, one must check that the existence of the second dark (unstable) species, S_2, does not produce any cosmological disaster in the early universe. Finally, we might actually be interested in varying the value of λ_1 above its minimal value (in order to be as general as possible).

In this subsection we discuss the various physical constraints to which the model is subject.

Invisible width of the SM Higgs boson. From the observed decay channels of the SM Higgs boson, an experimental constraint can be derived on its invisible decay width. Namely, using the recent ATLAS and CMS results [141, 231–233], we will impose $\mathrm{BR}(h \to inv) \leq 0.20$ (at a 90% confidence level) throughout this chapter. In the scenario presented here, the DM sector can contribute to the invisible width of the SM Higgs through the decays $h \to S_1 S_1$, $h \to S_1 S_2$, and $h \to S_2 S_2$, when these are kinematically allowed (see also Ref. [227]).

The corresponding decay widths at tree level read

$$\begin{aligned}
\Gamma_{h\to S_1 S_1} &= \frac{\lambda_1^2 v^2}{32\pi m_h}\left(1-\frac{4\,m_{S_1}^2}{m_h^2}\right)^{1/2}, \\
\Gamma_{h\to S_1 S_2} &= \frac{\lambda_{12}^2 v^2}{64\pi m_h}\left(1-\frac{(m_{S_2}+m_{S_1})^2}{m_h^2}\right)^{1/2}\left(1-\frac{(m_{S_2}-m_{S_1})^2}{m_h^2}\right)^{1/2},
\end{aligned}$$

$$\Gamma_{h\to S_2S_2} = \frac{\lambda_2^2 v^2}{32\pi m_h}\left(1-\frac{4\,m_{S_2}^2}{m_h^2}\right)^{1/2}. \tag{4.3}$$

In our calculation, we have included the radiative corrections to the S_1S_1h coupling (see Fig. 4.4), as explained in the previous section. As mentioned in Sec. 4.1, in the conventional SHP this constraint excludes areas with large coupling for small dark matter masses. In the ESHP, both λ_1 and λ_2 can be chosen small and, therefore, $h \to S_1S_2$ is the most relevant process, setting an upper bound on λ_{12}.

Lifetime of the extra scalar particle. The heavy scalar S_2 is unstable and decays into S_1 (plus SM products). We will require that the decay occurs before Big Bang nucleosynthesis, so as not to spoil its predictions. In fact, if S_2 is substantially heavier than S_1, namely $m_{S_2} > m_{S_1} + m_h$, it rapidly decays as $S_2 \to S_1 h$ through the corresponding trilinear coupling λ_{12}. However, if $m_{S_2} < m_{S_1} + m_h$, we need to consider the three-body decay $S_2 \to S_1 f\bar{f}$. The latter is in general fast enough when the $S_1 b\bar{b}$ channel is open, but the lifetime of S_2 increases rapidly below this mass. We have computed the lifetime of S_2 using CalcHEP [234], and excluded points in the scan where $\tau_{S_2} > 1$ s.

Direct detection. The tree-level scattering of S_1 off quarks occurs via a t-channel Higgs exchange, as depicted in Fig. 4.6, where the gray circle represents the sum of the (tree-level and 1-loop) vertices of Fig. 4.4. Since λ_1 can be very small, the constraints from direct detection experiments are substantially alleviated, in contrast with the situation of the canonical Higgs portal, as has also been observed in Ref. [227].

We have explicitly computed the spin-independent contribution to the DM-nucleon elastic scattering cross section, $\sigma^{SI}_{S_1p}$, which occurs through the exchange of a Higgs boson, as illustrated in Fig. 4.6. The Higgs-nucleon coupling can be parametrized as $f_N m_N/v$ where $m_N \simeq 0.946$ GeV is the mass of the nucleon. According to this, the spin-independent cross section, $\sigma^{SI}_{S_1p}$, reads

$$\sigma^{SI}_{S_1p} = \frac{\lambda_1^2 f_N^2 \mu^2 m_N^2}{4\pi m_h^4 m_{S_1}^2}\,, \tag{4.4}$$

where $\mu = m_N m_{S_1}/(m_N + m_{S_1})$ is the nucleon-DM reduced mass. The f_N parameter contains the nucleon matrix elements, and its full expression can be found, e.g., in ref. [201]. Using the values for the latter obtained from the lattice evaluation [235–240], one arrives at $f_N = 0.30 \pm 0.03$, in agreement with Ref. [201]. Finally, we have included one-loop contributions to the S_1S_1h coupling, shown in Fig. 4.4, according to the computation given in the Appendix A.

Then, we have implemented the most recent upper bounds obtained by the LUX collaboration [106] (which improves the bound obtained by PandaX-II [199]) for DM particles

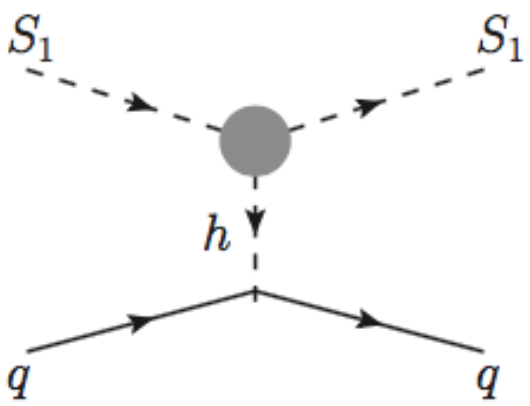

Figure 4.6: Diagrams contributing to the direct detection of S_1. The gray circle represents the sum of the (tree-level and 1-loop) vertices of Fig. 4.4.

with masses above 6 GeV [3]. Notice that since S_1 is a scalar field, there is no contribution to spin-dependent terms.

Although in principle we could also have inelastic scattering processes at tree level, $S_1 q \to S_2 q$, the typical mass difference in our scenario is such that $m_{S_2} - m_{S_1} > 1$ GeV, significantly larger than the kinetic energy of the incoming DM particle (which is smaller than ~ 1 MeV for DM particles lighter than ~ 1 TeV), and this process does not take place.

Indirect detection Regarding indirect dark matter searches, the most relevant bounds for this model can be derived from gamma-ray searches from dwarf spheroidal galaxies (for the continuum spectrum) and the galactic centre (for gamma ray lines and spectral features).

In order to apply the dwarf spheroidal galaxies data on the continuum, we have computed the thermally-averaged annihilation cross section, $\langle \sigma v \rangle$, in the dwarf galaxies using MicrOMEGAs [241, 242], assuming that the initial particles are at rest (a good approximation since the velocity of the DM is low). We have then confronted the results with the combined analysis of Fermi-LAT and MAGIC [243], considering the upper bounds on $\langle \sigma v \rangle$ for annihilation into $b\bar{b}$ (again a good approximation since the annihilation is through the Higgs and this is the main final state when it is open).

On the other hand, for gamma ray lines in the galactic centre, we have calculated the annihilation cross section into a pair of photons, $\langle \sigma v \rangle_{\gamma\gamma}$, again using MicrOMEGAs, and confronted it with the upper bound given by Fermi-LAT [244]. We have chosen the

[3]The SuperCDMS [102] and CRESST [104] collaborations have obtained more stringent constraints for light DM particles, but this range of masses is excluded in our model, mainly because of the experimental constraint on the invisible decay width of the Higgs boson.

Einasto [245, 246], profile for the DM halo, since is more restrictive than Navarro-Frenk-White (NFW) [247, 248] and has a good fit to results of numerical simulations. As in the SHP model, a Breit-Wigner enhancement near the Higgs resonance takes place,[4] although, given the small decay width of the Higgs boson, it only occurs for a narrow range of masses. This leads to a sizable annihilation cross section in that region.

Finally, let us recall that indirect detection constraints are very sensitive to whether the gamma-ray flux is re-scaled by the dark matter density squared (ξ^2).

4.3 Results

In this section we explore the parameter space of the ESHP model, incorporating all the experimental constraints and computing the theoretical predictions of observables for direct and indirect DM searches. As mentioned in the previous section, we have used MicrOMEGAs [241] to compute the relic abundance and indirect detection observables (the thermal average of the annihilation cross section of S_1 particles in the DM halo, $\langle\sigma v\rangle_0$, and the resulting gamma-ray flux). The spin independent S_1-nucleon scattering cross section, $\sigma^{SI}_{S_1 p}$, and the invisible Higgs decay width, have been computed including one-loop corrections, as explained in Section 4.2.2.

In order to facilitate the comparison of the model with the usual SHP, we have carried out a series of numerical scans, for fixed values of λ_{12}, in the three dimensional parameter space $\{m_{S_1}, \lambda_1, m_{S_2}\}$, searching for points where S_1 is a viable candidate for dark matter. Note that the first two parameters are those of the SHP, i.e. the mass and quartic coupling of the DM. As already mentioned, we will set λ_2 at its lowest natural value, $\lambda_2 = \lambda_{12}^2/(4\pi)^2$. This is also the lower limit of λ_1 in the scans.

We have represented the results of the scans in Figs. 4.7 and 4.8, where $\{m_{S_1}, \lambda_1\}$ and $\{m_{S_1}, m_{S_2}\}$ are plotted for fixed values of λ_{12}. From top to bottom, we have chosen $\lambda_{12} = 0.01$, 0.1, and 1, respectively, thereby gradually switching on the effect of the extra singlet in the model. The different experimental constraints are added sequentially from left to right. The left column includes the bounds from the invisible Higgs decay width and lifetime of S_2. The central column incorporates indirect detection bounds from Fermi-LAT results on the Galactic Centre and dSphs. Finally, in the right column we add the direct detection limits from LUX. In all the plots, black dots correspond to those in which the (thermal) relic abundance of S_1 matches the results from the Planck satellite, whereas grey points are those in which S_1 is a subdominant dark matter component.

[4] This has been studied in various models [249–253].

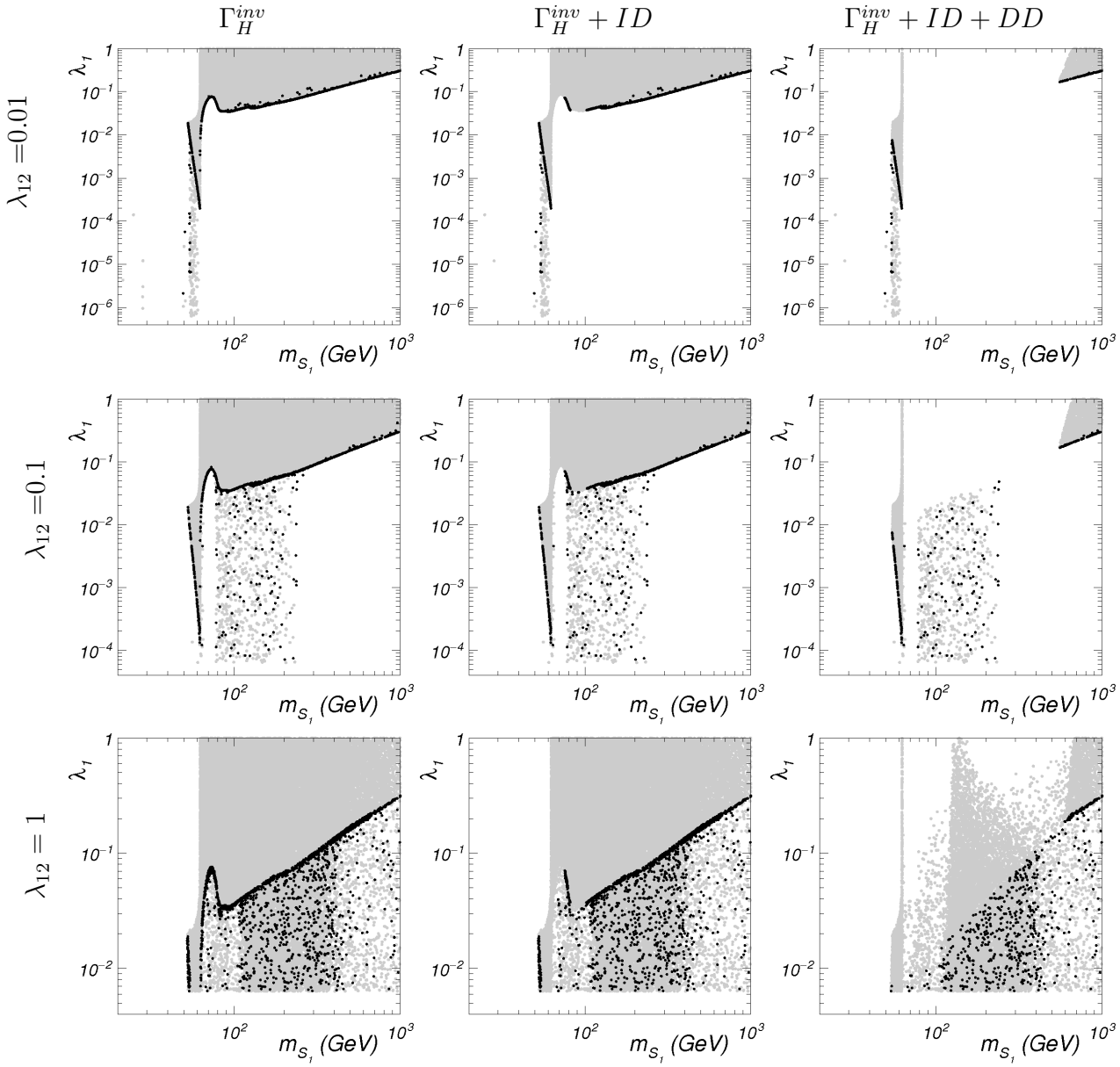

Figure 4.7: Effect of the experimental constraints in the $\{\lambda_1, m_{S_1}\}$ parameter space of the ESHP model. From up to down, we have fixed $\lambda_{12} = 0.01, 0.1, 1$, and $\lambda_2 = \lambda_{12}^2/(4\pi)^2$. In all the HP/Plots, black (gray) points correspond to those where $\Omega h^2 = 0.119 \pm 0.003$ ($\Omega h^2 < 0.116$). The left column incorporates only constraints from lifetime of S_2 and invisible decay width of the Higgs boson. The central column includes also the indirect detection (dSph and gamma ray lines). Finally, the bottom row includes the bound from the LUX constraint.

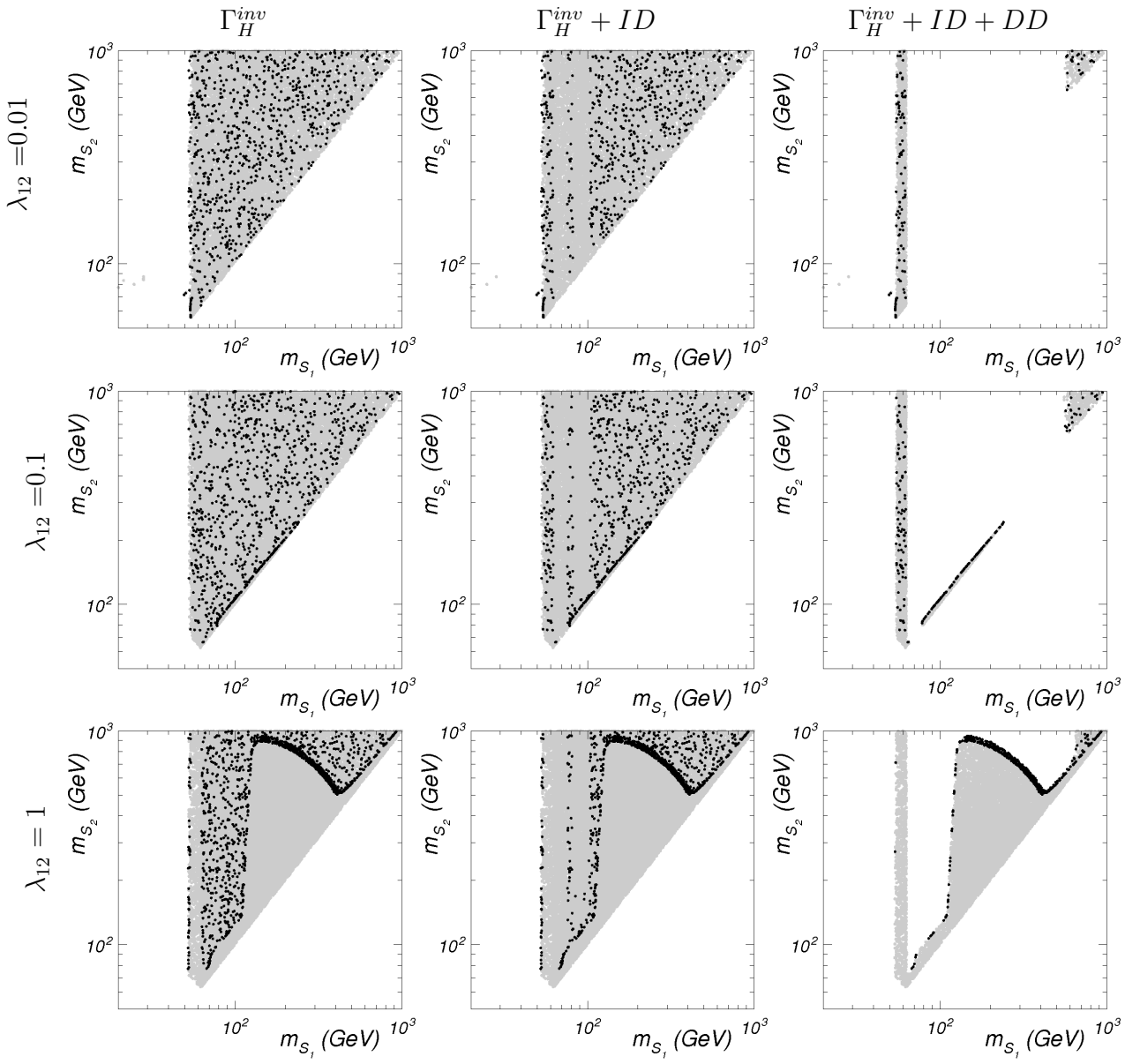

Figure 4.8: Effect of the experimental constraints in the $\{m_{S_1}, m_{S_2}\}$ parameter space of the ESHP model. We have used the same examples and colour conventions as in Fig. 4.7.

In all the plots of Fig. 4.7 an accumulation of black dots along a thick line is visible, which coincides with the relic-density line of the standard SHP (the black line of Fig. 4.2). For these points, the presence of the extra particle, S_2, has no effect, because the λ_{12} coupling is too small or/and S_2 is substantially heavier than S_1. These points appear as uniformly scattered in the $\{m_{S_1}, m_{S_2}\}$ plane in Fig. 4.8. Besides this (somehow trivial) thick line, there

are new regions of interest, which we discuss below.

The results for the top row ($\lambda_{12} = 0.01$) resemble those of the usual SHP due to the smallness of λ_{12}. This can also be checked from the fact that the black dots in the plots in the first row of Fig. 4.8, appear uniformly scattered in the allowed regions. Consequently, the parameter space is extremely constrained by the combined effect of of the invisible Higgs width, indirect detection and (most notably) direct detection limits. Once all the bounds are included, only the points in the Higgs resonance and those with $m_{S_1} > 500$ GeV survive. Still, when these results are compared to the left panel of Figure 4.2, we observe a new (small) population of points at the Higgs resonance, with very small values of the coupling λ_1. This occurs when the masses of S_2 and S_1 are close enough so that coannihilation effects become important (first diagram of Fig. 4.3). Away from the resonance region, the coannihilation effect is irrelevant due to the small size of λ_{12} assumed here, so the correct relic density is obtained only for the usual value of λ_1, independently of how close m_{S_1} and m_{S_2} are.

As we increase the value of λ_{12}, new areas of the parameter space become available. In the middle row of Fig. 4.7, ($\lambda_{12} = 0.1$), we observe a region of black dots with masses $m_{S_1} \approx 100 - 200$ GeV and a very small λ_1 coupling. These points have the correct relic abundance thanks to coannihilation effects, which requires $m_{S_1} \sim m_{S_2}$. They can be observed in the second row of Fig. 4.8 as a thick line of black dots in that range of masses.

When $\lambda_{12} = 1$ (last row of Fig. 4.7), the effect of the DM annihilation in two Higgses, $S_1 S_1 \to hh$, exchanging S_2 in $t-$channel as in the last diagram of Fig. 4.3, becomes more remarkable, as soon as it is kinematically allowed, i.e. for $m_{S_1} \geq m_h$. This is the reason for the denser clouds of black dots out from the standard Higgs-portal thick line. For smaller values of m_{S_1} co-annihilation is still the main responsible for DM annihilation, thus requiring the S_1, S_2 masses to be closer. All this can be seen in Fig. 4.8. In the bottom panels of that figure we see that, for $m_{S_1} \leq m_h$, there is a thin "black line" made of points close to $m_{S_1} = m_{S_2}$. The short distance of this line to the perfect degeneracy shows the required closeness between m_{S_1} and m_{S_2} to produce the amount of co-annihilation that gives the observed relic density. Below that line co-annihilation is too strong, so there are only gray dots (too low relic density). For $m_{S_1} \geq m_h$ the line moves far away from $m_{S_1} = m_{S_2}$. As mentioned above, this behavior is due to the opening of the $S_1 S_1 \to hh$ process with both Higgses on-shell, which occurs via exchange of S_2 in $t-$channel (see Fig. 4.3). This process is very efficient, thus m_{S_2} has to get much larger to appropriately decrease its effect and keep the relic density at the right value. However, as m_{S_1} continues to increase, the black line again approaches $m_{S_2} \simeq m_{S_1}$. The reason is that the larger m_{S_1} the less efficient the annihilation process, an effect that must be compensated in the $t-$channel diagram by a larger λ_{12} or a smaller m_{S_2}; and the latter is the only possibility since we have set $\lambda_{12} = 1$ in the plot. This can be easily understood by considering the $t-$channel diagram as generating an effective vertex, $S_1^2 h^2$, with strength $\lambda_{\text{eff}} \propto \lambda_{12}^2 / m_{S_2}^2$. In the next section we will elaborate more on this aspect.

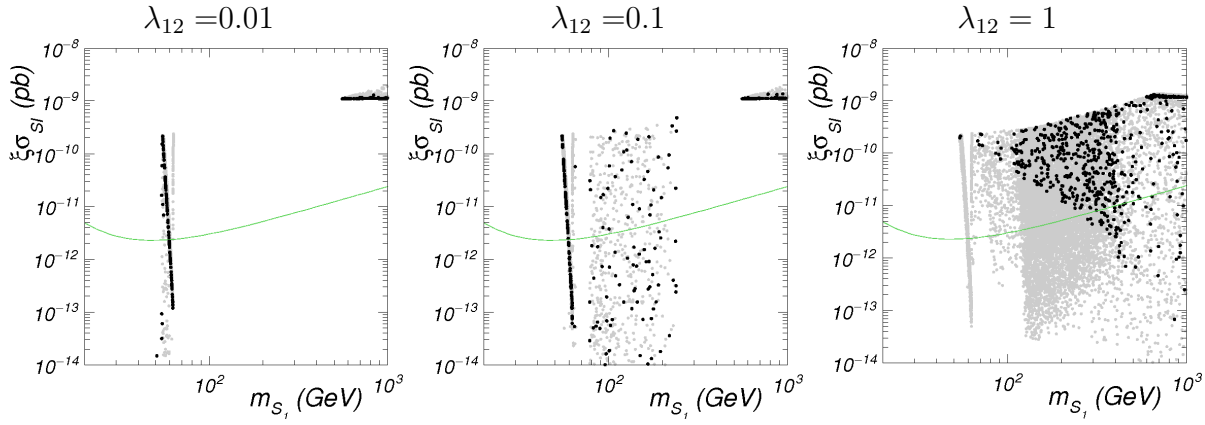

Figure 4.9: Spin-independent scattering cross section of S_1 with protons as a function of its mass in the ESHP model. From left to right, we have fixed $\lambda_{12} = 0.01, 0, 1$, and 1, respectively.

As in the case of the conventional SHP model, we expect future direct detection experiments (and in particular LZ) to be able to test large areas of the parameter space of our extended, ESHP, scenario. We represent in Fig. 4.9 the theoretical predictions for the elastic scattering cross section of S_1 with protons, after all experimental constraints are applied. We indicate by means of a green line the expected reach of LZ. As we can observe, although a large area of the parameter space might be probed by these searches, there is a substantial region for which the predictions are beyond LZ sensitivity. For $\lambda_{12} = 0.1 - 1$, this is possible for a range of DM masses between 100 GeV and 1 TeV (besides the usual narrow region at the Higgs resonance for $m_{S_1} \simeq m_h/2$), while satisfying the constraint on the relic abundance. None of these points can be probed by indirect detection either.

We should stress at this point that the solution put forward in this article is not unique. For example, using the same field content as the ESHP defined by equation (4.2), one could have constructed a secluded dark matter scenario in the same spirit as in Ref.[228], where the singlet S_1 only annihilates into a pair of semistable S_2 (which subsequently decay into SM particles). This would require a different choice of Z_2 charges, such that the terms $S_1^3 S_2$, $S_1 S_2^3$, and $S_1 S_2$ are forbidden.

4.4 Effective-theory description

As we have seen in the previous sections, the presence of the second particle, S_2, in the dark sector can enable the efficient annihilation of the DM particle, S_1, even if the usual quartic coupling of the latter, $\lambda_1 S_1^2 |H|^2$, is small enough to evade direct and indirect detection constraints.

Since $m_{S_2} > m_{S_1}$, one can wonder whether S_2 might be integrated-out. Then, one would be left with a usual Higgs-portal scenario with just one particle, S_1, plus some higher-order operators, involving S_1 and H. If this procedure is sound, these additional operators should be "clever" enough to mimic the effects of the heavy particle, S_2. Actually, the possibility of opening the allowed parameter-space of the Higgs-portal by adding new operators in the spirit of an effective field theory (EFT) has been considered in refs. [210, 211]. In our case, the coefficients of the EFT expansion are not completely independent, since they are determined by the ultraviolet (UV) completion, i.e., the Lagrangian of Eq. (4.2). As we are about to see, this produces a quite special EFT, which is indeed very efficient in rescuing the excluded regions of the usual Higgs-portal for singlet scalar DM. Without the knowledge of the UV completion, such EFT could be seen as designed ad hoc for that purpose.

In fact, it is not always possible to mimic the effects of S_2 by integrating it out in some approximation. In particular, when $m_{S_2} \simeq m_{S_1}$, such integration is not appropriate. Consequently, the EFT description is not suitable to describe the regions of the parameter space where co-annihilation effects are dominant, e.g., for $\lambda_{12} \lesssim 0.1$, see Figs. 4.7 and 4.8. However, there are other regimes in which S_2 is substantially (though not enormously) heavier than S_1, see for example Fig. 4.5 and the bottom row of Fig. 4.8. In those cases the EFT captures, at least qualitatively, the relevant physics.

Once S_2 is integrated out at tree-level from Eq. (4.2), the relevant new terms in the effective Lagrangian are

$$\Delta\mathcal{L}_{\text{eff}}(S_1, H) = \frac{1}{2}\frac{\lambda_{12}^2}{m_{S_2}^2}\, S_1^2 \left(|H|^2 - \frac{v^2}{2}\right)^2 + \cdots . \tag{4.5}$$

Of course, this operator arises from the third tree-level diagram in Fig. 4.3, with S_2 exchanged in $t-$channel. Here the dots stand for higher order terms in S_1 or H. An important property of $\Delta\mathcal{L}_{\text{eff}}$ is that, after EW breaking, the operator (4.5) has the form $\frac{1}{4}S_1^2(h^2+2vh)^2$, triggering a contribution to the $S_1^2h^2$ quartic coupling, without generating new cubic couplings, S_1^2h (as a usual quartic coupling does). This is extremely useful to enhance the S_1 annihilation without contributing to direct-detection processes or to the Higgs invisible-width (if S_1 is light enough).

Fig. 4.10 shows the performance of this Higgs-portal scenario with the presence of such extra operator, which we have parametrized as

$$\mathcal{L}_{\text{SHP}}^{'} = \mathcal{L}_{\text{SHP}} + \frac{1}{2}\frac{\lambda'}{(500\ \text{GeV})^2}\, S^2 \left(|H|^2 - \frac{v^2}{2}\right)^2 , \tag{4.6}$$

where $\mathcal{L}_{\text{SHP}}$ is the SHP Lagrangian, defined in equation (4.1), $\lambda' = \lambda_{12}^2(500\ \text{GeV}/m_{S_2})^2$ and to compare with the conventional SHP we have changed the notation and the dark matter candidate is called S. The lines shown in the $\{\lambda_S,\, m_S\}$ plane correspond to the correct relic

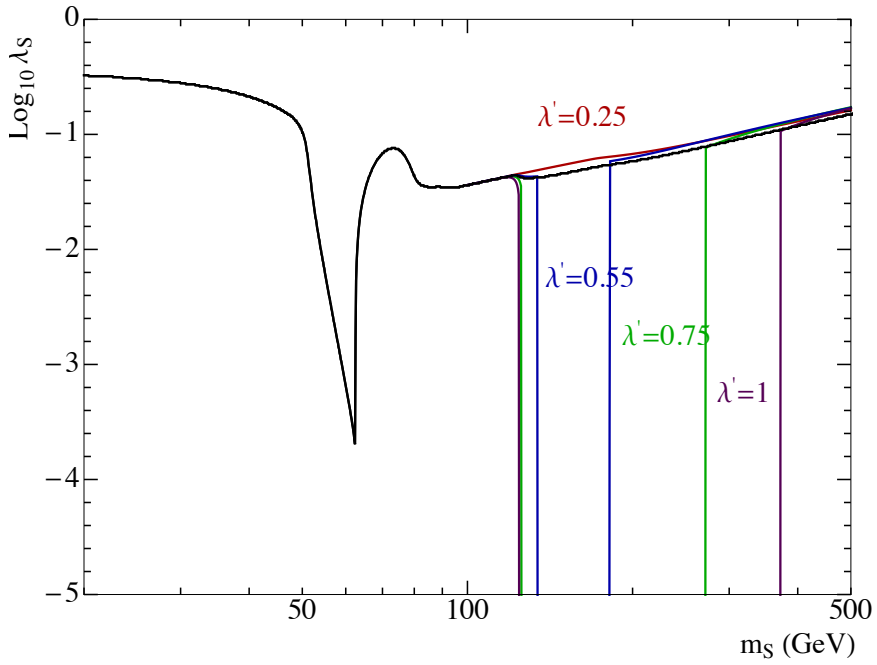

Figure 4.10: Contour lines of the correct relic DM abundance in an SHP effective theory consisting of the usual SHP Lagrangian plus an extra operator, as given in Eq. (4.6), for several values of the λ' coupling. This effective theory describes the ESHP in large regions of the parameter space.

abundance for different values of the effective coupling λ'. As we can observe, the contribution from the effective operator is triggered when the annihilation channel into a pair of Higgs bosons gets kinematically allowed. Then, for each value of λ' there are essentially two values of m_S for which this channel annihilates the required amount of dark matter (the lower one is not too far from the kinematic threshold, where the suppression due to the phase space is relevant). At those points, the value of λ_S becomes essentially irrelevant, For m_S beyond the higher of those two values, the effective operator becomes less efficient and eventually we recover the original SHP behaviour (black thick line). If we demand that $\lambda' < 1$, then the contribution from the effective operator is important for DM masses between 126 GeV and approximately 500 GeV. In this range of masses, the usual quartic coupling λ_S can be very small, thus helping to evade direct-detection limits.

In other words, in this region of DM masses, for any value of the λ_S coupling, there exists a value of λ' that allows to recover the correct relic density. Since $\lambda' = \lambda_{12}^2(500\ \text{GeV}/m_{S_2})^2$, there are many combinations of the two underlying parameters of the UV theory, $\{\lambda_{12}, m_{S_2}\}$, leading to the correct result. These findings are in good agreement with the results presented in the previous section (Fig. 4.7), in particular with those for large λ_{12} in the region of m_{S_1},

where the co-annihilation effects are not dominant.

4.5 Applying the ESHP to the Galactic Center Excess

The region around the Galactic Center (GC) is one of the richest in the gamma-ray sky. The Large Area Telescope (LAT) [254] onboard the *Fermi* satellite has revealed the γ-ray sky with unprecedented detail, and the measurements of gamma-rays coming from the GC have been studied thoroughly.

The emission measured by the LAT can be separated into different sources, most of which are point-like, and diffuse emission. The majority of diffuse gamma-ray emission comes from inelastic hadronic collisions, mostly through the decay of neutral pions. This component is produced in interactions of cosmic ray nuclei with interstellar gas. Another interstellar-emission component comes from the inverse Compton (IC) scattering of leptonic cosmic rays interacting with interstellar radiation field (ISRF). The ISRF consists basically of three components: starlight, infrared light emitted by dust, and the CMB radiation. The IC contribution is expected to be less structured compared to the hadronic component. On the other hand, at energies ≤ 10 GeV, bremsstrahlung emission from electrons and positrons interacting with interstellar gas can become important. Additionally, there is a diffuse emission component with approximately isotropic intensity over the sky. It is made of residual contamination from interactions of charged particles in the LAT (misclassified as gamma rays), unresolved extragalactic sources, and, possibly, truly diffuse extragalactic gamma-ray emission. Including a template compatible with the predictions of DM annihilating into SM particles, following a slightly contracted Navarro-Frenk-White (NFW) profile, substantially improves the description of the data. The emission assigned to this extra template is the so-called Galactic Center excess (GCE) [115, 167–170, 172, 173, 255–258]. In Ref [115], the Fermi-LAT collaboration modeled all these contributions, as shown in Fig. 4.11.

In this section we examine the capability of the ESHP model of DM to account for the CGE through the corresponding annihilations. We will work using the effective description model given in Sec. 4.4.

4.5.1 The Galactic Center Excess

In the recent analysis of ref. [259], to study the GCE a representative set of models from ref. [260] was taken into account, along with different lists of detected point sources. The bottom line is that there remains a GCE emission, now peaked at the ~ 3 GeV region, i.e. slightly shifted towards higher energies with respect to previous studies. In this section we will consider the GCE emission obtained by using the so-called Sample Model (light blue points in Fig. 4.12, see Sec. 2.2 of ref. [259] for details on the model) and a combination of

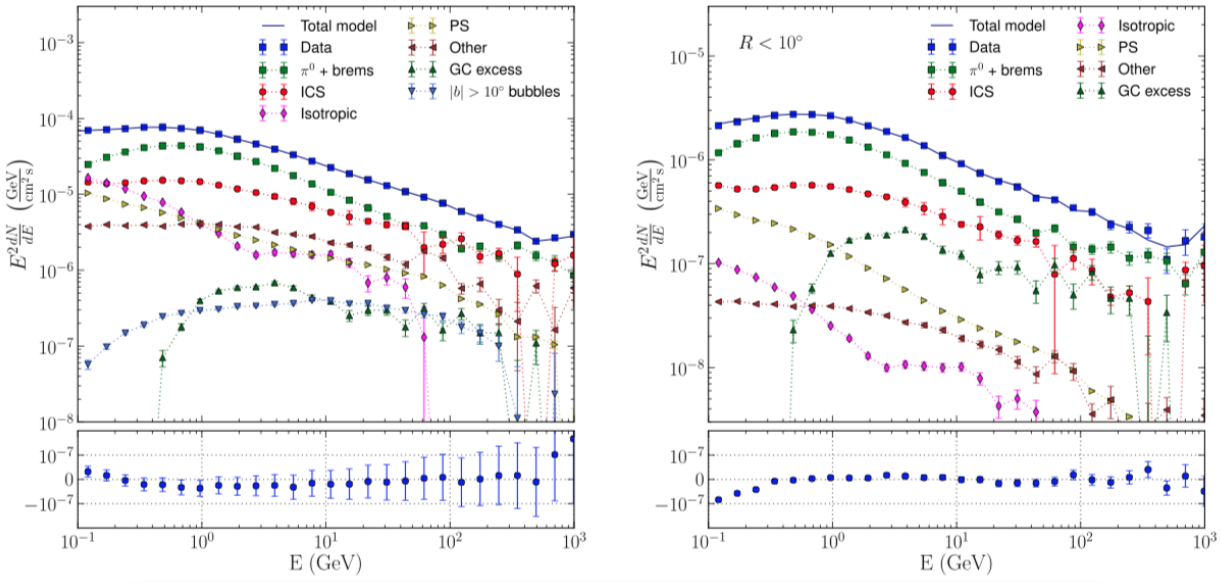

Figure 4.11: Modeling of the different components of the gamma-ray emission from the GC. Some templates are summed together in several groups for presentation. "π_0 + brems" includes the hadronic and bremsstrahlung components. "ICS" includes the three IC templates corresponding to the three radiation fields. 'Other" includes Loop I, Sun, Moon, and extended sources. GC excess is modeled by the gNFW template with index γ=1.25. Left: flux of the components integrated over the whole sky except for the PS mask. Right: flux of the components integrated inside 10^o radius from the GC; the model is the same as in the left panel, with the only difference being the area of integration for the flux. The bubbles are not present in the right panel, since the Sample Model includes the bubble template defined at latitudes $|b| < 10^o$. The pictures are extracted from ref. [115].

the covariance matrices derived in ref. [261] in order to perform the fits.

The nature of the GCE is under debate. Apart from the DM hypothesis, it has been proposed that the GCE can be due to collective emission of a population of point sources too dim to be detected individually [262–268], or the result of fresh cosmic-ray particles injected in the Galactic Center region interacting with the ambient gas or radiation fields, see for instance ref. [269, 270]. Indeed, some studies favour a point-source population as explanation to the GCE emission [271–274], however further investigations on the data are required, since the GCE could be the result of a combination of phenomena at work in the inner Galaxy, including DM annihilation [275]. On the other hand, the GCE may well have different origins below and above $\sim$ 10 GeV [259, 276]. The high energy tail ($E > 10$ GeV) could be due to the extension of the *Fermi* bubbles observed at higher latitudes [259] or some mismodeling of the interstellar radiation fields and a putative high-energy electron population [270]. At lower

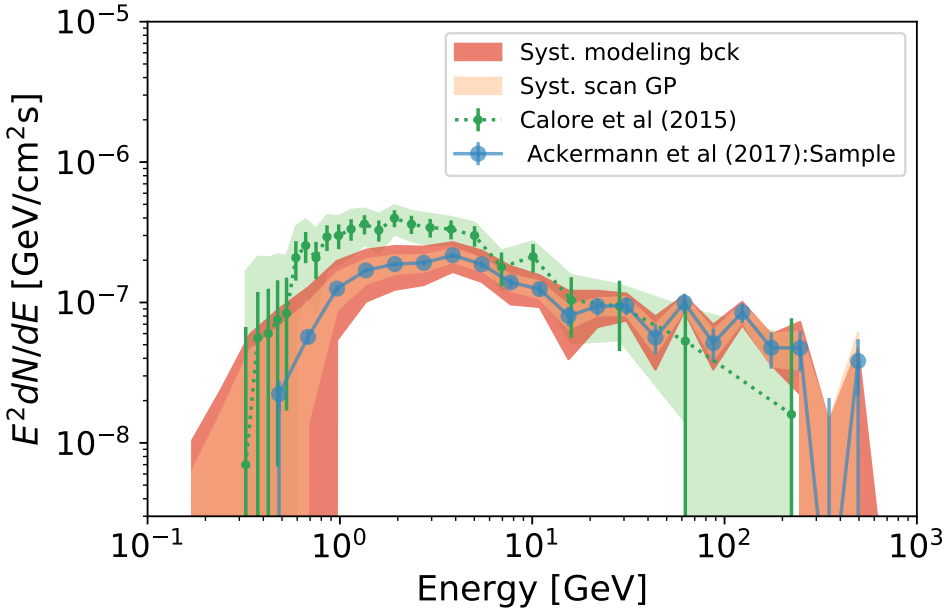

Figure 4.12: Blue points: GCE spectrum from ref. [259] using the Sample model, see the reference for more info. The light orange band represents the diagonal of the covariance matrix due to excesses along the Galactic Plane, obtained using the same procedure as for the GCE [261]. The dark orange band is the diagonal of the covariance matrix from variations in the GCE due to uncertainties in modelling diffuse emission from ref. [259]. For comparison we include the green points and shadow green area, obtained in the analysis of ref. [256].

energies ($E < 10$ GeV) the GCE might be due to DM annihilation, unresolved millisecond pulsars (MSP), or a combination of both, see for instance refs. [261, 275]. According to ref. [259], the interpretation of the GCE as a signal for DM annihilation is not robust, but is not excluded either. Actually, it has been claimed in refs. [277–279] that a population of γ-ray pulsars cannot be responsible for the entire GCE emission.

On the other side, the interpretation of the GCE as originated by DM (with or without an astrophysical source for the high energy tail) is not straightforward, particularly in theoretically-sound models (see, for instance, Refs. [181, 187, 209, 227, 280–298]). The most common difficulty is that a DM model able to reproduce the GCE also leads to predictions on DM direct detection which are already excluded by present experiments. The PICO-60 [299] (spin dependent cross-section) and XENON1T [300] (spin-independent cross-section) experiments provide the most stringent direct detection bounds, so far. Of course, things change for better if only a fraction of the low-energy GCE is associated to DM annihilation. For

example, in the recent paper [261] it is shown that supersymmetric DM could be well responsible of $\sim 40\%$ of the low-energy ($E < 10$ GeV) GCE emission. However, fitting the whole low-energy GCE just with DM emission is more challenging.

4.5.2 Fitting the Galactic-Center Excess in the ESHP model

We will assume the GCE is originated by two different sources: an astrophysical one plus the emission from DM annihilation,

$$\Phi_{\rm tot} = \Phi_{\rm astrophysical} + \Phi_{\rm DM}. \tag{4.7}$$

Concerning the astrophysical component, following the morphological studies in ref. [259], a sensible hypothesis is that it is a continuation to lower Galactic latitudes of the *Fermi* bubbles. Above 10° in Galactic latitude the spectral shape of the *Fermi* bubbles is well characterized by a power law, with index 1.9 ± 0.2, times an exponential cutoff, with cutoff energy 110 ± 50 GeV [301]. We assume the same modeling for the astrophysical component:

$$\Phi_{\rm astrophysical} = N\ E^{-\alpha} e^{E/E_{\rm cut}}. \tag{4.8}$$

We leave α as a free parameter to test if we can recover the known *Fermi*-bubble spectral index above 10° in Galactic latitude.

Regarding the DM part, we assume the S particles of the ESHP model acting as DM, and compute the corresponding emission spectrum in the ESHP parameter space, $\{\lambda_S, \lambda', m_S\}$ using MicrOmegas 4.3.2 [242]. Since the main annihilation channel is the one depicted in the central panel of Fig. 4.3 with $i, j = 1$, i.e. $SS \to hh$, most of the photons come from the subsequent decay of the Higgs-bosons into $b\bar{b}$, but there are other contributions coming from $h \to WW$ and even $h \to \gamma\gamma$ (the latter gives an interesting spectral feature, as we will see below). The prompt Galactic Center flux coming from DM annihilations, $\Phi_{\rm DM}$, is proportional to this spectrum times the so-called $J-$factor

$$J_{10^0} = \int_{\Delta\Omega} d\Omega \int_{\rm l.o.s.} ds \rho^2(r(s,\theta))\ , \tag{4.9}$$

where ρ is the DM density, r is the spherical distance from the Galactic Center, θ is the observational angle towards the GC and s is the line of sight (l.o.s.) variable. As usual, we assume a NFW profile

$$\rho(r) = \rho_s \left(\frac{r}{r_s}\right)^{-\gamma} \left(1 + \frac{r}{r_s}\right)^{-3+\gamma}\ , \tag{4.10}$$

where r_s is the scale radius (20 kpc), ρ_s a scale density fixed by requiring the local DM density at the 8.5 kpc Galactocentric radius to be 0.4 GeV cm^{-3}; and $\gamma = 1.25 \pm 0.8$, as given in ref. [259].

In summary, the fit contains 6 independent parameters: $\{N, \alpha, E_{\rm cut}\}$ (astrophysical part) and $\{\lambda_S, \lambda', m_S\}$[5] (DM part). In order to assess the quality of a fit we construct the χ^2-function:

$$\chi^2 = \sum_{i,j} (\Phi_i^{\rm obs} - \Phi_i^{\rm m}) \hat{\Sigma}^{-1}_{i,j} (\Phi_j^{\rm obs} - \Phi_j^{\rm m}). \tag{4.11}$$

Here i labels the energy-bin, $\Phi_i^{\rm m}$ is the flux for a model (m), defined by the values of the above six parameters, $\Phi_i^{\rm obs}$ is the derived flux with the Sample model, the light blue points in Fig. 4.12, and $\hat{\Sigma}^{-1}_{i,j}$ is the inverse of the covariance matrix, which was derived in ref. [275]. Note that the derived information on the GCE spectrum in ref. [259] is enclosed in $\{\Phi_i^{\rm obs}, \hat{\Sigma}^{-1}_{i,j}\}$. Since the functions used to fit the GCE are not linear, we cannot use the reduced χ^2 to compute $p-$values[6]. Instead, following ref. [275], we will proceed in this way:

1. For each point under consideration in the ESHP parameter-space (defined by $\{\lambda_S, \lambda', m_S\}$), we allow the astrophysical parameters, $\{N, \alpha, E_{\rm cut}\}$ to vary, in order to find the best fit to the data. This gives $\Phi^{\rm m}_{\rm best}$.
2. Create a set of 10^7 pseudo-random (mock) data normal-distributed with mean at $\Phi^{\rm m}_{\rm best}$, according to $\hat{\Sigma}_{i,j}$
3. Compute χ^2 for each data created in step 2.
4. Create a χ^2 distribution using the values from step 3.
5. The integrated χ^2 distribution up to the best-fit-χ^2 to the actual data, gives the $p-$value of the model.

It turns out that the shape of the χ^2 distribution is extraordinarily stable through the whole parameter space, so it can be settled once and for all, with a consequent saving of computation time. The χ^2 distribution is illustrated in Fig. 4.14 below.

In addition to the fit of the GCE data, we require that every point is not constrained by other DM detection observables like the spin-independent cross-section from the XENON1T experiment [300] and the thermal averaged annihilation cross section from the search of DM in dwarf spheroidal satellite galaxies of the Milky Way (dSphs) by the *Fermi*-LAT experiment [177].

The spin-independent cross section is evaluated analytically as in the previous sections (see Eq. 4.4 in Subsec. 4.2.2). In this section we impose the strongest results on spin-independent cross section, given by XENON1T.

[5] These are the parameters which define the ESHP model in its effective description given in Eq. 4.6

[6] For a detailed discussion see ref [302].

Concerning constraints from dSphs, we use gamLike 1.1 [303], a package designed for the evaluation of likelihoods for γ-ray searches which is based on the combined analysis of 15 dSphs using 6 years of *Fermi*-LAT data, processed with the pass-8 event-level analysis. For any point in the parameter space we scale the photon flux by the ξ^2 factor, with $\xi \equiv \Omega_S/\Omega_{CDM}$. GamLike provides a combined likelihood, with which we perform the test statistic [304]

$$TS = -2\ln(\mathcal{L}(\mu, \theta \mid D)/\mathcal{L}(\mu_0, \theta \mid D)) \,, \tag{4.12}$$

where μ denotes the parameters of the DM model, μ_0 corresponds to no-annihilating DM, θ are the nuisance parameters used in the *Fermi*-LAT analysis [177], and D is the γ-ray data set . To find a 90% upper limit on the DM annihilation cross-section we look for changes in $TS = 2.706$.

4.5.3 Results

Despite having just three parameters, $\{\lambda_S, \lambda', m_S\}$, the effective interpretation of the ESHP model has regions of the parameter space that could be contributing significantly to the GCE without conflicting with other observables. In fact, this holds even if one of the parameters, λ_S (the initial $S^2|H|^2$ coupling in the ordinary SHP model) is set to zero, since the $\lambda'-$coupling is enough to lead to sufficient DM annihilation to reproduce the correct relic density, without conflicting with direct-detection, as explained in Sec. 4.4. Then, the ESHP model may work with just two parameters, as the standard SHP. A representative point in the ESHP parameter space, not rejected as a possible explanation of a significant fraction of the GCE is illustrated in Fig. 4.13, which corresponds to the following values of the parameters:

$$\begin{aligned} &m_S = 131 \text{ GeV}, \quad \lambda_S = 0, \quad \lambda' = 0.58, \\ &\alpha = 1.5, \quad E_{\text{cut}} = 178 \text{ GeV} \,. \end{aligned} \tag{4.13}$$

Note that the λ_S coupling is set to zero, so the value of λ' is simply the required one to reproduce the correct relic density. The astrophysical exponent, α, becomes close to the estimations from the *Fermi*-bubble emission at high latitudes, $\alpha \simeq 1.9$.[7] The fit is quite good, with $p-$value=0.63 (coresponding to a $\chi^2 = 27.8$ for the 27 energy-bins). As mentioned in the previous section, this $p-$value is obtained from the associated χ^2 distribution, which for this particular point is shown in Fig. 4.14.

Fig. 4.13 also shows an amusing peculiarity. Namely, the $h \to \gamma\gamma$ decay contributes very little to the total flux, it is but located around a typical energy $E \simeq m_S/2 \simeq 65$ GeV. This

[7] Fixing α in the fitting procedure at the value preferred by the *Fermi*-bubble analysis, $\alpha = 1.9$, is also possible. Then typically, less flux from DM annihilation is required at low-energy and, consequently, the favoured values of the $\lambda'-$coupling are somewhat smaller.

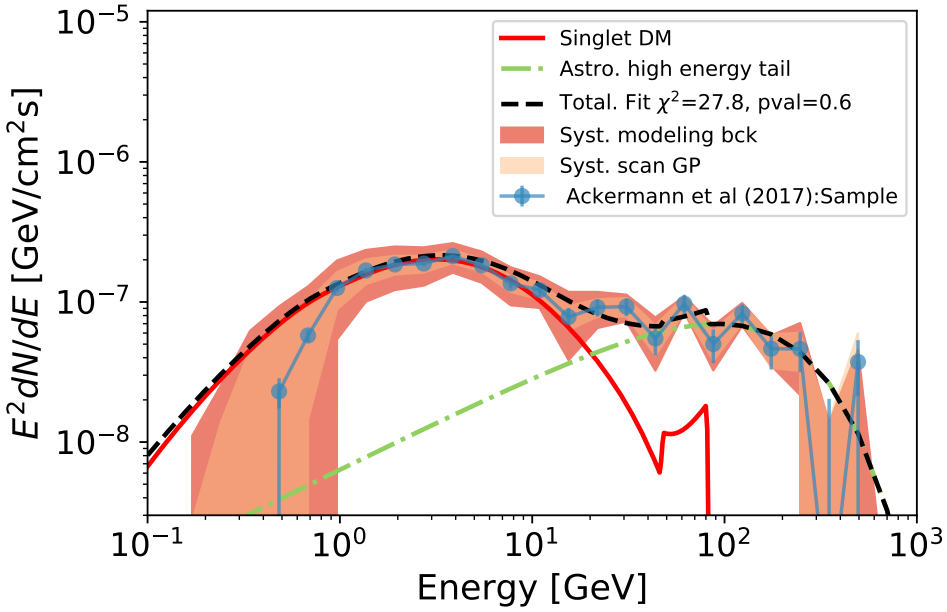

Figure 4.13: Fit to the GCE spectrum (blue dots of Fig. 4.12) by the combination of a power-law with an exponential cutoff, describing the astrophysical sources (green dash-dotted line), plus the contribution of DM annihilation, as given by the ESHP model (red line); with parameters given in Eq. (4.13). See eqs. (4.7-4.10) for further details. The black dashed line gives the final prediction of the model.

corresponds to a visible feature in the red line, which produces a bump in the total flux in a bin where data show a peak as well. The feature, however, is spread over the $\sim 40-80$ GeV range since the Higgs giving the two photons has a non-vanishing momentum. Consequently, the usual *Fermi*-LAT contraints on γ-lines are not applicable here. In addition, the total flux coming from this process is below the present limits on lines at $\sim$ 65 GeV [244]. So, even if it were concentrated at that energy it would be non-detectable yet. Nevertheless, it is not unthinkable that a future dedicated search could be sensitive to this feature.

Fig. 4.15 shows the $p-$value in the $\{m_S, \lambda_S\}$ plane, where λ' is adjusted for each point in order to reproduce the correct relic density. The XENON1T bound is also shown. As expected, it only gives restrictions when λ_S is sizeable, which is not necessary. The constraints from dSphs do not appear, as they do not give any constraint. Obviously, for small λ_S the plot lacks structure in the vertical axis.

Fig. 4.16 (left panel) is an equivalent plot where λ_S has been set to zero, so that $\{m_S, \lambda'\}$ are the only relevant parameters. Now, the value of the relic density depends on the point. The lower black curve corresponds to the Planck relic-density, hence it coincides

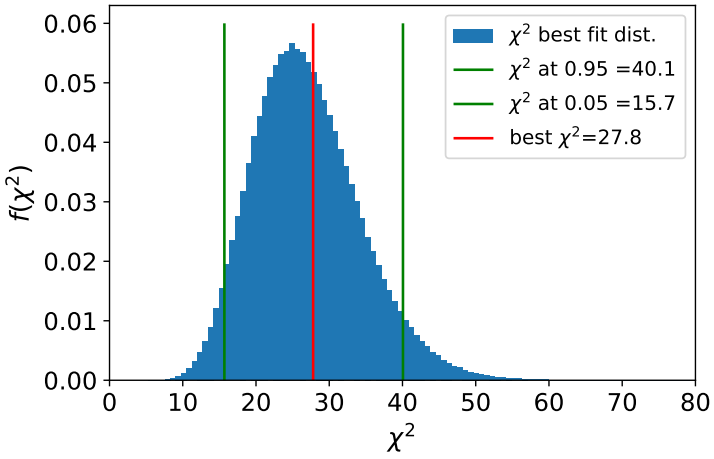

Figure 4.14: The blue histogram represents the distribution of χ^2 drawn from the best fit to the GCE spectrum in Fig. 4.13, green vertical lines correspond to upper and lowers limits at 5%. The red vertical line represents the best fit model in Fig.4.13.

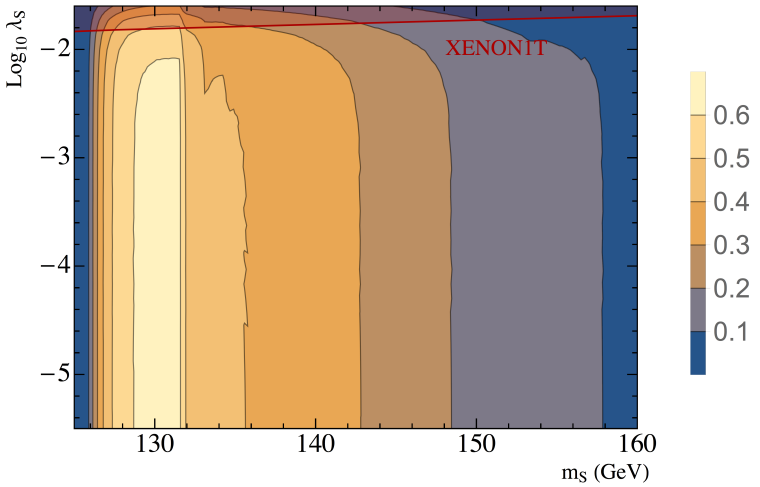

Figure 4.15: Contours of constant $p-$value in the $\{m_S, \lambda_S\}$ plane in the context of the ESHP model. The value of λ' is adjusted at each point in order to reproduce the correct relic density. The XENON1T direct-detection bound is shown (red line). For small λ_S the plot lacks structure in the vertical axis.

with the horizontal bottom line of Fig. 4.15. Below that curve the relic density is too high. The upper black curve corresponds to half of the relic density. Interestingly, models in the parameter space that reproduce the whole dark matter relic density with S particles are the

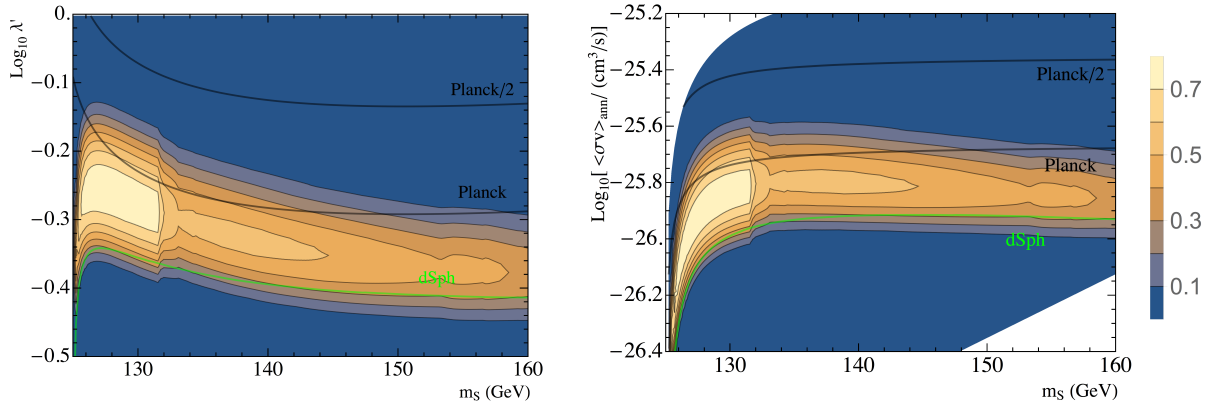

Figure 4.16: Contours of constant $p-$value in the $\{m_S, \lambda'\}$ plane (left panel) and the $\{m_S, \langle\sigma_{\rm ann} v\rangle\}$ plane (right panel), setting $\lambda_S = 0$. Now, the value of the relic density depends on the point, increasing in the downward direction. The lower (upper) black curve corresponds to (half of) the Planck relic-density. The green curve shows the lower bound on λ' from dwarf spheroidal observations.

ones with higher $p-$values. Indeed, the regions with an optimal fit of the GCE present a (slightly) too-large relic density, implying that the points along the "Planck"-line tend to produce (slightly) less GC flux than required (recall here that the annihilation cross section of dark matter increases as $(\lambda')^2$, while the J-factor goes as $\rho^2_{\rm DM} \sim (\lambda')^{-4}$). In consequence, the possibility commented in Subsec. 4.5.1 that only a fraction of the low-energy GCE is associated to DM annihilation is still the most advantageous one. However, in this scenario that fraction is remarkably close to the whole GCE.

The green curve gives the lower bound on λ' from dwarf observations, taking into account the previosly mentioned ξ^2 factor. Clearly, dSphs limits do not impose any constraint in practice. Actually, it is apparent that the green curve corresponds to $\xi > 1$. Therefore, assuming that in that region of the parameter space the relic density is the observed one (thanks to some unspecified mechanism), as it is sometimes done, then the dSphs limit becomes even weaker.

Fig. 4.16 (right panel) is the equivalent plot in the $\{m_S, \langle\sigma_{\rm ann} v\rangle\}$ plane.

To conclude this chapter, let us mention that we have studied the simplest extension of the singlet-scalar Higgs portal, consisting of the addition of an extra scalar to the model. This extension, that we call ESHP, despite its simplicity, is able to considerably relax the strong constraints affecting the Higgs portal model. Besides, the extended model is able to fit quite well the galactic center excess.

Chapter 5

Z' Portal. Minimal leptophobic anomaly free Z' model

In this chapter we consider an alternative candidate for a mediator of the DM, namely an extra vector boson. The main possibility in the SM is the Z boson, although, as we commented in Sec. 2.2 the $Z-$portal model is very constrained by experimental searches [79].

The existence of extra symmetries from the SM gauge group would imply the existence of an extra vector boson mediator, usually called Z'. Different options for this kind of mediator have been studied extensively in the literature [305–326], as they represent a very plausible scenario of BSM physics, e.g. in the context of GUT or string models. This chapter is focussed on this kind of models.

Usually, the analyses of these models have been done in the framework of the so called simplified DM models (SDMM), where the DM particle and the Z' mediator are the only extra fields. Still, there is a non-trivial parameter space, essentially given by the $Z'-$mass, its coupling to the DM particle, and the various couplings to the SM fields. Some of the most important constraints on that parameter space come from DD experiments [314, 320] and from di-lepton production at the LHC [317, 320]. These constraints are highly alleviated if the coupling of the Z' with DM is of the axial type, and if the Z' has leptophobic couplings to the SM particles, respectively.

On the other hand, as stressed in several articles [307, 309, 310, 314–317, 321, 327], simplified DM models are "too simple" concerning unitarity, gauge invariance and anomaly cancellation. In fact, the Z's in SDMM are typically anomalous. Then, in order to cancel the anomalies, additional fermions (besides the DM one) are mandatory. The authors of ref. [307, 309, 310, 314–316, 321, 327] performed a systematic search of (anomaly-free) Z' extensions either with axial DM-coupling or with leptophobia (or, equivalently, completions of gauged baryon number). In this chapter we follow a similar spirit, obtaining new general

results on this type of consistent Z' extensions. We will assume throughout the chapter that the DM particle is a Dirac fermion, χ, neutral under all the SM gauge symmetries. Then, we will determine the possible scenarios where the Z' is simultaneously leptophobic and with axial DM coupling. There are very few scenarios of that kind with a minimal dark spectrum. Finally, we study the phenomenology of these models, and discuss how they can be experimentally tested.

The results of this chapter have been published in [328].

5.1 Anomaly-free leptophobic Z's

It is easy to see that a consistent leptophobic $U(1)_{Y'}$ group, where leptons have vanishing $Y'-$charge, must be equivalent to baryonic number, $U(1)_B$, in the SM sector. The invariance of the leptonic Yukawa couplings,

$$y_i^e \bar{L}_i H e_i, \tag{5.1}$$

(where y_i are the Yukawa coupling constants, with i a family index in an obvious notation) requires the $Y'-$charge of the Higgs to vanish, $Y'_H = 0$. Then, invariance of the hadronic Yukawa couplings

$$y_{ij}^u \bar{Q}_i \bar{H} u_j, \qquad y_{ij}^d \bar{Q}_i H d_j \tag{5.2}$$

requires $Y'_Q = Y'_u = Y'_d$, which is equivalent to $U(1)_B$. So, in the following we will assume $U(1)_{Y'} \equiv U(1)_B$ in the SM sector, and therefore $Y' = 1/3$ for all quarks. Note that this is a completely generic result for any UV completion of the SM with a leptophobic, flavour-blind, $U(1)_{Y'}$ group.

A consequence of the previous result is that a (leptophobic) Z' couples to quarks in a purely vectorial way. This has important implications, especially for DD experiments. Namely, if the Z' couples also in a vectorial way to DM, then the effective operator for DD is spin-independent with no velocity-supression. Hence the model would be under extreme pressure from DD bounds as it has been shown for instance in Ref. [317, 320]. On the other hand, if the Z' coupling to DM is axial, then the effective DD operator is both spin-dependent and velocity-suppressed, so the model is safe from DD bounds. We will come back to this point in Sec. 5.3. Next, we examine further conditions imposed by the requirement of leptophobia.

Since $U(1)_{Y'} \equiv U(1)_B$ for the SM fields, there are two anomalies[1] which are not vanishing just within the SM sector, and thus require extra stuff: $SU(2)_L^2 \times U(1)_{Y'}$ and $U(1)_Y^2 \times U(1)_{Y'}$. The first one requires the presence of non-trivial representations under $SU(2)_L$. Since by assumption, the DM particle, χ, is a SM singlet, the most economical

[1] Previous systematic studies on anomaly cancellation conditions for $U(1)_B$ extensions have been performed in refs. [307, 310, 314–316, 329–338]).

extension is to add two $SU(2)_L$ doublets, ψ_L, ψ_R (the need of at least two of such doublets is obliged e.g. by the cancellation of Witten's $SU(2)$ global anomaly). The cancellation of the anomaly requires

$$SU(2)_L^2 \times U(1)_{Y'} \text{ anomaly} \longrightarrow Y'_{\psi_L} - Y'_{\psi_R} = -3. \tag{5.3}$$

Then, it is straightforward to check that the cancellation of the $U(1)_Y^2 \times U(1)_{Y'}$ anomaly demands extra particles. Otherwise, such cancellation would require[2] $Y_{\psi_L}^2 Y'_{\psi_L} - Y_{\psi_R}^2 Y'_{\psi_R} = 3/4$. In addition, the vanishing of the $U(1)_Y^3$ anomaly would impose $Y_{\psi_L} = Y_{\psi_R}$. These two conditions, together with Eq. (5.3), lead to $Y_{\psi_L}^2 = -1/4$, with no solution. In consequence, we need to add at least one extra singlet fermion, η, to the dark sector. In other words, the minimal dark sector for a leptophobic Z' is:

$$\text{minimal dark sector}: \quad \{\chi_{L,R},\ \psi_{L,R},\ \eta_{L,R}\}, \tag{5.4}$$

where χ is a SM singlet (and the DM particle), ψ is a $SU(2)_L$ doublet (and color singlet), and η is $SU(2)_L$ and color singlet.

Next, we re-examine the conditions imposed on the charges of the dark sector by the cancellation of the various anomalies:

$$SU(2)_L^2 \times U(1)_{Y'} \text{ anomaly} \longrightarrow Y'_{\psi_R} = 3 + Y'_{\psi_L}, \tag{5.5}$$

$$SU(2)_L^2 \times U(1)_{Y} \text{ anomaly} \longrightarrow Y_{\psi_L} = Y_{\psi_R} \equiv Y_\psi, \tag{5.6}$$

$$U(1)_Y^3 \text{ and } U(1)_Y \text{ anomalies} \longrightarrow Y_{\eta_L} = Y_{\eta_R} \equiv Y_\eta, \tag{5.7}$$

$$U(1)_Y^2 \times U(1)_{Y'} \text{ anomaly} \longrightarrow Y_\eta^2 (Y'_{\eta_L} - Y'_{\eta_R}) = \frac{3}{2} + 6Y_\psi^2, \tag{5.8}$$

$$U(1)_{Y'}^2 \times U(1)_{Y} \text{ anomaly} \longrightarrow 2Y_\psi ({Y'_{\psi_L}}^2 - {Y'_{\psi_R}}^2) = -Y_\eta ({Y'_{\eta_L}}^2 - {Y'_{\eta_R}}^2), \tag{5.9}$$

$$U(1)_{Y'} \text{ anomaly} \longrightarrow (Y'_{\chi_L} + Y'_{\eta_L}) - (Y'_{\chi_R} + Y'_{\eta_R}) = 6, \tag{5.10}$$

$$U(1)_{Y'}^3 \text{ anomaly} \longrightarrow ({Y'_{\chi_L}}^3 + {Y'_{\eta_L}}^3 + 2{Y'_{\psi_L}}^3) - ({Y'_{\chi_R}}^3 + {Y'_{\eta_R}}^3 + 2{Y'_{\psi_R}}^3) = 0. \tag{5.11}$$

Eqs. (5.5-5.10) can be solved analytically in a straightforward way, leaving $\{Y_\psi, Y_\eta, Y'_{\psi_R}, Y'_{\chi_R}\}$ as the remaining unknowns. Furthermore, Y_ψ and Y_η are chosen so that the corresponding electric charges are integer, to avoid cosmological disasters. This requires them to be $m+1/2$ and n respectively, with m, n integers. Then for each choice of $\{Y_\psi, Y_\eta\}$, there is a continuum of consistent values of $\{Y'_{\psi_R}, Y'_{\chi_R}\}$, although only two (or one in some cases) out of them present axial coupling of the Z' to the DM particle, χ, i.e. $Y'_{\chi_L} = -Y'_{\chi_R}$ (for details and explicit expressions see Appendix B). Besides, only for four special choices of $\{Y_\psi, Y_\eta\}$, the

[2] We use a normalization of the hypercharge, so that it coincides with the electric charge for $SU(2)_L-$singlets.

axial solutions correspond to rational $Y'-$charges (which actually happen to be identical in the four cases), namely

$$\begin{aligned} \{Y_\psi, Y_\eta\} &= \left\{\pm\frac{1}{2}, \pm 1\right\}, \left\{\pm\frac{7}{2}, \pm 5\right\}, \\ \left\{Y'_{\psi_L}, Y'_{\psi_R}, Y'_{\eta_L}, Y'_{\eta_R}, Y'_{\chi_L}, Y'_{\chi_R}\right\} &= \left\{-\frac{3}{2}, \frac{3}{2}, \frac{3}{2}, -\frac{3}{2}, \frac{3}{2}, -\frac{3}{2}\right\}. \end{aligned} \tag{5.12}$$

In addition, recall that all quarks have $Y' = 1/3$, i.e. their baryon number.

5.2 Anomaly-free leptophobic Z', with axial coupling to DM

As mentioned in the previous section, the requirement of axial coupling of the Z' mediator to DM has been advocated to diminish the pressure of DD bounds on the viability of the scenario. For example, in Ref. [313], a Z' with axial couplings to both the SM fields and the DM particle, was considered. In this way the $Z'-$mediation leads to spin-dependent effective operators for DD, which are much less constrained. However, as we have seen, if the Z' is leptophobic (which is desirable), then the coupling to the SM fields is vectorial, since $U(1)_{Y'}$ is equivalent to baryonic number in the observable sector. Hence a leptophobic Z' with axial DM coupling leads to effective operators

$$\bar{q}\gamma_\mu q \ \bar{\chi}\gamma_5\gamma^\mu\chi, \tag{5.13}$$

where q is a generic quark. Such operators induce DD interactions that are not only spin-dependent, but also velocity-suppressed. Consequently DD virtually does not impose constraints on a generic leptophobic Z', axially coupled to DM. These are of course good news for this kind of scenario.

An interesting fact is that, assuming minimal DM sector, a leptophobic, DM-axial Z' has completely determined Y' charges for both SM and dark fields, as shown in Eq. (5.12). This means that a usual parameter in SDMM, namely the relative strength of the SM and the DM $Z'-$couplings, is not free anymore. Consequently, a future detection of the Z' mediator at the LHC would also test this scenario. To be more precise, the absolute value of the Y' charge of the DM particle, χ, is 4.5 times larger than that of quarks. Actually, this goes in the right direction to explain why such Z' has not been discovered yet (if it exists, of course): the smaller the couplings to the quarks, the more suppressed the Z' production at the LHC.

Another relevant point has to do with baryon number violation. Since the SM baryonic number is being promoted to an anomaly-free gauge symmetry, which is spontaneously broken (so that the Z' is massive), one should be concerned about baryon-number violation

constraints. The most important of those are proton decay and neutron-antineutron oscillations. Proton decay cannot take place in this context since it needs lepton-number violation as well. On the other hand, neutron-antineutron oscillations represent a violation of baryon number in two units. However, from Eq. (5.12), it is clear that the scalar field breaking $U(1)_{Y'}$, say S, must have $Y'_S = \pm 3$, in order to trigger masses for the dark fields. Consequently, it is not possible to build an effective operator able to mediate neutron-antineutron oscillations. Incidentally, this argument also applies to proton decay, which needs $\Delta B = -1$.

In order to explore further the phenomenology of leptophobic, DM-axial, Z's, we will focus on one of the four models of Eq. (5.12), namely the one where the dark sector contains the following $SU(2)_L \times U(1)_Y \times U(1)_{Y'}$ (fermionic) representations:

$$\begin{aligned}
&\chi_L \left(1, \quad 0, \quad \frac{3}{2} \right), \\
&\chi_R \left(1, \quad 0, \quad -\frac{3}{2} \right), \\
&\psi_L \left(2, \quad -\frac{1}{2}, \quad -\frac{3}{2} \right), \\
&\psi_R \left(2, \quad -\frac{1}{2}, \quad \frac{3}{2} \right), \\
&\eta_L \left(1, \quad -1, \quad \frac{3}{2} \right), \\
&\eta_R \left(1, \quad -1, \quad -\frac{3}{2} \right).
\end{aligned} \tag{5.14}$$

In addition, the dark sector contains a complex scalar, S, with quantum numbers

$$S \left(1, \quad 0, \quad -3 \right). \tag{5.15}$$

All the previous fields are color singlets. In the SM sector, only the quarks have non-vanishing Y' charge: $Y' = 1/3$. The model defined in Eq. (5.14) belongs to a class of leptophobic models formulated in Refs. [309, 315], from which we have borrowed the notation. The specific charge-assignment (5.14) was explicitly considered in [316].

With the previous spectrum, the most general fermionic Lagrangian involving fields of the dark sector reads

$$\begin{aligned}
\mathcal{L}_{\text{fer}} \quad \supset \quad & \mathcal{L}_{\text{kin}} - y_1 \bar{\psi}_L H \eta_R - y_2 \bar{\psi}_L \bar{H} \chi_R - y_3 \bar{\psi}_R H \eta_L - y_4 \bar{\psi}_R \bar{H} \chi_L \\
- \quad & \lambda_\psi \bar{\psi}_L \psi_R S - \lambda_\eta \bar{\eta}_R \eta_L S - \lambda_\chi \bar{\chi}_R \chi_L S - \lambda_L \chi_L \chi_L S - \lambda_R \chi_R \chi_R S^\dagger \\
+ \quad & (\text{h.c.}).
\end{aligned} \tag{5.16}$$

Similarly, the scalar Lagrangian involving the S field is given by

$$\mathcal{L}_{\text{scal}} \quad \supset \quad \mathcal{L}_{\text{kin}} - m_S^2 |S|^2 - \lambda_S^2 |S|^4 - \lambda_{HS}^2 |H|^2 |S|^2. \tag{5.17}$$

Defining $S = \langle S \rangle + s$, the three parameters of Eq. (5.17) can be traded by $\langle S \rangle$, m_s and the mixing between the Higgs boson and the scalar singlet s. This mixing is constrained by Higgs measurements. For the sake of simplicity, we will take $\lambda_{HS} = 0$, so that there is no such mixing.

Notice that, even though the models in Eq. (5.14) with hypercharges $Y_\psi = \pm\frac{7}{2}$ and $Y_\eta = \pm 5$ have identical Y' charges than the one we are considering, with this minimal particle content (3 fermions, the complex scalar S and the gauge boson Z') they cannot be suitable DM models since the particular choice of hypercharges forbids operators coupling different dark fermions, like the ones in the first line of the Eq. (5.16). Thus an accidental flavour symmetry arises and the electrically charged fermions, ψ, η, become stable. This shortcoming might be avoided by enlarging the scalar sector with an extra Higgs with $Y_{H'} = \pm\frac{3}{2}$. Consequently, the model defined in Eqs. (5.14-5.17) is somehow the minimal model with a leptophobic Z' mediator, axially coupled to the dark matter.

Concerning the fermionic Lagrangian (5.16), it should be noticed that the "Majorana couplings", λ_L, λ_R, if sizable, lead to the mixing and splitting of the two lightest degrees of freedom in the dark sector, so that the coupling of the lightest dark particle (i.e. the dark matter) to the Z' would not be purely axial. This problem is avoided by noticing that taking $\lambda_L = \lambda_R = 0$, leads to a global $U(1)$ symmetry in the dark sector, under which all the dark fermions, $\{\chi, \psi, \eta\}$, transform with the same charge. This works exactly as a "dark leptonic number". Consequently, we will assume such global symmetry, and thus $\lambda_L = \lambda_R = 0$. (This assumption was not done in Ref. [316], so the model became non-axial.)

The extra fermionic fields in the dark sector, ψ and η, can have an interesting phenomenology in colliders since they are charged under the SM gauge group. Furthermore, if they are light enough, they can play a relevant role in the dark matter phenomenology, in particular its thermal production in the early universe. E.g., if their masses are close enough to the DM one, their presence triggers efficient co-annihilation processes with the DM particle. However, since we are interested in exploring characteristics of the simplest scenario, we will make the assumption that the ψ and η masses are large enough to integrate these fields out. In that regime we recover a scenario which is similar to SDMM, but with some differences, e.g. the correlation between the coupling of the Z' to the SM and dark fields (which are taken as free parameters in SDMM). In this way, we get a truly realistic a SDMM (as it emerges from an anomaly-free model), whose performance is worth to examine. As we are about to see, even in that case, the extra fields leave a footprint in the low-energy theory in the form of an effective operator. The present analysis can be thus considered as the study of a portion of the parameter space of the theory, but of course the remaining regions are also interesting and would require a specific study.

On the other hand, the "dark scalar", s, may play a relevant role in DM annihilation at the early universe, due for instance to the $s-$channel process $\chi\chi \to s \to Z'Z'$. Depending on the values of m_χ and m_s, this diagram can be competitive with the diagram $\chi\chi \to Z'Z'$,

where χ propagates in $t-$channel. (Both diagrams are shown in see Fig. 5.1 below.) Actually, for $m_s \sim 2\ m_\chi$ the $s-$mediated annihilation becomes resonant and dominant ('$s-$funnel'). The effect of the $s-$field in the DM phenomenology has been discussed in Ref. [240]. Along the chapter we will consider two possibilities, namely a heavy scalar, $m_s^2 \gg m_\chi^2$, and a not-too-heavy one, in order to show its impact on the DM physics and phenomenological prospects.

Hence, after integration of the extra dark fermions, we end up with an effective theory where the dark sector contains just the DM field, χ, besides the scalar s and the Z' mediator. In addition there is an effective dimension-5 operator, $\sim |H|^2 \bar{\chi}_L \chi_R$, which arises upon the integration of the ψ field. Thus, the relevant DM Lagrangian of the effective theory reads

$$\mathcal{L}_{\rm eff}^{\rm DM} = \mathcal{L}_{\rm kin} - \lambda_\chi \bar{\chi}_R \chi_L S + \frac{1}{\Lambda} \bar{\chi}_R \chi_L |H|^2 + \cdots + (\text{h.c.}), \tag{5.18}$$

where it is understood that $\mathcal{L}_{\rm kin}$ contains the gauge interactions with the Z' and

$$\frac{1}{\Lambda} = \frac{y_2 y_4}{m_\psi}. \tag{5.19}$$

Note that this operator is exactly the one of a fermionic singlet Higgs$-$portal. Therefore, a $Z'-$framework naturally leads to a Higgs$-$portal, thus representing an interesting UV completion of it. Nevertheless this "Higgs$-$portal" operator is not going to play any relevant role in the DM phenomenology. The reason is that if the effective coupling $1/\Lambda$ is large enough to contribute to the DM annihilation in the early universe, then the strong constraints from direct (and indirect) detection rule out the scenario in most of the parameter space (except very close to the Higgs$-$funnel, $m_\chi \simeq m_h/2$). This will be discussed below. Consequently, we will assume in (most of) what follows that $1/\Lambda$ is small enough to be neglected.

In this regime, the model is thus described by three parameters: the $U(1)_{Y'}$ gauge coupling, g_B[3]; the $Z'-$mass, $m_{Z'}$ (or, equivalently, $\langle S \rangle$); and the dark matter mass, $m_\chi \simeq \lambda_\chi \langle S \rangle$. In the case of a not-too-heavy $s-$field, there is one extra relevant parameter, m_s (the coupling of s to $\chi\chi$, λ_χ, is determined by the value of m_χ). This is to be compared with ordinary SDMM, where there are four parameters, since the gauge coupling of the Z' to quarks (g_q) and to DM ($g_{\rm DM}$) are taken as independent parameters. As explained above, in our scenario, the cancellation of anomalies fixes the ratio between them: $g_{\rm DM}/g_q = 4.5$.

Still, we will see that the model is perfectly viable and quite predictive.

[3]The notation g_B stems from the equivalence of $U(1)_{Y'}$ and $U(1)_B$ for the SM fields.

5.3 Phenomenology of the Model

5.3.1 Kinetic mixing

As it is well known, the presence of more than one $U(1)$ factor in the gauge group leads to the possibility of kinetic terms which mix the corresponding gauge fields. In our case, such kinetic-mixing term takes the form

$$\mathcal{L}_{\rm kin} \supset -\frac{1}{2}\,\epsilon\, F^{Y}_{\mu\nu}\, F^{Y'\mu\nu}. \tag{5.20}$$

where $F^{Y(Y')}$ is the field-strength tensor of the $U(1)_{Y(Y')}$ gauge factor.

It is reasonable to assume that $\epsilon = 0$ at some unknown high-energy scale, Λ', above which the theory enters a different ultraviolet regime. Still, since quarks couple to both $U(1)$ gauge bosons, quark loops generate a non-vanishing value of ϵ at lower energies, $\mu = m_{Z'}$ [332]

$$\epsilon = \frac{e g_q}{2\pi^2 \cos\theta_W} \log\frac{\Lambda'}{\mu} \simeq 0.02\; g_q\; \log\frac{\Lambda'}{\mu}, \tag{5.21}$$

where $g_q = g_{Y'}/3$. Note that this result is completely general for any leptophobic model since, as commented in Sec. 5.1, leptophobia implies that $U(1)_{Y'}$ is equivalent to baryon number for the SM fields. In addition to quarks, there are loops involving the η, ψ fields, which are also charged under both $U(1)$s. However, the fact that their coupling to $U(1)_Y$ ($U(1)_{Y'}$) are vectorial (axial) makes their contributions to ϵ to cancel. In consequence, Eq. (5.21) holds. The previous mixing leads to relevant phenomenological constraints, e.g. from EW observables and di-lepton production at the LHC, which will be discussed in Sec. 5.4.

In order to prepare the model for the phenomenological analysis, one has to properly normalize and diagonalize the gauge kinetic terms. We have followed here the analysis of Refs. [80, 317]. To summarize, after appropriate redefinition of the $U(1)_{Y'}$ gauge boson, the kinetic terms get diagonal and normalized, while the covariant derivative takes the form

$$\mathcal{D}_\mu = \partial_\mu + i g_s T^a G^a_\mu + i g t^a W^a_\mu + i g' Y B_\mu + i(\tilde{g} Y + g_B Y') B'_\mu. \tag{5.22}$$

where G_μ, W_μ, B_μ are the ordinary gauge bosons of $SU(3)_c \times SU(2)_L \times U(1)_Y$; B'_μ is the gauge boson of $U(1)_{Y'}$ (with a small admixture of B_μ) and

$$\tilde{g} = \frac{\epsilon}{\sqrt{1-\epsilon^2}}\; g' \simeq \epsilon g'. \tag{5.23}$$

The final physical fields, A_μ, Z_μ, Z'_μ, are obtained upon diagonalization of the gauge-boson mass matrix:

$$\begin{pmatrix} B_\mu \\ W^3_\mu \\ B'_\mu \end{pmatrix} = \begin{pmatrix} \cos\theta_w & -\sin\theta_w \cos\theta' & \sin\theta_w \sin\theta' \\ \sin\theta_w & \cos\theta_w \cos\theta' & -\cos\theta_w \sin\theta' \\ 0 & \sin\theta' & \cos\theta' \end{pmatrix} \begin{pmatrix} A_\mu \\ Z_\mu \\ Z'_\mu \end{pmatrix}, \tag{5.24}$$

where θ_w is the weak angle and θ' is the mixing between the Z and Z' fields, given by[4]

$$\theta' \simeq \epsilon \sin\theta_w \frac{m_Z^2}{m_{Z'}^2 - m_Z^2}. \tag{5.25}$$

All these relations will be applied below. For a detailed review on the kinetic mixing see Appendix C.

5.3.2 Dark Matter Constraints

From the Lagrangian of the model (5.18), the thermal production of dark matter in the early universe is controlled by the DM annihilation processes of Figs. 5.1, 5.2.

Keeping for the moment the assumption that the effective coupling, $1/\Lambda$, in Eq.(5.18) is small (which is perfectly reasonable), the main annihilation channels of DM come from the first two diagrams of Fig. 5.1 (and the other three as well if s is light enough). Thus the annihilation rate depends on the main three parameters of the model, $\{g_B, m_{Z'}, m_\chi\}$ (plus m_s if the $s-$field is relevant). Recall that the relative couplings of Z' to quarks and DM are determined by g_B, namely $g_q = \frac{1}{3}g_B$, $g_{\rm DM} = \frac{3}{2}g_B$. Consequently, for each value of $\{m_{Z'}, m_\chi, m_s\}$, there is always a (unique) value of g_B (maybe in the non-perturbative regime) which leads to the correct relic DM density, $\Omega_{\rm DM}h^2 = 0.1188$ [20].

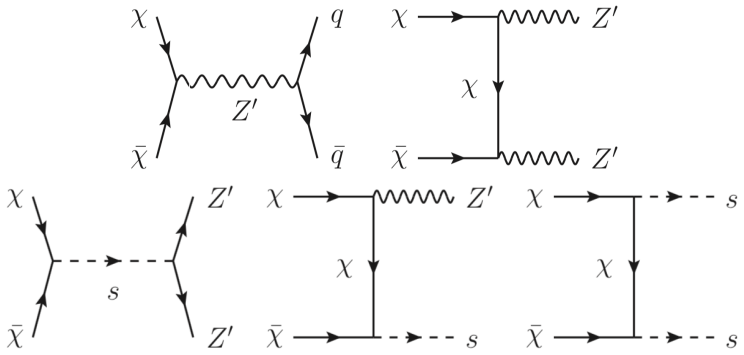

Figure 5.1: Feynman diagrams, relevant for DM annihilation in the model.

This is illustrated in Fig. 5.3 in the $m_\chi - g_B$ plane for several choices of $m_{Z'}$ and two choices of the scalar mass, $m_s = 15$ TeV (i.e. irrelevant) and $m_s = 2$ TeV. Interestingly, the value of g_B remains in the perturbative regime in most of the parameter space. For each curve, the two resonances, $2m_\chi \sim m_{Z'}, m_s$, and the threshold of two Z's are visible. Note that the values of g_B are almost the same in both panels, unless $m_s \lesssim 2m_\chi$, i.e. when the effects of the scalar in the DM annihilation are non-negligible.

[4]Eq. (5.25) is accurate enough for small ϵ; the complete expression can be found e.g. in ref.[80], Eq. (44).

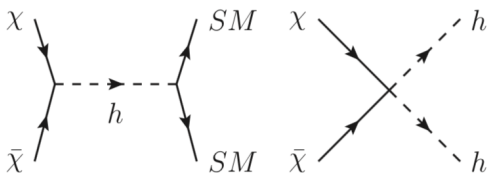

Figure 5.2: Feynman diagrams arising from the effective operator (5.18), that contribute to DM annihilation in the model.

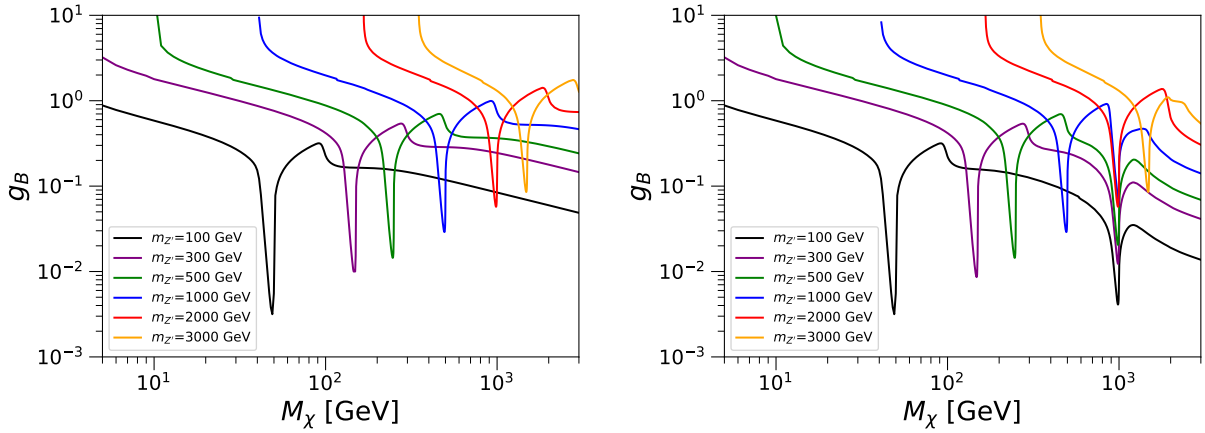

Figure 5.3: Values of the g_B coupling that reproduce the observed DM relic density as a function of the DM mass for several choices of $m_{Z'}$. The left (right) panel shows the $m_s = 15$ TeV ($m_s = 2$ TeV) case.

Concerning bounds from direct and indirect detection, as mentioned in previous sections, the fact that the Z' couples to DM (SM quarks) in an axial (vectorial) way, implies that the effective DD interaction is spin-dependent and velocity-suppressed [73]. Analogously, indirect detection (ID) is velocity-suppressed as well [73]. Consequently, there are virtually no bounds from DD or ID on the model (for $1/\Lambda$ small). Actually, the most important constraints on the model (and the opportunity to probe it experimentally) come from collider measurements, which we examine in the next subsections.

Let us finish this subsection by discussing the role of the effective "Higgs−portal" operator of Eq. (5.18) in the DM phenomenology. This interaction leads to the DM annihilation processes of Fig. 5.2. In Fig. 5.4 we have plotted (black line) the corresponding spin-independent DM-nucleon cross section as a function of m_χ when the value of the effective coupling, $1/\Lambda$, is adjusted to reproduce the relic density; showing as well the region excluded by the current XENON1T limits [108]. Only a narrow range of m_χ around the Higgs-funnel region is still surviving. Hence the effective Higgs−portal operator must be

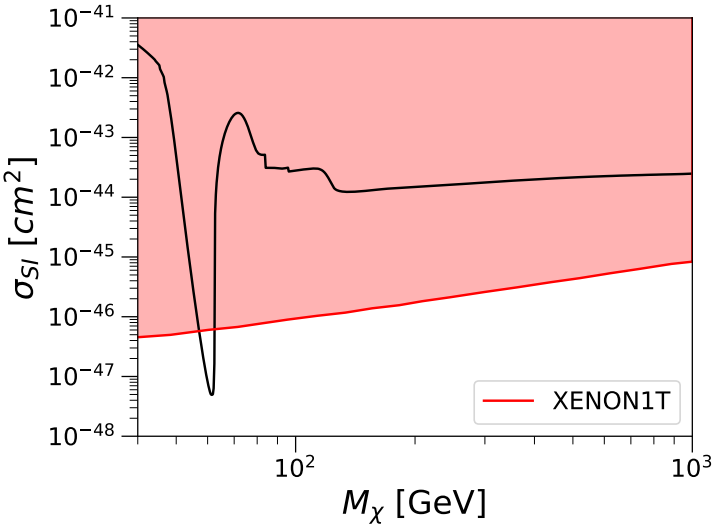

Figure 5.4: DM-nucleon spin-independent cross-section as a function of the DM mass when DM annihilation occurs thanks to the effective operator of Eq. (5.18). The black line corresponds to the observed relic density. The red-shaded area is excluded by current XENON1T constraints.

suppressed enough to avoid these strong bounds (fortunately this is perfectly sensible from (5.19)), and it is reasonable to assume that all the DM annihilation occurs through the diagrams of Fig. 5.1.

5.3.3 Bounds from EW observables and LHC

As mentioned above, the presence of a kinetic mixing, ϵ, between the two $U(1)$ gauge groups is unavoidable due to radiative corrections involving quarks. In the following we will assume that ϵ is initially vanishing at some unknown UV scale, Λ', so that its effective value at the $m_{Z'}$ scale is given by Eq. (5.21). We will derive results for two representative choices of the UV scale: $\log(\Lambda'/m_{Z'}) = 1,\ 4.6$ (the latter corresponds to $\Lambda' = 100\ m_{Z'}$).

A non-vanishing ϵ induces important physical effects which constrain the model. The most relevant ones are electroweak precision observables (EWPO) particularly, S and T, and the production of di-leptons at the LHC.

Concerning the first ones, we use the well-known expressions for the oblique parameters S and T [317]

$$\alpha_{\rm em}\ S \quad = \quad 4c_w^2 s_w \theta' \left(\epsilon - s_w \theta'\right),$$

$$\alpha_{\rm em}\ T \ = \ \theta'^2 \left(\frac{m_{Z'}^2}{m_Z^2} - 2 \right) + 2 s_w \theta' \epsilon, \tag{5.26}$$

and take $S = 0.03 \pm 0.10$ and $T = 0.05 \pm 0.12$ as values derived from the global fit to the electroweak precision data performed in Ref. [339].

We recall that the mixing angle θ' involved in Eq. (5.26) is given in terms of ϵ and $m_{Z'}$ by Eq. (5.25). Obviously, for a given ϵ, the larger $m_{Z'}$ the smaller θ'. Consequently, EW observables can be relevant at small $m_{Z'}$.

Regarding di-leptons, the kinetic mixing triggers couplings of the Z' to leptons, as it is clear from Eqs. (5.22), (5.24) (the precise expressions for the couplings to ℓ_L, ℓ_R leptons can be found in Refs. [80, 317]). Hence, production of Z's at the LHC leads to the possibility of di-leptons at the final state. LHC has provided strong constraints on the di-lepton search using 36.1 fb^{-1} of data at $\sqrt{s} = 13$ TeV. Ref. [340] gives bounds on the coupling of Z' to leptons as function of $m_{Z'}$ for several representative examples of the associated $U(1)_{Y'}$. More precisely, that reference provides an analysis on the bounds on a Z' corresponding to $B - L$, which is identical to ours for quarks, and thus for Z' production. Then the ratio of the braching fraction of Z' into leptons in the $B - L$ model over the one in ours can be straightforwardly derived from the respective couplings of both Z's to leptons. In addition, it has to be taken into account that, depending on the value of $m_{Z'}$, the gauge boson can decay into top-antitop and/or $\chi\chi$ (with appropriate kinematical factors), which modifies further the braching fraction into leptons. We have taken into account all these details in order to extract the bounds from di-leptons, which will be shown in the next subsection.

Bounds from di-leptons are stronger for smaller $m_{Z'}$. Hence, as for EWPO, the constraints on our model due to kinetic mixing are specially relevant in the range of light Z'. Needless to say, the larger the UV scale, Λ', the larger the radiatively induced ϵ and thus the stronger both types of bounds.

Constraints from di-jet searches turn out to be the dominant ones in most of the parameter space. We have translated the last ATLAS results on di-jets [341–345] into bounds on the scenario at hand. As for the above di-lepton bounds, this entails to take into account that, depending on the value of $m_{Z'}$, the gauge boson can decay into top-antitop and/or $\chi\chi$ (with appropriate kinematical factors), thus modifying the branching fraction into di-jets. In the $m_{Z'} \sim 140 - 500$ GeV mass window, where UA2 [346] and CDF [347] experiments have better sensitivity than LHC experiments, the limits are however weaker than mono-jet bounds, which are discussed next.

Finally, mono-jet production at the LHC from ISR in the $q\bar{q} \to Z' \to \chi\chi$ process leads to important constraints on the model, which are specially relevant in the region of light Z'. This type of signatures are characterized by a high-p_T object recoiling against $\not{E}_T$ which can be triggered at the ATLAS and CMS detectors. Our application of the mono-jet constraints is based on its implementation in MicrOMEGAS [348], with 20.3 fb^{-1} of data collected at

$\sqrt{s} = 8$ TeV [349][5].

5.4 Results

We have scanned the DM mass and Z' mass plane randomly for two different values of the scalar s-field mass ($m_s = 2, 15$ TeV) requiring each point to fulfill the central value of the Planck measured DM relic density $\Omega h^2 = 0.1188$, measured by Planck [20]. This procedure fixes the coupling g_B. Besides, we impose a 2σ cut on the S and T oblique parameters and apply 95% C.L. exclusion limits from LHC searches of di-leptons, di-jets and mono-jets as it has been discussed in Sec. 5.3.

For the calculation of the relic density the program MicrOMEGAS [348] has been used. MicrOMEGAS is based on the CalcHEP [234] package which is used to calculate the tree level cross sections relevant for DM annihilations and thus the DM relic density. The implementation of the model in CalcHEP format has been done using the FeynRules package [350].

As explained in previous subsections, our model, which is representative of a leptophobic Z' axially coupled to DM with minimal dark sector, has only three relevant parameters: $\{g_B, m_{Z'}, m_\chi\}$, plus m_s if the scalar is not too heavy. We have considered here the simplest possibility where effective interactions due to the extra dark fermions, ψ and η, are negligible since their masses are substantially bigger than $m_{Z'}, m_\chi$. The study of phenomenological implications of these extra dark fermions is left for a future work. It was shown in Subsec. 5.3.2 that for any choice of $m_{Z'}, m_\chi, m_s$, there is a unique value of g_B leading to the correct thermal relic density, $\Omega_{\rm DM} h^2$. Fig. 5.5 shows such value of g_B in the $m_{Z'} - m_\chi$ plane for two regimes of m_s. In most of the interesting parameter space g_B is well inside the perturbative regime, which we have taken as $g_B < 4\sqrt{\pi}$ (see [351] for a detailed discussion). However, the most important restrictions from the perturbativity requirement come from the fermionic Yukawa couplings, $\lambda_{\chi,\psi,\eta}$, and, the scalar one, λ_S. The latter is the most constraining one in the regime where $m_s > 2m_\chi$ (left plot of Figure 5.5), i.e. when the scalar plays a negligible role for the DM annihilation in the early universe. In contrast, when the scalar plays a role ($m_s \lesssim 2m_\chi$), the required value of g_B becomes smaller. This is illustrated in the right plot of Figure 5.5 for $m_s = 2$ TeV. As a consequence, for a given value of $m_{Z'}$, the VEV $\langle S \rangle$ becomes larger and all the (fermionic and scalar) couplings smaller. Then, the perurbative limits exclude a much smaller region in the parameter space, as shown in the figure. The resonance region, $2m_\chi \sim m_{Z'}, m_s$ is also visible in the figure.

The trend in both cases is that the larger (smaller) m_χ ($m_{Z'}$) the smaller g_B. As we shall see shortly, this will be, in general terms, the region safe with respect to the various constraints and, consequently, it becomes larger in the regime where the scalar field plays a

[5] We have checked that the coverage of current 13 TeV data is similar.

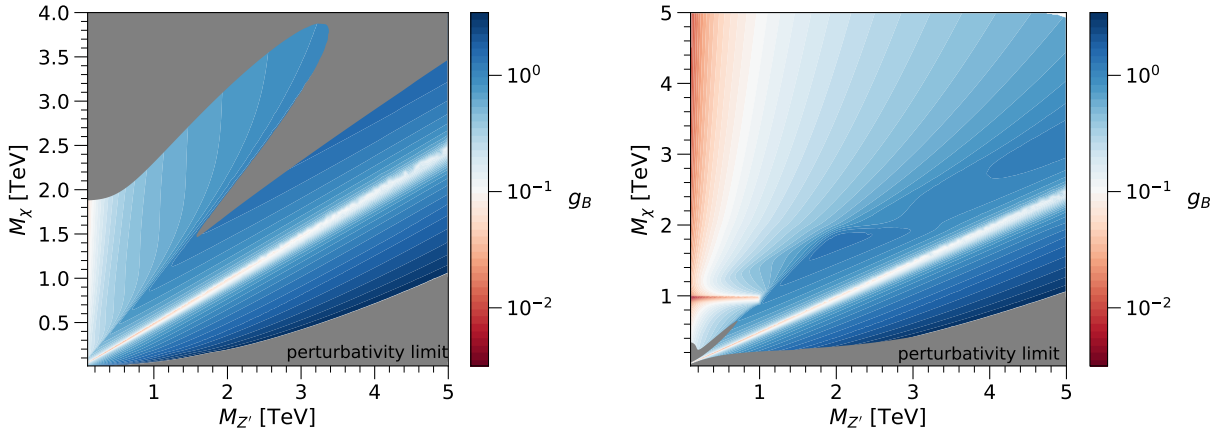

Figure 5.5: The logarithmic-scale colorbar gives the values of the g_B coupling that fit the observed DM relic density in the $m_{Z'} - m_\chi$ plane. The left (right) panel shows the $m_s > 2m_\chi$ ($m_s = 2$ TeV) case. The grey-shaded region is excluded by the perturbativity condition in the various couplings.

significant role.

Next we show the phenomenological bounds on the model in the same $m_{Z'} - m_\chi$ plane, assuming at any point the value of g_B leading to the correct $\Omega_{\rm DM}$, as given in Fig. 5.5.

Fig. 5.6 shows the constraints on the model discussed in the previous subsection for $\log(\Lambda'/m_{Z'}) = 1$. As expected, di-jet production (pink region) gives the dominant constraint in most of the parameter space. It essentially excludes the whole 500 GeV $\lesssim m'_Z \lesssim$ 3000 GeV region, except around the Z' and s resonances, $2m_\chi \sim m_{Z'}, m_s$. Notice that the constraints from a correct relic density are also incorporated, as every point in the $m_{Z'} - m_\chi$ plane has the correct relic density, according to Fig. 5.5.

For the value of Λ' considered (a rather low one), the kinetic mixing is not sizeable and does not lead to relevant constraints from EWPO and di-lepton production. The corresponding bounds on the plane are close to the perturbativity one, and always weaker than other phenomenological constraints. For $m'_Z \lesssim 500$ GeV the most important bounds come from mono-jet production (green area). Still there is a lot of viable parameter space in this regime of relatively light Z'. Fig. 5.7 shows the constraints when the UV scale is large, $\Lambda' = 100\, m_{Z'}$. Bounds from di-jets and mono-jets remain as before, since they are essentially independent of the kinetic mixing. However, bounds from di-leptons become now important in the region of light Z', excluding new areas in that regime. In contrast, EWPO bounds remain unimportant. Still, there remain large viable regions for $m'_Z \lesssim 500$ GeV, especially for a not very heavy scalar (last two panels).

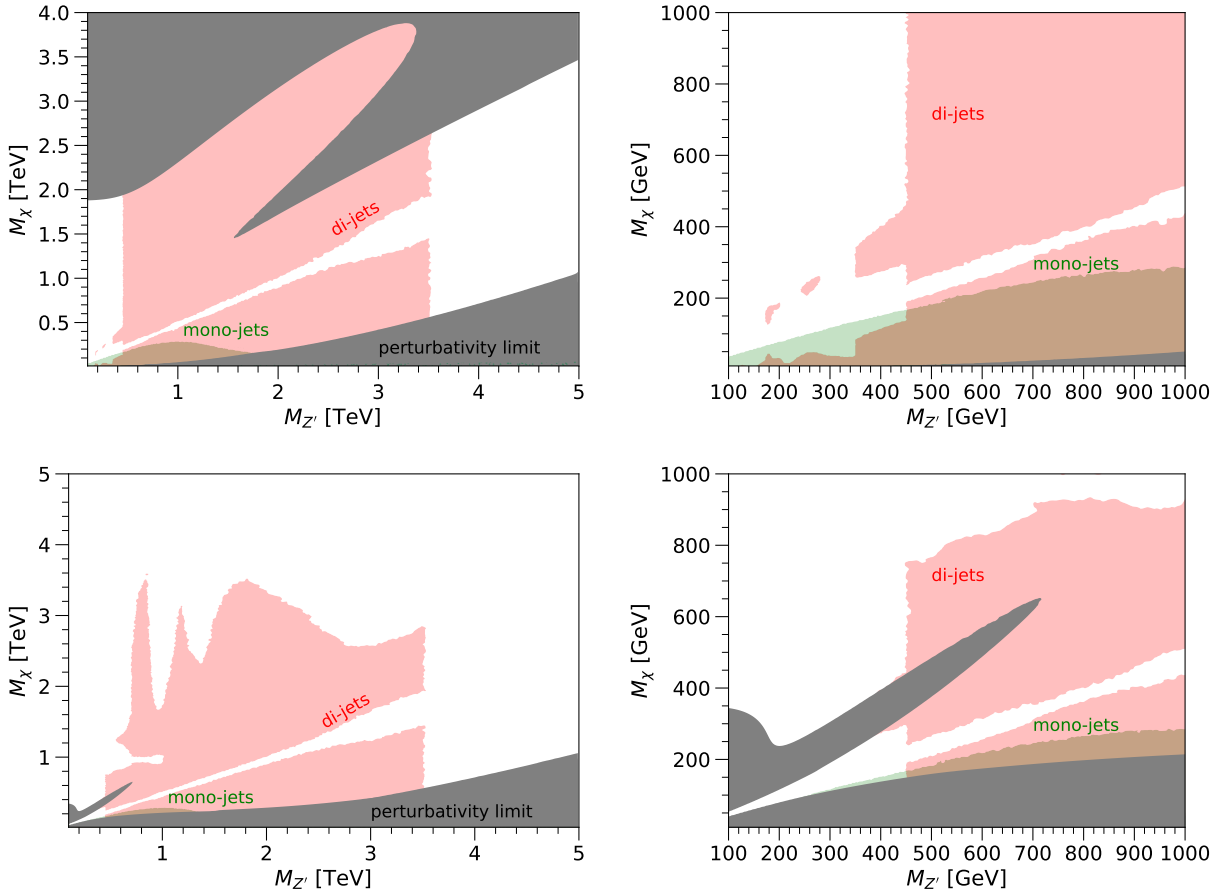

Figure 5.6: Areas in the $m_{Z'} - m_\chi$ plane forbidden by constraints from di-jets (pink) and mono-jets (green); for $\log(\Lambda'/m_{Z'}) = 1$ (see Eq. 5.21). The value of the g_B coupling is adjusted at every point to reproduce the observed DM relic density. In the grey region one of the couplings becomes non-perturbative. Upper (lower) panels show the case where $m_s > 2m_\chi$ ($m_s = 2$ TeV). Left panels show the full range of $m_{Z'}$ considered while in the right ones we zoom in the region of Z' masses up 1 TeV.

To summarize, in this chapter we have analyzed the scenario of a leptophobic Z' mediator axially coupled to the DM. Looking for a UV complete model, with anomaly cancellation, we found several solutions for three fermions in the dark sector. We studied the phenomenology of a significant one, and, although affected by some collider physics constraints, we have obtained a parameter space completely safe from DD and ID experiments.

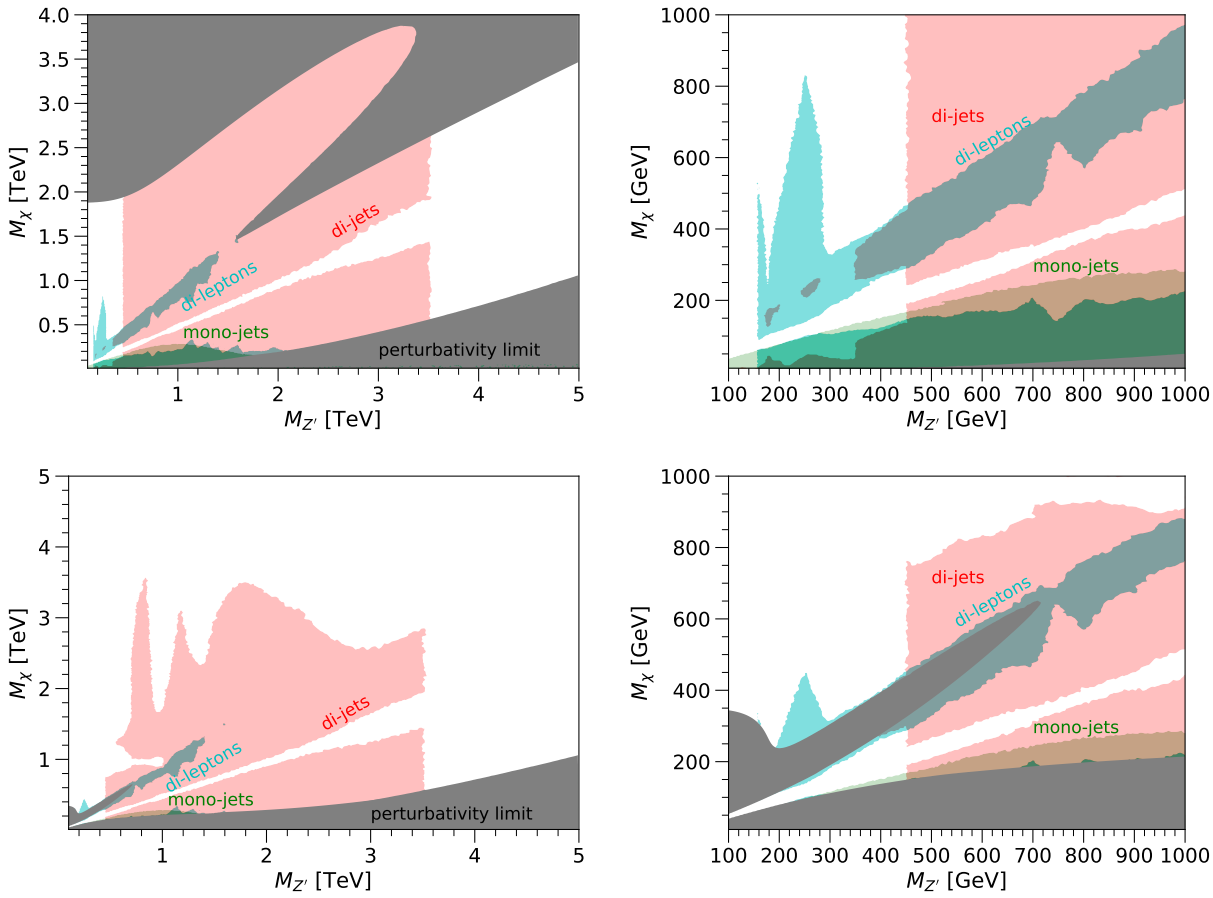

Figure 5.7: The same as Fig. 5.6 for $\Lambda' = 100\ m_{Z'}$. The turquoise-shaded area is excluded by di-lepton resonance searches.

Chapter 6

Conclusions

In this thesis we have studied the problem of the nature of dark matter, focusing on weakly interacting massive particles. In this context, we have studied their production in early universe and its phenomenology for direct and indirect searches and collider experiments. To explore these physics, simplified DM models are very popular. However, they are limited by its simplicity and most of them are very constrained by experimental bounds. For these reasons, we have studied two DM models taking a step further from the SDMM. First, an extension of the Higgs portal model to alleviate the strong bounds that constrain it. Second, an anomaly free Z' portal model which is leptophobic and axially coupled to DM.

In particular, conventional Higgs portal consists of a new singlet-scalar, S, coupled to the Higgs, with a Z_2 symmetry to guarantee the stability of the DM. With such a simple construction the model is able to reproduce the correct relic density. However, different experiments have tested the model, resulting in a severely constrained parameter space, as can be seen in Fig. 4.2. Right now, only a small region around the Higgs resonance, i.e. $m_{DM} \simeq m_h/2$, and large DM masses are allowed.

Nevertheless, the economy of the model makes it very appealing. For this reason, in Chapter 4 we have explored a simple extension of it, by adding just an extra scalar-singlet. This new scalar, S_2, is coupled to the Higgs boson, just as the DM candidate, S_1, but now an additional mixed coupling, $S_1 S_2 H H^\dagger$, plus extra terms coupling both singlet-scalars, are allowed, which may keep them in equilibrium. The coupling among the three scalars also permits the heavy one to decay into the DM particle after the freeze-out. One remarkable implication of the extra term is the possible coannihilation effects between the two scalars. The new scalar can also mediate the annihilation of S_1 exchanging an S_2 in t-channel.

We have seen that these two effects are so important that can carry out completely the annihilation of dark particles in the early universe leading to a correct relic density, as shown in Fig. 4.5. This fact allows the model to relax the coupling between S_1 and the Higgs, $S_1 S_1 H H^\dagger$, which is responsible for the direct detection constraints, i.e. the strongest

bounds on the singlet-scalar Higgs portal.

For simplicity, we considered a minimal value for the $S_2 S_2 H H^\dagger$ coupling. Hence, the only two new parameters of the model are the coannihilation coupling λ_{12} and the mass of the new scalar. With just these two extra parameters, four in total, we have shown that the usual bounds become extremely relaxed. As ilustrated in Figs 4.7 and 4.8, we rescue large areas for DM masses above 50 GeV. Recall that in the case of the usual singlet-scalar Higgs portal, the whole parameter space for masses below 500 GeV was excluded, except a narrow region around the Higgs resonance.

We have also studied the case where the coannihilation effect is off due to a large difference of masses between the two scalars. In this regime the model can be analyzed in terms of an effective field theory, by integrating-out the heavy scalar. Then, the Lagrangian is as the one for the usual singlet-scalar Higgs portal plus an extra dimension-6 operator, which allows a relaxation of the direct detection bounds for masses over 125 GeV, as shown in Fig. 4.10. This effect is relevant for masses over the Higgs mass, since the effective operator involves the annihilation of two DM particles into two Higgs bosons, exchanging a heavy scalar in the t-channel. For DM masses lower than the Higgs mass, the Higgses are produced off-shell and the phase-space suppresses the annihilation processes, so the effective operator is not relevant.

In the previous studies we have taken into account all the phenomenological constraints on the model, including direct and indirect detection searches and LHC phenomenology.

After addressing the relic density problem, we focused our attention to the galactic center excess, detected by the *Fermi*-LAT Collaboration. This excess is peaked at around 3 GeV. Its origin is unknown and many possibilities have been considered, typically a combination of *Fermi*-bubble-like emission plus another source.

We tested how DM, more concretely the extended singlet-scalar Higgs portal presented here, could account for the extra source. In most of the DM models it is difficult to find a choice of parameters that fits the galactic center excess and avoids all the constraints, specially the ones from DD, as happens in the usual singlet-scalar Higgs portal. Considering the effective approach of the ESHP, we analyzed how this model could actually fit the peak of the GCE between 1-10 GeV, assuming an extra astrophysical *Fermi*-Bubble-like contribution for the large mass region. Interestingly, we found areas of the parameter space of the ESHP that reproduce the correct relic density, that are in agreement with the experimental bounds and simultaneously present a good fit to the GCE. An example of this is illustrated in Fig. 4.13, which shows a fit with a p-value of 0.63, for a DM mass of $m_S \simeq 130$ GeV. This point is of special interest since the annihilation channel $h \to \gamma\gamma$ is concentrated at $E \simeq m_S/2 \simeq 65$ GeV, producing a bump in a bin where data show a peak as well.

Doing a scan in the parameter space of the ESHP, demanding the correct relic density, we showed that some of the parameter space leads to a good fit of the GCE avoiding at the same time the experimental constraints from DD and ID.

In summary, the extended singlet-scalar Higgs portal, despite its simplicity, has a very rich phenomenology able to avoid experimental constraints from direct and indirect detection and collider physics and it can also fit quite well the excess from the galactic center.

In Chapter 5 we have studied other kind of mediator, the so-called Z'-portal. This mediator arises from an extra $U(1)$ gauge symmetry, spontaneously broken if the mediator is massive. This kind of mediators is also experimentally restricted, specially by direct detection and di-lepton searches at colliders. For these reasons, we focused on the search of a mediator that could alleviate these two constraints. For di-lepton searches, the simplest way is to consider a mediator that does not couple to leptons while for the direct detection constraints, an axial coupling to DM would drastically relax the bound since the effective quark-DM interactions would be spin-dependent, much less restrictive than the spin-independent ones.

Taking these considerations into account, we studied the simplest leptophobic Z' solution, namely a flavor blind symmetry where all the families are charged equally. This basically corresponds to taking baryon number as the new gauge symmetry. We searched for consistent ultraviolet completions of this scenario, i.e., with a complete cancellation of anomalies from the new symmetry of the theory, with the minimal amount of extra particles. The latter consists in two $SU(2)_L$ fermionic singlets, one of them a $U(1)_Y$ singlet (the DM particle), and a $SU(2)_L$ fermionic doublet. We find an infinite number of anomaly free models of this kind. The set becomes much reduced if an axial coupling of the mediator with the DM candidate is required.

We studied the phenomenology of a representative axial model, assuming that the only relevant fermion of the dark sector is the SM singlet, i.e., the dark matter particle. The other two dark fermions are assumed to be heavier so that they can be integrated out, leaving a dimension-5 Higgs-portal-like operator. Hence, the only new particles in the model are the DM candidate, χ, the Z' boson and the scalar that breaks the symmetry, S. The dimension-5 operator is strongly constrained by direct detection as it happens with the original Higgs portal, hence the effective coupling should be very small. Then, the only four relevant parameters of the model are the masses of the three new particles, m_χ, m_S and $m_{Z'}$ and the extra gauge coupling, g_B. This scenario is very similar to a simplified DM model, except that in a SDMM the couplings of the new vector boson with the DM and the SM are completely independent, while here the anomaly cancellation relates them, $g_q/g_{DM} = 2/9$. This hierarchy is actually very convenient to avoid LHC bounds and to produce the correct relic density.

In order to study the phenomenology of the model, we first solved the g_B parameter in terms of the others (m_χ, m_S and $m_{Z'}$) through the requirement of a correct relic density. Then, we analyzed the experimental bounds on the model. By construction, the coupling of the Z' with the quarks is vectorial, while we chose an axial coupling with the DM. This configuration implies a spin-dependent and velocity suppressed DD cross section which is essentially invisible to direct detection experiments. On the other hand, the leptophobia of

the mediator relaxes the constraints from di-lepton searches. However, depending on the mixing between the two $U(1)$ symmetries the effective coupling to leptons might be sizable. In fact, even considering a null mixing at a UV scale, radiative corrections could trigger a sizable mixing. Besides these two bounds, we also included bounds from mono-jet and di-jet production at LHC.

In Figs 5.6 and 5.7 we see the effect of these bounds in the parameter space, for two different choices of the UV scale where the mixing vanishes. The main bounds come from di-jets searches, resulting in strong restrictions in the mass of the Z' mediator between 500 GeV and 3 TeV. The bounds become less restrictive if the scalar, S, is light enough to play a role in the phenomenology, for example $m_S = 2$ TeV, as shown in the bottom panels of Figs 5.6 and 5.7, where high values of DM mass are safe from di-jet searches.

Collider searches are the natural way to probe this model, exploring areas that are now allowed. In addition, the extra fermions are charged, so that if their masses were of the same order as the DM particle, they could produce interesting phenomenology at colliders that could help testing the model as well as coannihilation effects in the early universe.

To conclude, simplified DM models (as the singlet-scalar Higgs portal and $Z'-$SDMM) are a good first approximation to the DM issue. However, they are probably too simple, since they are strongly constrained by experimental searches and, on the other hand, there is no reason to think that the dark sector consists of just one particle. Therefore, it is natural to consider a larger dark sector, as shown in the two models analyzed in this thesis. The extra particles can relax the constraints imposed on the simplified models and also give a richer phenomenology accessible at experiments, specially at colliders. Hence, it is worth to keep studying different possibilities for an ultimate DM model, waiting for a positive signal at the experiments.

Conclusiones

En esta tesis hemos estudiado el problema de la naturaleza de la materia oscura, centrándonos en partículas masivas que interaccionan débilmente. En este contexto, hemos estudiado su producción en el universo temprano y su fenomenología en experimentos de detección directa e indirecta y búsquedas en colisionadores. Para explorar la física detrás de esto, los modelos simplificados de materia oscura son muy populares. Sin embargo, están limitados por su simplicidad y muchos de ellos están muy restringidos por límites experimentales. Por estas razones, hemos estudiado dos modelos de materia oscura dando un paso más allá de los modelos simplificados. Primero, una extensión del modelo portal de Higgs para relajar los fuertes límites que lo restringen. Segundo, un modelo portal de Z', sin anomalías, pidiendo leptofobia y que se acople de manera axial a la materia oscura.

En particular, el modelo portal de Higgs consiste en un nuevo singlete escalar, S, acoplado al Higgs, con una simetría Z_2 para garantizar la estabilidad de la materia oscura. Con esta simple construcción el modelo es capaz de reproducir la densidad reliquia de materia oscura. Sin embargo, diferentes experimentos han testado el modelo, lo cual ha resultado en un espacio de parámetros muy constreñido, como se puede ver en la Fig. 4.2. Ahora mismo, solo una pequea región en la resonancia con el Higgs, es decir $m_{DM} \simeq m_h/2$, y masas grandes de materia oscura están permitidas.

No obstante, la economía del modelo lo hace muy interesante. Por esta razón, en el Capítulo 4 hemos explorado una extensión simple del modelo, añadiendo solo un singlete escalar extra. Este nuevo escalar, S_2, se acopla al Higgs, de la misma manera que el candidato a materia oscura, S_1, pero ahora un acoplamiento mixto adicional, $S_1 S_2 H H^\dagger$, además de términos extra acoplando ambos escalares, están permitidos, los cuales permiten que estén en equilibrio. El acoplamiento entre los tres escalares también permite que el escalar pesado decaiga en la partícula de materia oscura después del *freeze-out*. Una consecuencia interesante de este término extra es la posibilidad de efectos de coaniquilación entre los dos escalares. El escalar nuevo también puede mediar la aniquilación de S_1 intercambiando un S_2 en canal t.

Hemos visto que estos dos efectos son de gran importancia y pueden acarrear por completo la aniquilación en el universo temprano consiguiendo la densidad de materia os-

cura correcta, como podemos ver en la Fig. 4.5. Este hecho permite al modelo relajar el acoplamiento entre S_1 y el Higgs, $S_1 S_1 H H^\dagger$, el cual es responsable de la restricción por detección directa, es decir el limite más fuerte del portal de Higgs con un escalar singlete.

Por simplicidad, hemos considerado un valor mínimo para el acoplamiento $S_2 S_2 H H^\dagger$. Así los únicos parámetros nuevos del modelo son el acoplamiento de coaniquilación, λ_{12}, y la masa del nuevo escalar. Con solo estos dos parámetros, cuatro en total, hemos visto que las restricciones habituales se relajan severamente. Como se ilustra en las Figs. 4.7 y 4.8, rescatamos áreas grandes por encima de 50 GeV. Recordar que en el caso del portal de Higgs con un escalar singlete habitual, todo el espacio de parámetros para masas por encima de 500 GeV estaba excluido, a excepción de una pequeña región en la resonancia del Higgs.

También hemos estudiado el caso donde los efectos de coaniquilación no están presentes debido a una diferencia de masas grande entre los dos escalares. En este caso el modelo se puede analizar en términos de una teoría de campos efectiva, integrando fuera del espectro el campo más pesado. En ese caso, el Lagrangiano es el mismo del portal de Higgs habitual añadiendo un operador de dimensión 6, el cual permite relajar los límites de detección directa para masas mayores que 125 GeV, como se muestra en la Fig. 4.10. Este efecto es relevante para masas mayores que la masa del Higgs, ya que el operador efectivo incluye la aniquilación de dos partículas de materia oscura en dos bosones de Higgs, intercambiando un escalar pesado en canal t. Para masas menores de que masa del Higgs, los Higgses están producidos fuera de la capa de masas y el espacio de fases suprime los procesos de aniquilación, por tanto el operador efectivo no es relevante.

En los estudios anteriores se han tenido en cuenta todas las restricciones fenomenológicas del modelo, incluyendo detección directa e indirecta y búsquedas en el LHC.

Después de solucionar el problema de la densidad reliquia, nos centramos en el exceso del centro galáctico, detectado por la colaboración *Fermi*-LAT. Este exceso tiene un máximo alrededor de 3 GeV. Su origen es desconocido y se han considerado muchas posibilidades, por ejemplo una combinación de una emisión de tipo burbujas de *Fermi* más otra fuente.

Testamos cómo la materia oscura, y más concretamente el portal de Higgs extendido que se ha presentado aquí, podría dar cuenta de la fuente extra. En la mayoría de los modelos de materia oscura es difícil encontrar una elección de parámetros que acomode el exceso del centro galáctico y que evite todas las restricciones, en especial las de detección directa, como pasa con el portal de Higgs con un escalar singlete habitual. Considerando la aproximación efectiva del portal de Higgs con dos escalares singletes, analizamos cómo de bien era el modelo capaz de acomodar el pico del exceso entre 1 y 10 GeV, asumiendo una contribución astrofísica extra del tipo burbuja de *Fermi* para la zona de masas grandes. Es interesante ver que encontramos áreas del espacio de parámetros del portal de Higgs con dos escalares singletes que reproduce la densidad reliquia correcta, está a salvo de las restricciones experimentales y además acomoda bien el exceso galáctico. Un ejemplo de esto se puede ver en la Fig. 4.13, que muestra un ajuste con valor de p de 0.63, para una masa

de la materia oscura de $m_S \simeq 130$ GeV. Este punto tiene un interés especial ya que el canal de aniquilación $h \to \gamma\gamma$ está concentrado en $E \simeq m_S/2 \simeq 65$ GeV, produciendo un pico en los datos que coincide con las medidas.

Escaneando el espacio de parámetros del portal de Higgs con dos escalares singletes, pidiendo la densidad reliquia correcta, mostramos que para algunos puntos del espacio de parḿetros se produce un buen acomodamiento del exceso del centro galáctico evitando al mismo tiempo las restricciones experimentales de detección directa e indirecta.

En resumen, el portal de Higgs con dos escalares singletes, a pesar de su simplicidad, tiene una rica fenomenología capaz de evitar los límites experimentales de detección directa e indirecta y de colisionadores y además es capaz de acomodar bastante bien el exceso del centro galáctico.

En el Capítulo 5 hemos estudiado otro tipo de mediador, el llamado portal de Z'. Este mediador proviene de una simetría gauge $U(1)$, que está espontáneamente rota si el mediador es masivo. Este tipo de mediadores también está restringido por los experimentos, en particular por detección directa y búsquedas de di-leptones en colisionadores. Por estas razones, buscamos la manera de relajar estas restricciones. Para las búsquedas de di-leptones, la manera más fácil es considerar un mediador que no se acople a leptones mientras que para detección directa, un acoplamiento axial con la materia oscura relaja drásticamente el límite ya que la interacción efectiva entre los quarks y la materia oscura sería dependiente del spin, mucho menos restrictiva que la independiente del spin.

Tomando todo esto en cuenta, hemos estudiado la solución más simple para un Z' leptofóbico, una simetría en la que las tres familias están cargadas de igual manera. Esto corresponde a tomar número bariónico como una nueva simetría gauge. Buscamos escenarios con completitud ultravioleta, es decir, con una completa cancelación de anomalías debido a la nueva simetría de la teoría, con un número mínimo de partículas. El mínimo consiste en dos fermiones singletes bajo $SU(2)_L$, uno de ellos singlete bajo $U(1)_Y$ (la materia oscura), y un doblete fermiónico de $SU(2)_L$. Encontramos infinitas soluciones con cancelación de anomalías para esta configuración. El número de soluciones se reduce drásticamente si consideramos un acoplo axial con la materia oscura.

Estudiamos la fenomenología de un modelo representativo axial, asumiendo solo como fermión relavante del sector oscuro el singlete bajo el Modelo Estándar, es decir, la materia oscura. Se asume que los otros dos fermiones oscuros son mas pesados y por tanto pueden ser integrados fuera del espectro, quedando un operador de dimensión 5 similar a un portal de Higgs. Así, las únicas partículas nuevas en el modelo son el candidato a materia oscura, χ, el bosón Z' y el escalar que rompe la simetría, S. El operador de dimensión 5 está muy restringido por detección directa, como ocurre con el portal de Higgs original, con lo cual el acoplamiento efectivo debería ser muy pequeño. Por tanto, los cuatro únicos parámetros relevantes del modelo son las masas de las tres partículas nuevas, m_χ, m_S y $m_{Z'}$, y el acoplamiento gauge, g_B. Este escenario es similar a un modelo simplificado de materia

oscura, excepto que en el modelo simplificado los acoplamientos del nuevo boson vector son independientes, mientras que en este caso la cancelación de anomalías los relaciona, $g_q/g_{DM} = 2/9$. Esta jerarquía es muy conveniente para evitar límites de búsquedas de LHC y producir la densidad reliquia correcta.

Para estudiar la fenomenología del modelo, primero despejamos el parámetro g_B en términos de los otros (m_χ, m_S and $m_{Z'}$) exigiendo que la densidad reliquia sea la correcta. Luego, analizamos los límites experimentales del modelo. Por construcción, el acoplamiento de la Z' con los quarks es vectorial, mientras que elegimos un acoplamiento axial con la materia oscura. Esta configuración implica una sección eficaz de detección directa dependiente del spin y suprimida con la velocidad, lo cual es prácticamente invisible para búsquedas de detección directa. Por otro lado, la leptofobia del mediador relaja las restricciones de búsquedas de di-leptones. No obstante, dependiendo de la mezcla entre las dos simetrías $U(1)$ el acoplamiento efectivo con los leptones puede ser considerable. De hecho, incluso considerando una mezcla nula a una determinada escala ultravioleta, correcciones radiativas pueden desarrollar una mezcla considerable. Además de estos límites, también incluimos límites por producción de mono-jets y di-jets en el LHC.

En las Figs. 5.6 y 5.7 vemos el efecto de estos límites en el espacio de parámetros, para dos elecciones diferentes de la escala ultravioleta donde la mezcla es nula. El límite más fuerte viene de búsquedas de di-jets, lo que se traduce en fuertes restricciones en la masa del mediador Z' entre 500 GeV y 3 TeV. El límite se vuelve menos restrictivo si el escalar, S, es ligero y juega un papel en la fenomenología, por ejemplo $m_S = 2$ TeV, como se muestra en los paneles inferiores de las Figs. 5.6 y 5.7, donde valores altos de la masa de la materia oscura están a salvo de las búsquedas de di-jets.

Las búsquedas en colisionadores son la manera más natural de probar este modelo, explorando áreas que están ahora permitidas. Además, los fermiones extra están cargados, por tanto, si su masa son del mismo orden que la materia oscura, podrían producir fenomenología interesante en colisionadores que podría ayudar a testar el modelo como también efectos de coaniquilación en el universo temprano.

Para concluir, modelos simplificados de materia oscura (como el portal de Higgs con un escalar singlete o el modelo simplificado del portal Z') son una buena primera aproximación al problema de la materia oscura. Sin embargo, son probablemente demasiado simples, ya que estan fuertemente limitados por búsquedas experimentales y, por otro lado, no hay motivo alguno para pensar que el sector oscuro está compuesto de solo una partícula. Por tanto, es natural considerar un sector oscuro más grande, como se muestra en los dos modelos analizados en esta tesis. Las partículas extra pueden relajar las restricciones impuestas en los modelos simplificados y dar una fenomenología más rica accesible en los experimentos, especialmente en colisionadores. Por todo esto, merece la pena seguir estudiando diferentes posibilidades de una teoría última para un modelo de materia oscura, esperando una señal positiva por parte de los experimentos.

Appendix A

Radiative contributions to the $S_1 S_1 h$ vertex

In this appendix we compute the dominant radiative contributions for relevant physical processes involving DM in the context of the ESHP model, defined by the Lagrangian of eq.(4.2). We will do it in the framework of the EW symmetry broken theory.

Assuming, for simplicity and convenience, a small λ_2 coupling, as has been done throughout the chapter 4, the most important radiative corrections are those contributing to the $S_1 S_1 h$ vertex, in particular the three 1-loop diagrams depicted in Fig. 4.4. This vertex plays a crucial role for a number of DM processes; namely DM annihilation in the early universe, direct and indirect DM detection, and contributions to the invisible width of the Higgs boson. Other relevant DM processes, in particular $S_1 S_1 \to hh$, receive radiative corrections as well, but they are much smaller than the contribution from the tree-level diagram in which a S_2 particle is exchanged in $t-$channel, see Fig. 4.3.

Therefore, in order to evaluate radiative corrections, the relevant terms of the Lagrangian in the broken phase are

$$\mathcal{L} \supset -\frac{1}{4!}\lambda h^4 - \frac{1}{3!}\lambda_1 v h^3 - \frac{1}{2}\lambda_{12} S_1 S_2 h^2 - \lambda_{12} v S_1 S_2 h - \frac{1}{3!}\lambda_{31} S_1^3 S_2 \ . \tag{A.1}$$

In the following we will compute them, using the conventions of Ref. [352] for Feynman rules.

Let us start with the one-loop diagrams involving two propagators (second and third diagrams of Fig. 4.4). Their contribution to the vertex is given by

$$\frac{iv}{16\pi^2}\left[\lambda_{31}\lambda_{12} B_0(p_h^2; m_{S_1}, m_{S_2}) + \lambda_{12}^2 \left(B_0(p_{S_1}^2; m_{S_2}, m_h) + B_0(p_{S_1'}^2; m_{S_2}, m_h)\right)\right] \ , \tag{A.2}$$

where p_{S_1} and $p_{S_1'}$ represent the momenta of the two S_1 particles entering the vertex, and

$$B_0(p^2, m_1, m_2) = (\text{Divergent part}) + \mathcal{B}(p^2, m_1, m_2) \ , \tag{A.3}$$

with

$$\mathcal{B}(p^2, m_1, m_2) = -\int_0^1 dx \log \frac{x m_1^2 + (1-x) m_2^2 - x(1-x)p^2}{m_1 m_2} \ . \tag{A.4}$$

In our case, the divergent part and the momentum-independent piece of $\mathcal{B}(p^2, m_1, m_2)$ can be absorbed in the renormalized value of λ_1. Moreover, $\mathcal{B}(p^2, m_1, m_2)$ can be expanded in powers of the momentum, as

$$\mathcal{B}(p^2, m_1, m_2) = 1 - \frac{m_1^2 + m_2^2}{m_1^2 - m_2^2} \log \frac{m_1}{m_2} + p^2 F(m_1, m_2) + \mathcal{O}(p^4) \ , \tag{A.5}$$

with

$$F(m_1, m_2) = \frac{m_1^4 - m_2^4 - 2m_1^2 m_2^2 \log \frac{m_1^2}{m_2^2}}{2(m_1^2 - m_2^2)^3} \ . \tag{A.6}$$

Keeping just the term proportional to p^2 turns out to be a good approximation in most cases (recall here that the $p-$independent terms in Eq. (A.5) are absorbed in a finite renormalization of λ_1). Hence, a good approximation for the contribution to the $S_1 S_1 h$ vertex from the one-loop diagrams involving two propagators is

$$\Gamma^{(2)} \simeq \frac{iv}{16\pi^2} \left[\lambda_{31}\lambda_{12} p_h^2 F(m_{S_1}, m_{S_2}) + \lambda_{12}^2 (p_{S_1}^2 + p_{S_1'}^2) F(m_{S_2}, m_h) \right] \ . \tag{A.7}$$

Alternatively, this contribution to the vertex can be viewed as the Feynman rule stemming from the corresponding term in the effective action, namely

$$16\pi^2 \Delta^{(2)} \mathcal{L} = -\frac{1}{2} \lambda_{31}\lambda_{12} v F(m_{S_1}, m_{S_2}) \ S^2 \partial^2 h - \lambda_{12}^2 v \, F(m_{S_2}, m_h) \ S(\partial^2 S) h \ . \tag{A.8}$$

This is a convenient way to encode these contributions in the MicrOMEGAs code, as we have done throughout the chapter.

Let us now consider the one-loop diagrams involving three propagators (fourth diagram of Fig. 4.4). The main difference with the previous two diagrams is that this represents a finite contribution which should be entirely counted, even the momentum-independent contribution, since the latter corresponds to a $S_1^2 |H|^4$ operator in the unbroken theory and cannot be absorbed in a finite renormalization of λ_1. Using the same momentum expansion as before, the corresponding contribution to the $S_1 S_1 h$ vertex reads

$$\Gamma^{(3)} \simeq \frac{i}{16\pi^2} \lambda_{12}^2 \lambda v^3 \left[F_3(m_{S_2}, m_h, m_h) \right. \tag{A.9}$$

$$\left. + (p_{S_1}^2 + p_{S_1'}^2) G(m_{S_2}, m_h, m_h) + p_h^2 G(m_h, m_h, m_{S_2}) \right] , \tag{A.10}$$

with

$$
\begin{aligned}
F_3(m_1,m_1,m_2) &= -\frac{m_1^2-m_2^2-m_2^2\log\frac{m_1^2}{m_2^2}}{(m_1^2-m_2^2)^2}\ , \\
G(m_1,m_1,m_2) &= -\frac{m_1^6-6m_1^4m_2^2+3m_1^2m_2^4+2m_2^6+6m_1^2m_2^4\log\left(\frac{m_1^2}{m_2^2}\right)}{12m_1^2(m_1^2-m_2^2)^4}\ , \\
G(m_1,m_2,m_1) &= -\frac{m_1^4+4m_1^2m_2^2-5m_2^4-2m_2^2(2m_1^2+m_2^2)\log\left(\frac{m_1^2}{m_2^2}\right)}{4(m_1^2-m_2^2)^4}\ .
\end{aligned}
\tag{A.11}
$$

The corresponding terms in the effective action read

$$
\begin{aligned}
16\pi^2\Delta^{(3)}\mathcal{L} &= \frac{1}{2}\lambda_{12}^2\lambda v^3\Big[\ F_3(m_{S_2},m_h,m_h)\ S^2h \\
&\quad -2G(m_{S_2},m_h,m_h)S(\partial^2S)h - G(m_h,m_h,m_{S_2})\ S^2\partial^2h\ \Big]\ .
\end{aligned}
\tag{A.12}
$$

Appendix B

Anomaly-free completions of $U(1)_B$

As discussed in Section 5.1 any consistent leptophobic, flavour-blind, $U(1)_{Y'}$ group must be equivalent to baryonic number, $U(1)_B$, in the SM sector. Furthermore, anomaly-cancellation requires the presence of extra particles. Then, assuming that the DM particle, χ, is a fermion with vanishing hypercharge, the minimal content of the dark sector contains an additional doublet, ψ and an additional singlet, η:

$$\text{minimal dark sector}: \quad \{\chi_{L,R},\ \psi_{L,R},\ \eta_{L,R}\}, \tag{B.1}$$

In this appendix we fully classify the possible assignments of Y, Y' to these fields, consistent with anomaly-cancellation, paying special attention to the axial cases. Notice that the requirement of non-fractional electric charges implies $Y_\psi = m + 1/2, Y_\eta = n$, with m, n integers, a condition that we will assume in what follows.

A useful observation is that the anomaly-cancelation conditions, listed in the equations (5.5-5.11), are invariant under the three independent transformations:

$$Y_{\psi,\eta} \to -Y_{\psi,\eta}, \tag{B.2}$$

$$Y'_{(\psi,\eta)_L} \leftrightarrow -Y'_{(\psi,\eta)_R}, \tag{B.3}$$

$$Y'_{\chi_L} \leftrightarrow -Y'_{\chi_R}. \tag{B.4}$$

Hence, in general the solutions to the anomaly-cancellation conditions come in sets of 8 possibilities related by these transformations.

B.1 Classification of solutions

In this section we will derive the possible values of the extra hypercharges (Y') of the fields in the dark sector (B.1) for any choice of Y_ψ, Y_η.

From Eqs.(5.5-5.8) we can solve $Y'_{\psi_L}, Y'_{\eta_L}, Y'_{\chi_L}$ in terms of the other charges:

$$\begin{aligned} Y'_{\psi_L} &= Y'_{\psi_R} - 3 \\ Y'_{\eta_L} &= Y'_{\eta_R} + \frac{3}{2Y_\eta^2}(1+4Y_\psi^2) \\ Y'_{\chi_L} &= Y'_{\chi_R} - \frac{3}{2Y_\eta^2}(1+4Y_\psi^2) + 6 \end{aligned} \tag{B.5}$$

The value of Y'_{η_R} can be derived from Eq.(5.9), which, thanks to Eqs.(B.5) becomes linear in Y'_{ψ_R}:

$$Y'_{\eta_R} = \frac{2Y_\eta(-3+2Y'_{\psi_R})}{1+4Y_\psi^2} - \frac{3(1+4Y_\psi^2)}{4Y_\eta^2} \tag{B.6}$$

So far we have expressed $Y'_{\psi_L}, Y'_{\eta_L}, Y'_{\chi_L}, Y'_{\eta_R}$ in terms of $Y_\psi, Y_\eta, Y'_{\psi_R}, Y'_{\chi_R}$. Now, for a given choice of Y_ψ, Y_η, the values of Y'_{ψ_R}, Y'_{χ_R} are related by the only remaining anomaly-cancelation condition, namely Eq.(5.11), which, thanks to Eqs.(B.5) becomes quadratic in the unknowns:

$$\begin{aligned} \frac{1}{32Y_\eta^6(1+4Y_\psi^2)} \quad & \big\{9(-16Y_\eta^4(6+Y'_{\chi_R})^2)(1+4Y_\psi^2)^2 + 24Y_\eta^2(6+Y'_{\chi_R}))(1+4Y_\psi^2)^3 - 9(1+4Y_\psi^2)^4 \\ & -64Y_\eta^6(9-(-3+Y'_{\psi_R})Y'_{\psi_R} + 45Y_\psi^2 + Y'_{\chi_R}(6+Y'_{\chi_R}))(1+4Y_\psi^2))\big\} = 0 \end{aligned} \tag{B.7}$$

Consequently, one would expect that for any choice of Y_ψ, Y_η there is a continuum of solutions. Still one has to require that these solutions are real. Let us examine closely this issue. Solving Y'_{χ_R} in Eq.(B.7) gives

$$Y'_{\chi_R} = 3\left(-1+\frac{1+4Y_\psi^2}{4Y_\eta^2}\right) \pm \frac{\sqrt{D}}{4Y_\eta^2(1+4Y_\psi^2)(-1+4Y_\eta^2-4Y_\psi^2)} \tag{B.8}$$

with

$$\begin{aligned} D = \; & -\frac{1}{Y_\eta^6}(-1+4Y_\eta^2-4Y_\psi^2)(1+4Y_\psi^2) \\ & \times \left[-16Y_\eta^4((-3+Y'_{\psi_R})Y'_{\psi_R} - 9Y_\psi) + 9(1+4Y_\psi^2)^3 - 36(Y_\eta + 4Y_\eta Y_\psi^2)^2\right] \end{aligned} \tag{B.9}$$

Obviously, real solutions correspond to $D \geq 0$. Let us note that the extremal point of the quadratic expression (B.9) always lies at $Y'_{\psi_R} = 3/2$ (this is a consequence of the symmetry (B.3) and the first equation of (B.5)). At this extremal point D reads

$$D^{\text{extr}} = -\frac{9}{Y_\eta^6}(-1+4Y_\eta^2-4Y_\psi^2)(1+4Y_\psi^2)(1-2Y_\eta^2+4Y_\psi^2)^2 \tag{B.10}$$

On the other hand, the coefficient of $(Y'_{\psi_R})^2$ in (B.9) reads

$$\frac{16}{Y_\eta^2}(-1+4Y_\eta^2-4Y_\psi^2)(1+4Y_\psi^2) \tag{B.11}$$

Since expressions (B.10) and (B.11) have opposite signs, it turns out that for any choice of Y_ψ, Y_η there is indeed a continuum of values of Y'_{ψ_R} that lead to real solutions:

$$\text{If } -1+4Y_\eta^2-4Y_\psi^2>0, \qquad Y'_{\psi_R}\le Y'^{\,(1)}_{\psi_R} \quad \& \quad Y'_{\psi_R}\ge Y'^{\,(2)}_{\psi_R}$$

$$\text{If } -1+4Y_\eta^2-4Y_\psi^2<0, \qquad Y'^{\,(1)}_{\psi_R}\le Y'_{\psi_R}\le Y'^{\,(2)}_{\psi_R}$$

where

$$Y'^{\,(1,2)}_{\psi_R}=\frac{3}{2}\mp\frac{3|1-2Y_\eta^2+4Y_\psi^2|}{4Y_\eta^2}\sqrt{(1+4Y_\psi^2)} \tag{B.12}$$

Then, for each allowed value of Y'_{ψ_R}, the corresponding value of Y'_{χ_R} is given by Eq.(B.8).

B.2 Special Choices of Y_ψ, Y_η

There are four special choices of Y_ψ, Y_η that lead to a substantial simplification of the solutions and, besides, allow for generic rational solutions. Namely, for

$$\{\pm Y_\psi,\pm Y_\eta\}=\left\{\frac{1}{2},1\right\},\left\{\frac{7}{2},5\right\}\ , \tag{B.13}$$

Eqs.(B.5) become

$$\begin{aligned} Y'_{\psi_L} &= Y'_{\psi_R}-3,\\ Y'_{\eta_L} &= Y'_{\eta_R}+3,\\ Y'_{\chi_L} &= Y'_{\chi_R}+3. \end{aligned} \tag{B.14}$$

The value of Y'_{η_R} becomes

$$\begin{aligned} Y'_{\eta_R}&=\frac{1}{8}(-24+8Y'_{\psi_R}), \quad \text{for} \quad \{\pm Y_\psi,\pm Y_\eta\}=\left\{\frac{1}{2},1\right\},\\ Y'_{\eta_R}&=\frac{1}{5}(-18+7Y'_{\psi_R}), \quad \text{for} \quad \{\pm Y_\psi,\pm Y_\eta\}=\left\{\frac{7}{2},5\right\}. \end{aligned} \tag{B.15}$$

The value of Y'_{χ_R}, Eq.(B.8), gets also drastically simplified:

$$Y'_{\chi_R}=-3+Y'_{\psi_R},\quad -Y'_{\psi_R}\ , \qquad \text{for} \quad \{\pm Y_\psi,\pm Y_\eta\}=\left\{\frac{1}{2},1\right\},$$

$$Y'_{\chi_R} = \frac{1}{5}(-6 - Y'_{\psi_R}), \quad \frac{1}{5}(-9 + Y'_{\psi_R}) \quad , \qquad \text{for} \quad \{\pm Y_\psi, \pm Y_\eta\} = \left\{\frac{7}{2}, 5\right\}. \tag{B.16}$$

Note that, in each case, the two solutions for Y'_{χ_R} are related by the symmetry (B.4) and Eq.(B.14).

A crucial consequence of the previous equations is that, in the special cases (B.13), for any rational choice of Y'_{ψ_R}, the rest of the $Y'-$charges become rational as well. This cannot be guaranteed for any other choice of Y_ψ, Y_η. As a matter of fact, in general it does not hold, except by accident. In Table B.1 we list accidental rational possibilities, which do not belong to the special choices (B.13).

Y_ψ	Y_η	Y'_{ψ_L}	Y'_{ψ_R}	Y'_{η_L}	Y'_{η_R}	Y'_{χ_L}	Y'_{χ_R}
3/2	1	-9	0	-9	-6	3	-12
3/2	1	3/8	75/8	3/8	27/8	69/8	-51/8
3/2	2	3/8	-15/8	3/8	27/8	33/8	3/8
3/2	3	5/3	-8/3	-4	-1	-11/3	-16/3

Table B.1: Accidental rational solutions to the anomaly equations. For each case, there are seven additional solutions, which can be obtained by using the transformations (B.2-B.4).

Some of the previous features come from the fact that the special choices (B.13) are the only ones for which $1 - 2Y_\eta^2 + 4Y_\psi^2 = 0$. This also implies that $D^{\text{extr}} = 0$ in Eq.(B.10). Since, on the other hand, $-1+4Y_\eta^2-4Y_\psi^2 > 0$, it turns out that all values of Y'_{ψ_R} are allowed, in particular all rationals.

B.3 Axial coupling of the dark matter

In this section we particularise to the case where the coupling of the extra gauge boson to the dark matter is axial, i.e.

$$Y'_{\chi_L} = -Y'_{\chi_R}. \tag{B.17}$$

Let us start by noting that the two generic solutions of Y'_{χ_R} given in Eq.(B.8) are related by the symmetry transformation (B.4). Therefore, the axial case (B.17) occurs when the two solutions coincide, i.e. when $D = 0$. This happens precisely for $Y'_{\psi_R} = Y'^{(1)}_{\psi_R}, Y'^{(2)}_{\psi_R}$, given in Eq.(B.12).

Consequently, for any choice of Y_ψ, Y_η, there are two solutions of axial DM, with Y'_{ψ_R} given by Eq.(B.12); Y'_{χ_R}, given by Eq.(B.8), which in this case simplifies to

$$Y'_{\chi_R} = 3\left(-1 + \frac{1 + 4Y_\psi^2}{4Y_\eta^2}\right) \tag{B.18}$$

and the remaining charges given by Eqs.(B.5, B.6).

Notice that the two values $Y'^{(1)}_{\psi_R}, Y'^{(2)}_{\psi_R}$ are symmetrical with respect to $Y'_{\psi_R} = 3/2$ (as implied by the symmetry (B.2) and Eq.(B.5)). This means that the solutions are *not* axial for the other dark fields, ψ and η, *except* in the special cases (B.13), where $Y'^{(1)}_{\psi_R} = Y'^{(2)}_{\psi_R} = 3/2$. For each of these special cases there is a unique axial solution, which, in addition, is axial in all the dark fields as well. These are the ones given in Eq.(5.12) of the Sec. 5.2. Note also that these are the only axial solutions whose charges are rational.

Appendix C

$Z - Z'$ mixing

C.1 Kinetic mixing

The presence of an extra $U(1)$ symmetry in the gauge symmetry group allows kinetic terms mixing the corresponding gauge fields. In this Appendix we discuss the diagonalization of the gauge bosons. For the case of a gauge group $SU(3)_C \times SU(2)_L \times U(1)_Y \times U(1)_{Y'}$, where in our case $U(1)_{Y'}$ corresponds to the baryonic number, the Lagrangian involving the two gauge bosons and the kinetic mixing is given by

$$\mathcal{L}_{\text{kin}} \supset -\frac{1}{4}\, F^{Y}_{\mu\nu}\, F^{Y\mu\nu} - \frac{1}{4}\, F^{Y'}_{\mu\nu}\, F^{Y'\mu\nu} - \frac{1}{2}\, \epsilon\, F^{Y}_{\mu\nu}\, F^{Y'\mu\nu}, \tag{C.1}$$

where ϵ is the kinetic mixing and $F^{Y,Y'}_{\mu\nu} = \partial_\mu A^{Y,Y'}_\nu - \partial_\nu A^{Y,Y'}_\mu$ are the field strengths.

With a simple rotation of $\pi/4$, we can eliminate the kinetic mixing of the two gauge fields,

$$\begin{pmatrix} A^{Y}_{\mu} \\ A^{Y'}_{\mu} \end{pmatrix} = \frac{1}{\sqrt{2}} \begin{pmatrix} 1 & -1 \\ 1 & 1 \end{pmatrix} \begin{pmatrix} \bar{B}^{1}_{\mu} \\ \bar{B}^{2}_{\mu} \end{pmatrix}, \tag{C.2}$$

leaving a Lagrangian after the rotation as

$$\mathcal{L}_{\text{kin}} \supset -\frac{1-\epsilon}{4}\, F^{\bar{1}}_{\mu\nu}\, F^{\bar{1}\mu\nu} - \frac{1+\epsilon}{4}\, F^{\bar{2}}_{\mu\nu}\, F^{\bar{2}\mu\nu}. \tag{C.3}$$

Now we re-escale the vector-boson fields to normalize the gauge terms,

$$\begin{pmatrix} \bar{B}^{1}_{\mu} \\ \bar{B}^{2}_{\mu} \end{pmatrix} = \begin{pmatrix} \frac{1}{\sqrt{1-\epsilon}} & 0 \\ 0 & \frac{1}{\sqrt{1+\epsilon}} \end{pmatrix} \begin{pmatrix} B^{1}_{\mu} \\ B^{2}_{\mu} \end{pmatrix}, \tag{C.4}$$

So the total transformation is given by the matrix $\mathcal{R}_\epsilon$,

$$\begin{pmatrix} A_\mu^Y \\ A_\mu^{Y'} \end{pmatrix} = \frac{1}{\sqrt{2}} \begin{pmatrix} \frac{1}{\sqrt{1-\epsilon}} & -\frac{1}{\sqrt{1+\epsilon}} \\ \frac{1}{\sqrt{1-\epsilon}} & \frac{1}{\sqrt{1+\epsilon}} \end{pmatrix} \begin{pmatrix} B_\mu^1 \\ B_\mu^2 \end{pmatrix} = \mathcal{R}_\epsilon \begin{pmatrix} B_\mu^1 \\ B_\mu^2 \end{pmatrix}, \tag{C.5}$$

and the Lagrangian in the new basis (B^1, B^2) after the previous rotation reads,

$$\mathcal{L}_{\text{kin}} \supset -\frac{1}{4} F^1_{\mu\nu}\, F^{1\mu\nu} - \frac{1}{4} F^2_{\mu\nu}\, F^{2\mu\nu}. \tag{C.6}$$

The interaction terms of the original Lagrangian were in the covariant derivatives,

$$\mathcal{D}^\mu = \partial^\mu + i Q^T G A^\mu, \tag{C.7}$$

where $Q^T = (q_Y\ q'_Y)$ is the charge array, $G = \text{diag}(g_Y, g_{Y'})$ with $g_{Y,Y'}$ the original couplings and $A_\mu^T = (A_\mu^Y\ A_\mu^{Y'})$. Applying the previous rotation, Eq. (C.5), the interaction terms in the new basis read

$$\mathcal{D}^\mu = \partial^\mu + i Q^T G \mathcal{R}_\epsilon \bar{B}^\mu = \partial^\mu + i Q^T G' \bar{B}^\mu, \tag{C.8}$$

where $\bar{B}_\mu^T = (B_\mu^1\ B_\mu^2)$ and

$$G' = G\mathcal{R}_\epsilon = \begin{pmatrix} g_{11} & g_{12} \\ g_{21} & g_{22} \end{pmatrix}. \tag{C.9}$$

It is convenient for the calculations to introduce a rotation matrix

$$O_R = \frac{1}{\sqrt{g_{22}^2 + g_{21}^2}} \begin{pmatrix} g_{22} & -g_{21} \\ g_{21} & g_{22} \end{pmatrix}. \tag{C.10}$$

Applying this rotation to the interaction terms we can parametrize the coupling matrix G in terms of three couplings as follows

$$\mathcal{D}^\mu = \partial^\mu + i Q^T G' O_R^T O_R \bar{B}^\mu = \partial^\mu + i Q^T \tilde{G} B^\mu, \tag{C.11}$$

with

$$\tilde{G} = G' O_R^T = \begin{pmatrix} g' & \tilde{g} \\ 0 & g_B \end{pmatrix}. \tag{C.12}$$

and

$$B_\mu = \begin{pmatrix} B_\mu \\ B'_\mu \end{pmatrix} = O_R \begin{pmatrix} B_\mu^1 \\ B_\mu^2 \end{pmatrix}. \tag{C.13}$$

The new couplings, g', $\tilde{g}$ and g_B are related to the original couplings $g_{Y,Y'}$ by

$$g' = g_Y, \quad \tilde{g} = \frac{g_Y \epsilon}{\sqrt{1-\epsilon^2}}, \quad g_B = \frac{g_{Y'}}{\sqrt{1-\epsilon^2}}. \tag{C.14}$$

Therefore, for the gauge symmetry group $SU(3)_C \times SU(2)_L \times U(1)_Y \times U(1)_{Y'}$, assuming the kinetic mixing between the two $U(1)$ symmetries, the covariant derivative in the new basis is given by

$$\mathcal{D}_\mu = \partial_\mu + i g_S T^a G^a_\mu + i g t^a W^a_\mu + i g' Y B_\mu + i(\tilde{g} Y + g_B Y') B'_\mu. \tag{C.15}$$

Looking at Eq. (C.14) we can see that in the case of a null kinetic mixing parameter, $\epsilon = 0$, the new coupling $\tilde{g}$ becomes zero and the couplings g' and g_B recover the original values g_Y and $g_{Y'}$, respectively, as expected.

C.2 Scalar sector and spontaneous symmetry breaking

Now we focus on the scalar potential. In our model we require the existence of an extra scalar to give masses to the extra vector boson and the new fermions. Now the scalar sector is composed by the Higgs boson, H, and the new complex scalar, S. The most general Lagrangian is the following

$$V(H,S) = \mu^2 H^\dagger H + m_S S^\dagger S + \lambda (H^\dagger H)^2 + \lambda_S (S^\dagger S)^2 + \lambda_{HS} (H^\dagger H)(S^\dagger S). \tag{C.16}$$

The stability of the potential is achieved if the conditions $\lambda > 0$, $\lambda_S > 0$ and $4\lambda\lambda_S - \lambda_{HS}^2 > 0$ are accomplished. To give masses to the fermions and vector bosons both symmetries must be broken and the two scalars acquire a vacuum expectation value

$$\langle H \rangle = \frac{1}{\sqrt{2}} \begin{pmatrix} 0 \\ v \end{pmatrix}, \qquad \langle S \rangle = \frac{v_S}{\sqrt{2}}, \tag{C.17}$$

which can be related with the parameters of the Lagrangian in Eq. (C.16) through the minimization conditions

$$v^2 = \frac{2 m_S^2 \lambda_{HS} - 4\mu^2 \lambda_S}{4\lambda\lambda_S - \lambda_{HS}}, \qquad v_S^2 = \frac{2\mu^2 \lambda_{HS} - 4 m_S^2 \lambda}{4\lambda\lambda_S - \lambda_{HS}}. \tag{C.18}$$

After the symmetry breaking, the mass matrix for the scalars is

$$m^2_{scalar} = \begin{pmatrix} 2\lambda v^2 & \lambda_{HS} v v_S \\ \lambda_{HS} v v_S & 2\lambda_S v_S^2 \end{pmatrix}, \tag{C.19}$$

which can be diagonalized by a simple rotation to a new scalar basis (h_1 h_2)

$$\begin{pmatrix} h_1 \\ h_2 \end{pmatrix} = \frac{1}{\sqrt{2}} \begin{pmatrix} \cos\theta & -\sin\theta \\ \sin\theta & \cos\theta \end{pmatrix} \begin{pmatrix} H \\ S \end{pmatrix}. \tag{C.20}$$

The masses of the new eigenstates are given by

$$m^2_{h_{1,2}} = \lambda v^2 + \lambda_S v_S^2 \mp \sqrt{(\lambda v^2 - \lambda_S v_S^2)^2 + (\lambda_{HS} v v_S)^2}, \tag{C.21}$$

and the rotation angle θ is

$$\tan 2\theta = \frac{\lambda_{HS} v v_S}{\lambda v^2 - \lambda_S v_S^2}. \tag{C.22}$$

With simple calculations we can express the original parameters λ, λ_S and λ_{HS} in terms of the masses and the angle

$$\begin{aligned} \lambda &= \frac{1}{4v^2}(m^2_{h_1}(1+\cos 2\theta) + m^2_{h_2}(1-\cos 2\theta)), \\ \lambda_S &= \frac{1}{4v_S^2}(m^2_{h_1}(1-\cos 2\theta) + m^2_{h_2}(1+\cos 2\theta)), \\ \lambda_{HS} &= \sin 2\theta \left(\frac{m^2_{h_2} - m^2_{h_1}}{2 v v_S}\right). \end{aligned} \tag{C.23}$$

After spontaneous symmetry breaking we can obtain the mass matrix for the neutral gauge bosons from the Lagrangian terms,

$$\left(\frac{g}{2}W^2_\mu - \frac{g'}{2}B_\mu - \frac{\tilde{g}}{2}B'_\mu\right)^2 \frac{v^2}{2} + \left(g_B Y'_S B'_\mu\right)^2 \frac{v_S^2}{2}. \tag{C.24}$$

Then, we can diagonalize the mass matrix to obtain the mass eigenstates with a rotation matrix of the form

$$\begin{pmatrix} B^\mu \\ W^\mu_3 \\ B'^\mu \end{pmatrix} = \begin{pmatrix} \cos\theta_\omega & -\sin\theta_\omega \cos\theta' & \sin\theta_\omega \sin\theta' \\ \sin\theta_\omega & \cos\theta_\omega \cos\theta' & -\cos\theta_\omega \sin\theta' \\ 0 & \sin\theta' & \cos\theta' \end{pmatrix} \begin{pmatrix} A^\mu \\ Z^\mu \\ Z'^\mu \end{pmatrix} \tag{C.25}$$

where θ_ω is the Weinberg angle and θ' is given by

$$\tan 2\theta' = \frac{2\tilde{g}\sqrt{g^2 + g'^2}}{\tilde{g}^2 + (2 g_B Y'_S v_S/v)^2 - g^2 - g'^2} \tag{C.26}$$

With this rotation we obtain a massless vector boson which corresponds to the photon, A, and two massive vector bosons, the SM Z boson and the new Z', with masses

$$m^2_{Z,Z'} = (g^2 + g'^2)\frac{v^2}{8}\left[1 + \frac{\tilde{g} + 4g_B Y'_S v_S^2/v^2}{g^2 + g'^2} \mp \frac{2\tilde{g}}{\sqrt{g^2 + g'^2}\sin 2\theta'}\right] \tag{C.27}$$

LEP experiment [353] imposes a severe bound on this angle θ', $|\theta'| \lesssim 10^{-3}$, so we can approximate the expression for the mixing angle,

$$\theta' \simeq \epsilon \sin\theta_\omega \frac{m_Z^2}{m_{Z'}^2 - m_Z^2}, \tag{C.28}$$

and the vector boson masses,

$$m_Z^2 \simeq \frac{v^2}{4}(g^2 + g'^2), \qquad m_{Z'}^2 \simeq \frac{v^2}{4}(\tilde{g}^2 + (2g_B Y'_S v_S/v)^2). \tag{C.29}$$

Notice that with this approximation the mass of the Z boson is the usual SM one.

Agradecimientos

Qué mejor manera de terminar esta tesis que se ha gestado durante cuatro años que dando las gracias a todas esas personas que me han acompañado y ayudado en el viaje y que sin ellos no hubiese sido posible recorrerlo.

Empezando por Alberto. Cuando empecé en el doctorado era prácticamente un analfabeto en esto de la física teórica y la investigación y tengo que agradecerte tu infinita paciencia, especialmente durante el inicio. Me has inculcado muchas cosas durante estos cuatro años y he aprendido y disfrutado muchísimo trabajando contigo. Y además valoro mucho todas las veces que me has apoyado y animado cuando yo era demasiado crítico con el trabajo o conmigo mismo. Y por todo esto te tengo que dar las gracias.

En segundo lugar me tengo que acordar de la gente con la que más he trabajado y de la cual he aprendido muchísimo durante este tiempo. Por un lado, Jesús, gracias por todo, especialmente por toda la ayuda durante la primera mitad del doctorado en la que trabajamos juntos. Gracias a ti aprendí a ser mucho más riguroso de lo que era con mi trabajo. A David, que me introdujiste en el mundo de la materia oscura, gracias por tu entusiasmo, da gusto trabajar con gente tan positiva. Y por supuesto a Roberto, gracias por toda la ayuda que me has dado durante la última mitad del doctorado, trabajar contigo ha sido un verdadero placer y tengo que agradecerte tu paciencia, sobretodo en temas de computación que en ocaciones ha sido una odisea y siempre me has ayudado muchísimo.

Los primeros agradecimientos fuera del apartado laboral que quiero dar es sin duda para Xabi y Josu. Gracias por acoger al tío raro y asustado que casi no hablaba cuando llegó al IFT y hacerle sentir uno más desde el primer momento. Sois dos espejos donde mirarse y ejemplos a seguir. Gracias por todos esos momentos en los que intentabais hacerme creer que no era el único que se sentía imbécil en este trabajo, aunque me costaba y sigue costando creer que a vosotros os pase, la verdad. Y por supuesto valoro muchísimo que no todo fuese trabajo en ese despacho. Gracias por los videos de los Simpson, memes, pochas (saludos del último rey) y demás risas echadas en ese despacho. Y también los esfuerzos para que me pusiese en forma, tanto de Xabi con el fútbol o Josu con el gimnasio. Se os ha echado de menos este último periodo de tesis. Eso sí, lo del phenocoffee no te lo perdonaré jamás Xabi, jamás.

Y cuando me dejaron solo en ese despacho entró al rescate Claudia. Aunque no hemos coincidido mucho en este año y medio me gustaría agradecerte todo lo que has hecho por mí. Gracias por toda la ayuda, que ha sido mucha, desde preguntas de física dignas de un chaval de la ESO, hasta de habla tanto en ingles (todos recordamos ese *encodes* salvador) como en castellano, y computacionales, porque ese Feynrules no corría ni aunque me fuese la vida en ello y tuviste que venir tu a solucionarlo. Gracias por todo el apoyo también, que no ha sido poco. Por todas las risas durante la hora de la comida y en el despacho. Por las escobas a falta de pochas. Por el día de depositar el troncho este, en el que evité el tabardillo de milagro. Y mucho más. Y por encima de todo, gracias por todo lo no relacionado con el trabajo, tanto dentro como fuera del IFT, de verdad.

El siguiente en llegar fue Gallego, con su alegría innata. Siempre con un buenos días al llegar (al llegar yo, porque creo que no hubo un día que llegase yo antes que tú). Gracias por todo el apoyo y por tener el despacho calentito en invierno cuando llegábamos. Un placer haber coincido contigo.

Y además de estos cuatro del 413, hay más gente del IFT que me ha acompañado durante estos años. Empezando por Aitor. Ese Euro-Leicester fue mítico. Gracias por no matar a El Nuevo, porque sinceramente hubiese sido un marrón importante. Deberíamos de haber escrito algún tipo de diario de esos dos años con esos dos personajes, queda pendiente. Y Uga, el otro accionista de casa Sushi y broncaner número dos. A ver si consigues llevarme a escalar, no desistas.

Gracias a los que me acogisteis al llegar, en especial a Victor, que aunque poco coincidimos me ayudaste en los comienzos, especialmente con Micromegas, y Ander, por las risas, las pochas y las partidas de ping-pong. Y a los que llegasteis después, Guille, Salva, Judit, Fernando, Álvaro, Raquel, Roberto y todos los que me dejo.

Sin olvidar a todas la gente que trabaja en el IFT y que me ha hecho la vida mas fácil. Principalmente a Isabel, Mónica Encinas, Mónica Vergel, Rebeca y María Hortal, que han tenido que aguantar que en cada viaje subiese a preguntar por el 14A y demás burocracia.

Por otro lado, hay mucha gente que me ha acompañado en la distancia. Y aquí tengo que empezar por Rubén. Doctorados paralelos, aunque a ti no te engañaron y te fuiste a ganar panoja. Comenzamos el doctorado con grandes ilusiones y sue nos y los hemos mantenido juntos hasta el final. Los ánimos constantes, especialmente a primera hora de la mañana, los memes y tweets puntuales para desconectar brevemente y demás momentos son de agradecer. La siguiente visita es en Segovia a que me pagues el cochinillo y después a Hawaii.

Gracias a Nicolás y Gabriel, lástima que se acaben los ratos en vuestro piso y los cines pero bueno, ahora habrá que ir a Lisboa. A Marina por todo el apoyo siempre con todo y por el tiempo que coincidimos durante tu máster en la capital, te echo de menos por allí. A Núria por el apoyo y sacar un ratito cada vez que vuelvo un finde para vernos. Y a Violeta por el apoyo y los ratos en Madrid que afortunadamente han vuelto.

Y para acabar, gracias a la familia. Porque no había comida familiar en el que no cayese un "¿pero tú trabajas?" o un "¿y allí que haces?". No sé si al final os habréis enterado de qué es lo que hago o al menos de que trata lo que estudio pero gracias por todo el apoyo durante este tiempo.

Bibliography

[1] A. Pich, in *Fundamental physics: Selected topics on high-energy and astroparticle physics. Proceedings, 25th International Winter Meeting, Formigal, Spain, March 3-7, 1997* (1997) pp. 1–30, arXiv:hep-ph/9711279 [hep-ph]

[2] F. W. Bessel, Mon. Not. Roy. Astron. Soc. **6**, 136 (1844)

[3] Kelvin, B. (1904), Baltimore lectures on molecular dynamics and the wave theory of light, https://archive.org/details/baltimorelecture00kelviala,

[4] Poincare, H. (1906), L' Astronomie , 158.,

[5] E. Öpik. 1915. Bull. de la Soc. Astr. de Russie 21, 150.,

[6] E. Hubble and M. L. Humason, Astrophys. J. **74**, 43 (1931)

[7] F. Zwicky, Helv. Phys. Acta **6**, 110 (1933), [Gen. Rel. Grav.41,207(2009)]

[8] V. C. Rubin and W. K. Ford, Jr., Astrophys. J. **159**, 379 (1970)

[9] K. G. Begeman, A. H. Broeils, and R. H. Sanders, Mon. Not. Roy. Astron. Soc. **249**, 523 (1991)

[10] F. Zwicky, Astrophys. J. **86**, 217 (1937)

[11] J. Bekenstein and M. Milgrom, Astrophys. J. **286**, 7 (1984)

[12] D. Clowe, M. Bradac, A. H. Gonzalez, M. Markevitch, S. W. Randall, C. Jones, and D. Zaritsky, Astrophys. J. **648**, L109 (2006), arXiv:astro-ph/0608407 [astro-ph]

[13] A. N. Taylor, S. Dye, T. J. Broadhurst, N. Benitez, and E. van Kampen, Astrophys. J. **501**, 539 (1998), arXiv:astro-ph/9801158 [astro-ph]

[14] D. Clowe, A. Gonzalez, and M. Markevitch, Astrophys. J. **604**, 596 (2004), arXiv:astro-ph/0312273 [astro-ph]

[15] U. G. Briel and J. P. Henry, (1997), arXiv:astro-ph/9711237 [astro-ph]

[16] N. Jarosik *et al.*, Astrophys. J. Suppl. **192**, 14 (2011), arXiv:1001.4744 [astro-ph.CO]

[17] http://www.esa.int/spaceinimages/Images/2013/03/Planck_CMB,

[18] R. K. Sachs and A. M. Wolfe, Astrophys. J. **147**, 73 (1967), [Gen. Rel. Grav.39,1929(2007)]

[19] D. J. Eisenstein *et al.* (SDSS), Astrophys. J. **633**, 560 (2005), arXiv:astro-ph/0501171 [astro-ph]

[20] P. A. R. Ade *et al.* (Planck), Astron. Astrophys. **594**, A13 (2016), arXiv:1502.01589 [astro-ph.CO]

[21] J. R. Bond, G. Efstathiou, and J. Silk, Phys. Rev. Lett. **45**, 1980 (1980), [,61(1980)]

[22] A. G. Doroshkevich, Y. B. Zeldovich, R. A. Sunyaev, and M. Khlopov, Sov. Astron. Lett. **6**, 252 (1980), [Pisma Astron. Zh.6,457(1980)]

[23] D. N. Schramm and G. Steigman., Astrophysical Journal, 243:1, January 1981. doi: 10.1086/158559.

[24] B. Zeldovich, J. Einasto, and S. F. Shandarin., Nature, 300: 407?413, December 1982. doi: 10.1038/300407a0.

[25] J. R. Bond and A. S. Szalay., Astrophysical Journal, 274:443?468, November 1983. doi: 10.1086/161460.

[26] S. D. M. White, C. S. Frenk, and M. Davis, Astrophys. J. **274**, L1 (1983), [,80(1984)]

[27] S. Dodelson and L. M. Widrow, Phys. Rev. Lett. **72**, 17 (1994), arXiv:hep-ph/9303287 [hep-ph]

[28] P. Langacker, (1989)

[29] K. Abazajian, G. M. Fuller, and M. Patel, Phys. Rev. **D64**, 023501 (2001), arXiv:astro-ph/0101524 [astro-ph]

[30] A. Merle, A. Schneider, and M. Totzauer, JCAP **1604**, 003 (2016), arXiv:1512.05369 [hep-ph]

[31] A. Kusenko, Phys. Rev. Lett. **97**, 241301 (2006), arXiv:hep-ph/0609081 [hep-ph]

[32] K. Petraki and A. Kusenko, Phys. Rev. **D77**, 065014 (2008), arXiv:0711.4646 [hep-ph]

[33] A. Merle, V. Niro, and D. Schmidt, JCAP **1403**, 028 (2014), arXiv:1306.3996 [hep-ph]

[34] A. Merle and M. Totzauer, JCAP **1506**, 011 (2015), arXiv:1502.01011 [hep-ph]

[35] S. L. Glashow, Nucl. Phys. **22**, 579 (1961)

[36] A. Salam, *8th Nobel Symposium Lerum, Sweden, May 19-25, 1968*, Conf. Proc. **C680519**, 367 (1968)

[37] S. Weinberg, Phys. Rev. Lett. **19**, 1264 (1967)

[38] A. Strumia and F. Vissani, (2006), arXiv:hep-ph/0606054 [hep-ph]

[39] S. Weinberg, Phys. Rev. Lett. **43**, 1566 (1979)

[40] M. Gell-Mann, P. Ramond, and R. Slansky, *Supergravity Workshop Stony Brook, New York, September 27-28, 1979*, Conf. Proc. **C790927**, 315 (1979), arXiv:1306.4669 [hep-th]

[41] P. Minkowski, Phys. Lett. **67B**, 421 (1977)

[42] R. N. Mohapatra and G. Senjanovic, Phys. Rev. Lett. **44**, 912 (1980), [,231(1979)]

[43] T. Yanagida, Prog. Theor. Phys. **64**, 1103 (1980)

[44] C. A. Baker *et al.*, Phys. Rev. Lett. **97**, 131801 (2006), arXiv:hep-ex/0602020 [hep-ex]

[45] R. D. Peccei and H. R. Quinn, Phys. Rev. **D16**, 1791 (1977)

[46] R. D. Peccei and H. R. Quinn, Phys. Rev. Lett. **38**, 1440 (1977), [,328(1977)]

[47] S. Weinberg, Phys. Rev. Lett. **40**, 223 (1978)

[48] F. Wilczek, Phys. Rev. Lett. **40**, 279 (1978)

[49] R. Eichler *et al.* (SINDRUM), Phys. Lett. **B175**, 101 (1986)

[50] M. S. Turner, *BNL Workshop: Axions 1989:0001-38*, Phys. Rept. **197**, 67 (1990)

[51] G. G. Raffelt, Phys. Rept. **198**, 1 (1990)

[52] D. A. Dicus, E. W. Kolb, V. L. Teplitz, and R. V. Wagoner, Phys. Rev. **D18**, 1829 (1978)

[53] D. A. Dicus, E. W. Kolb, V. L. Teplitz, and R. V. Wagoner, Phys. Rev. **D22**, 839 (1980)

[54] G. G. Raffelt and D. S. P. Dearborn, Phys. Rev. **D36**, 2211 (1987)

[55] D. S. P. Dearborn, D. N. Schramm, and G. Steigman, Phys. Rev. Lett. **56**, 26 (1986), [,276(1985)]

[56] J. R. Ellis and K. A. Olive, Phys. Lett. **B193**, 525 (1987)

[57] H.-T. Janka, W. Keil, G. Raffelt, and D. Seckel, Phys. Rev. Lett. **76**, 2621 (1996), arXiv:astro-ph/9507023 [astro-ph]

[58] W. Keil, H.-T. Janka, D. N. Schramm, G. Sigl, M. S. Turner, and J. R. Ellis, Phys. Rev. **D56**, 2419 (1997), arXiv:astro-ph/9612222 [astro-ph]

[59] G. Raffelt and D. Seckel, Phys. Rev. Lett. **60**, 1793 (1988)

[60] M. S. Turner, Phys. Rev. Lett. **60**, 1797 (1988)

[61] B. Patt and F. Wilczek, (2006), arXiv:hep-ph/0605188 [hep-ph]

[62] D. Feldman, Z. Liu, and P. Nath, Phys. Rev. **D75**, 115001 (2007), arXiv:hep-ph/0702123 [HEP-PH]

[63] A. Falkowski, J. Juknevich, and J. Shelton, (2009), arXiv:0908.1790 [hep-ph]

[64] B. Batell, M. Pospelov, and A. Ritz, Phys. Rev. **D80**, 095024 (2009), arXiv:0906.5614 [hep-ph]

[65] P. Crivelli, A. Belov, U. Gendotti, S. Gninenko, and A. Rubbia, JINST **5**, P08001 (2010), arXiv:1005.4802 [hep-ex]

[66] X. Chu, T. Hambye, and M. H. G. Tytgat, JCAP **1205**, 034 (2012), arXiv:1112.0493 [hep-ph]

[67] R. Essig *et al.*, in *Proceedings, 2013 Community Summer Study on the Future of U.S. Particle Physics: Snowmass on the Mississippi (CSS2013): Minneapolis, MN, USA, July 29-August 6, 2013* (2013) arXiv:1311.0029 [hep-ph]

[68] W.-Z. Feng, G. Shiu, P. Soler, and F. Ye, JHEP **05**, 065 (2014), arXiv:1401.5890 [hep-ph]

[69] W.-Z. Feng, G. Shiu, P. Soler, and F. Ye, Phys. Rev. Lett. **113**, 061802 (2014), arXiv:1401.5880 [hep-ph]

[70] Y. Bai and J. Berger, JHEP **08**, 153 (2014), arXiv:1402.6696 [hep-ph]

[71] K. Blum, M. Cliche, C. Csaki, and S. J. Lee, JHEP **03**, 099 (2015), arXiv:1410.1873 [hep-ph]

[72] J. F. Cherry, A. Friedland, and I. M. Shoemaker, (2014), arXiv:1411.1071 [hep-ph]

[73] G. Arcadi, Y. Mambrini, and F. Richard, JCAP **1503**, 018 (2015), arXiv:1411.2985 [hep-ph]

[74] JHEP **05**, 036 (2017), arXiv:1701.08134 [hep-ph]

[75] JHEP **08**, 004 (2015), arXiv:1501.03799 [hep-ph]

[76] Phys. Rev. **D90**, 114018 (2014), arXiv:1406.1043 [hep-ph]

[77] T. Robens and T. Stefaniak, Eur. Phys. J. **C75**, 104 (2015), arXiv:1501.02234 [hep-ph]

[78] A. Falkowski, C. Gross, and O. Lebedev, JHEP **05**, 057 (2015), arXiv:1502.01361 [hep-ph]

[79] M. Escudero, A. Berlin, D. Hooper, and M.-X. Lin, JCAP **1612**, 029 (2016), arXiv:1609.09079 [hep-ph]

[80] C. Coriano, L. Delle Rose, and C. Marzo, JHEP **02**, 135 (2016), arXiv:1510.02379 [hep-ph]

[81] E. Gildener and S. Weinberg, Phys. Rev. **D13**, 3333 (1976)

[82] S. Weinberg, Phys. Rev. **D13**, 974 (1976), [Addendum: Phys. Rev.D19,1277(1979)]

[83] E. Gildener, Phys. Rev. **D14**, 1667 (1976)

[84] L. Susskind, Phys. Rev. **D20**, 2619 (1979)

[85] G. 't Hooft, C. Itzykson, A. Jaffe, H. Lehmann, P. K. Mitter, I. M. Singer, and R. Stora, NATO Sci. Ser. B **59**, pp.1 (1980)

[86] J.-L. Gervais and B. Sakita, Nucl. Phys. **B34**, 632 (1971), [,154(1971)]

[87] Yu. A. Golfand and E. P. Likhtman, JETP Lett. **13**, 323 (1971), [Pisma Zh. Eksp. Teor. Fiz.13,452(1971)]

[88] J. Wess and B. Zumino, Nucl. Phys. **B70**, 39 (1974), [,24(1974)]

[89] C. Regis *et al.* (Super-Kamiokande), Phys. Rev. **D86**, 012006 (2012), arXiv:1205.6538 [hep-ex]

[90] G. R. Farrar and P. Fayet, Phys. Lett. **76B**, 575 (1978)

[91] P. Fayet, Nucl. Phys. **B90**, 104 (1975)

[92] P. Fayet, Phys. Lett. **69B**, 489 (1977)

[93] A. Salam and J. A. Strathdee, Nucl. Phys. **B87**, 85 (1975)

[94] H. Goldberg, Phys. Rev. Lett. **50**, 1419 (1983), [,219(1983)]

[95] J. R. Ellis, J. S. Hagelin, D. V. Nanopoulos, and M. Srednicki, Phys. Lett. **127B**, 233 (1983)

[96] J. R. Ellis, J. S. Hagelin, D. V. Nanopoulos, K. A. Olive, and M. Srednicki, *Particle physics and cosmology: Dark matter*, Nucl. Phys. **B238**, 453 (1984), [,223(1983)]

[97] L. M. Krauss, Nucl. Phys. **B227**, 556 (1983)

[98] L. E. Ibanez, Phys. Lett. **137B**, 160 (1984)

[99] J. S. Hagelin, G. L. Kane, and S. Raby, Nucl. Phys. **B241**, 638 (1984)

[100] P. Gondolo and G. Gelmini, Nucl. Phys. **B360**, 145 (1991)

[101] D. G. Cerdeno and A. M. Green, , 347 (2010), arXiv:1002.1912 [astro-ph.CO]

[102] R. Agnese *et al.* (SuperCDMS), Phys. Rev. Lett. **112**, 241302 (2014), arXiv:1402.7137 [hep-ex]

[103] R. Agnese *et al.* (SuperCDMS), Phys. Rev. **D97**, 022002 (2018), arXiv:1707.01632 [astro-ph.CO]

[104] G. Angloher *et al.* (CRESST), Eur. Phys. J. **C76**, 25 (2016), arXiv:1509.01515 [astro-ph.CO]

[105] F. Petricca *et al.* (CRESST), in *15th International Conference on Topics in Astroparticle and Underground Physics (TAUP 2017) Sudbury, Ontario, Canada, July 24-28, 2017* (2017) arXiv:1711.07692 [astro-ph.CO]

[106] D. S. Akerib *et al.* (LUX), Phys. Rev. Lett. **118**, 021303 (2017), arXiv:1608.07648 [astro-ph.CO]

[107] X. Cui *et al.* (PandaX-II), Phys. Rev. Lett. **119**, 181302 (2017), arXiv:1708.06917 [astro-ph.CO]

[108] E. Aprile *et al.* (XENON), Phys. Rev. Lett. **121**, 111302 (2018), arXiv:1805.12562 [astro-ph.CO]

[109] R. Agnese *et al.* (SuperCDMS), Phys. Rev. **D95**, 082002 (2017), arXiv:1610.00006 [physics.ins-det]

[110] D. S. Akerib *et al.* (LUX-ZEPLIN), (2018), arXiv:1802.06039 [astro-ph.IM]

[111] J. Billard, L. Strigari, and E. Figueroa-Feliciano, Phys. Rev. **D89**, 023524 (2014), arXiv:1307.5458 [hep-ph]

[112] T. R. Slatyer, in *Proceedings, Theoretical Advanced Study Institute in Elementary Particle Physics : Anticipating the Next Discoveries in Particle Physics (TASI 2016): Boulder, CO, USA, June 6-July 1, 2016* (2018) pp. 297–353, arXiv:1710.05137 [hep-ph]

[113] J. Rico, M. Wood, A. Drlica-Wagner, and J. Aleksi? (MAGIC, Fermi-LAT), *Proceedings, 34th International Cosmic Ray Conference (ICRC 2015): The Hague, The Netherlands, July 30-August 6, 2015*, PoS **ICRC2015**, 1206 (2016), arXiv:1508.05827 [astro-ph.HE]

[114] L. Oakes, A. Viana, E. M. Cea, L. Rinchiuso, U. Schwanke, M. Cirelli, P. Panci, F. Sala, J. Silk, and M. Taoso (HESS), *The Fluorescence detector Array of Single-pixel Telescopes: Contributions to the 35th International Cosmic Ray Conference (ICRC 2017)*, PoS **ICRC2017**, 905 (2018), [35,905(2017)], arXiv:1708.04858 [astro-ph.HE]

[115] M. Ackermann *et al.* (Fermi-LAT), Astrophys. J. **840**, 43 (2017), arXiv:1704.03910 [astro-ph.HE]

[116] M. G. Aartsen *et al.* (IceCube), Eur. Phys. J. **C78**, 831 (2018), arXiv:1804.03848 [astro-ph.HE]

[117] A. Albert *et al.* (ANTARES), (2017), arXiv:1711.01496 [astro-ph.IM]

[118] M. Aguilar *et al.* (AMS 01), Phys. Lett. **B646**, 145 (2007), arXiv:astro-ph/0703154 [ASTRO-PH]

[119] M. Aguilar *et al.* (AMS), Phys. Rev. Lett. **110**, 141102 (2013)

[120] O. Adriani *et al.* (PAMELA), Nature **458**, 607 (2009), arXiv:0810.4995 [astro-ph]

[121] F. Kahlhoefer, Int. J. Mod. Phys. **A32**, 1730006 (2017), arXiv:1702.02430 [hep-ph]

[122] U. Haisch, F. Kahlhoefer, and E. Re, JHEP **12**, 007 (2013), arXiv:1310.4491 [hep-ph]

[123] M. Aaboud *et al.* (ATLAS), JHEP **06**, 059 (2016), arXiv:1604.01306 [hep-ex]

[124] C. Collaboration (CMS), (2016)

[125] G. Aad *et al.* (ATLAS), JHEP **11**, 099 (2011), arXiv:1110.2299 [hep-ex]

[126] A. M. Sirunyan *et al.* (CMS), JHEP **03**, 061 (2017), [Erratum: JHEP09,106(2017)], arXiv:1701.02042 [hep-ex]

[127] V. Khachatryan *et al.* (CMS), Phys. Rev. **D91**, 092005 (2015), arXiv:1408.2745 [hep-ex]

[128] G. Aad *et al.* (ATLAS), JHEP **09**, 037 (2014), arXiv:1407.7494 [hep-ex]

[129] G. Aad *et al.* (ATLAS), Phys. Rev. Lett. **115**, 131801 (2015), arXiv:1506.01081 [hep-ex]

[130] C. Collaboration (CMS), (2017)

[131] T. A. collaboration (ATLAS), (2016)

[132] G. Aad *et al.* (ATLAS), Phys. Rev. **D93**, 072007 (2016), arXiv:1510.06218 [hep-ex]

[133] M. Aaboud *et al.* (ATLAS), Phys. Lett. **B765**, 11 (2017), arXiv:1609.04572 [hep-ex]

[134] C. Collaboration (CMS), (2016)

[135] T. Lin, E. W. Kolb, and L.-T. Wang, Phys. Rev. **D88**, 063510 (2013), arXiv:1303.6638 [hep-ph]

[136] C. Arina *et al.*, JHEP **11**, 111 (2016), arXiv:1605.09242 [hep-ph]

[137] C. Collaboration (CMS), (2016)

[138] U. Haisch and E. Re, JHEP **06**, 078 (2015), arXiv:1503.00691 [hep-ph]

[139] U. Haisch, P. Pani, and G. Polesello, JHEP **02**, 131 (2017), arXiv:1611.09841 [hep-ph]

[140] J. Andrea, B. Fuks, and F. Maltoni, Phys. Rev. **D84**, 074025 (2011), arXiv:1106.6199 [hep-ph]

[141] V. Khachatryan *et al.* (CMS), JHEP **02**, 135 (2017), arXiv:1610.09218 [hep-ex]

[142] G. Aad *et al.* (ATLAS), Eur. Phys. J. **C75**, 337 (2015), arXiv:1504.04324 [hep-ex]

[143] G. Aad *et al.* (ATLAS), JHEP **11**, 206 (2015), arXiv:1509.00672 [hep-ex]

[144] V. Silveira and A. Zee, Phys. Lett. **161B**, 136 (1985)

[145] J. McDonald, Phys. Rev. **D50**, 3637 (1994), arXiv:hep-ph/0702143 [HEP-PH]

[146] C. P. Burgess, M. Pospelov, and T. ter Veldhuis, Nucl. Phys. **B619**, 709 (2001), arXiv:hep-ph/0011335 [hep-ph]

[147] H. Davoudiasl, R. Kitano, T. Li, and H. Murayama, Phys. Lett. **B609**, 117 (2005), arXiv:hep-ph/0405097 [hep-ph]

[148] V. Barger, P. Langacker, M. McCaskey, M. J. Ramsey-Musolf, and G. Shaughnessy, Phys. Rev. **D77**, 035005 (2008), arXiv:0706.4311 [hep-ph]

[149] R. N. Lerner and J. McDonald, Phys. Rev. **D80**, 123507 (2009), arXiv:0909.0520 [hep-ph]

[150] B. Grzadkowski and J. Wudka, Phys. Rev. Lett. **103**, 091802 (2009), arXiv:0902.0628 [hep-ph]

[151] B. Feldstein, A. L. Fitzpatrick, and E. Katz, JCAP **1001**, 020 (2010), arXiv:0908.2991 [hep-ph]

[152] S. Chang, A. Pierce, and N. Weiner, Phys. Rev. **D79**, 115011 (2009), arXiv:0808.0196 [hep-ph]

[153] K. R. Dienes, J. Kumar, B. Thomas, and D. Yaylali, Phys. Rev. **D90**, 015012 (2014), arXiv:1312.7772 [hep-ph]

[154] J. Fan, M. Reece, and L.-T. Wang, JCAP **1011**, 042 (2010), arXiv:1008.1591 [hep-ph]

[155] J. B. Dent, B. Dutta, J. L. Newstead, and L. E. Strigari, Phys. Rev. **D93**, 075018 (2016), arXiv:1602.05300 [hep-ph]

[156] V. Gluscevic, M. I. Gresham, S. D. McDermott, A. H. G. Peter, and K. M. Zurek, JCAP **1512**, 057 (2015), arXiv:1506.04454 [hep-ph]

[157] J. Kumar and D. Marfatia, Phys. Rev. **D88**, 014035 (2013), arXiv:1305.1611 [hep-ph]

[158] C. Savage, G. Gelmini, P. Gondolo, and K. Freese, JCAP **0904**, 010 (2009), arXiv:0808.3607 [astro-ph]

[159] X.-G. He, T. Li, X.-Q. Li, J. Tandean, and H.-C. Tsai, Phys. Rev. **D79**, 023521 (2009), arXiv:0811.0658 [hep-ph]

[160] M. Farina, D. Pappadopulo, and A. Strumia, Phys. Lett. **B688**, 329 (2010), arXiv:0912.5038 [hep-ph]

[161] A. Bandyopadhyay, S. Chakraborty, A. Ghosal, and D. Majumdar, JHEP **11**, 065 (2010), arXiv:1003.0809 [hep-ph]

[162] X.-G. He and J. Tandean, JHEP **12**, 074 (2016), arXiv:1609.03551 [hep-ph]

[163] V. Bonnivard, C. Combet, D. Maurin, and M. G. Walker, Mon. Not. Roy. Astron. Soc. **446**, 3002 (2015), arXiv:1407.7822 [astro-ph.HE]

[164] K. Ichikawa, M. N. Ishigaki, S. Matsumoto, M. Ibe, H. Sugai, K. Hayashi, and S.-i. Horigome, Mon. Not. Roy. Astron. Soc. **468**, 2884 (2017), arXiv:1608.01749 [astro-ph.GA]

[165] N. Klop, F. Zandanel, K. Hayashi, and S. Ando, Phys. Rev. **D95**, 123012 (2017), arXiv:1609.03509 [astro-ph.CO]

[166] S. Ipek, D. McKeen, and A. E. Nelson, Phys. Rev. **D90**, 055021 (2014), arXiv:1404.3716 [hep-ph]

[167] T. Daylan, D. P. Finkbeiner, D. Hooper, T. Linden, S. K. N. Portillo, N. L. Rodd, and T. R. Slatyer, Phys. Dark Univ. **12**, 1 (2016), arXiv:1402.6703 [astro-ph.HE]

[168] D. Hooper and L. Goodenough, Phys. Lett. **B697**, 412 (2011), arXiv:1010.2752 [hep-ph]

[169] D. Hooper and T. Linden, Phys. Rev. **D84**, 123005 (2011), arXiv:1110.0006 [astro-ph.HE]

[170] L. Goodenough and D. Hooper, (2009), arXiv:0910.2998 [hep-ph]

[171] K. N. Abazajian and M. Kaplinghat, Phys. Rev. **D86**, 083511 (2012), [Erratum: Phys. Rev.D87,129902(2013)], arXiv:1207.6047 [astro-ph.HE]

[172] C. Gordon and O. Macias, Phys. Rev. **D88**, 083521 (2013), [Erratum: Phys. Rev.D89,no.4,049901(2014)], arXiv:1306.5725 [astro-ph.HE]

[173] M. Ajello *et al.* (Fermi-LAT), Astrophys. J. **819**, 44 (2016), arXiv:1511.02938 [astro-ph.HE]

[174] A. Berlin, D. Hooper, and G. Krnjaic, Phys. Rev. **D94**, 095019 (2016), arXiv:1609.02555 [hep-ph]

[175] A. De Simone, G. F. Giudice, and A. Strumia, JHEP **06**, 081 (2014), arXiv:1402.6287 [hep-ph]

[176] D. Hooper, C. Kelso, and F. S. Queiroz, Astropart. Phys. **46**, 55 (2013), arXiv:1209.3015 [astro-ph.HE]

[177] M. Ackermann *et al.* (Fermi-LAT), Phys. Rev. Lett. **115**, 231301 (2015), arXiv:1503.02641 [astro-ph.HE]

[178] JCAP **1509**, 023 (2015), arXiv:1504.04276 [astro-ph.HE]

[179] M. Cirelli and G. Giesen, JCAP **1304**, 015 (2013), arXiv:1301.7079 [hep-ph]

[180] A. Berlin, D. Hooper, and S. D. McDermott, Phys. Rev. **D89**, 115022 (2014), arXiv:1404.0022 [hep-ph]

[181] JHEP **06**, 008 (2016), arXiv:1510.07562 [hep-ph]

[182] A. Beniwal, F. Rajec, C. Savage, P. Scott, C. Weniger, M. White, and A. G. Williams, Phys. Rev. **D93**, 115016 (2016), arXiv:1512.06458 [hep-ph]

[183] S. Profumo, L. Ubaldi, and C. Wainwright, Phys. Rev. **D82**, 123514 (2010), arXiv:1009.5377 [hep-ph]

[184] F. S. Sage and R. Dick, (2016), arXiv:1604.04589 [astro-ph.HE]

[185] M. Duerr, P. Fileviez Perez, and J. Smirnov, Phys. Lett. **B751**, 119 (2015), arXiv:1508.04418 [hep-ph]

[186] JCAP **1606**, 050 (2016), arXiv:1603.08228 [hep-ph]

[187] Phys. Rev. **D90**, 055026 (2014), arXiv:1407.0174 [hep-ph]

[188] JHEP **06**, 152 (2016), arXiv:1509.04282 [hep-ph]

[189] H. Han and S. Zheng, Nucl. Phys. **B914**, 248 (2017), arXiv:1510.06165 [hep-ph]

[190] J. Kozaczuk and T. A. W. Martin, JHEP **04**, 046 (2015), arXiv:1501.07275 [hep-ph]

[191] X.-G. He, T. Li, X.-Q. Li, and H.-C. Tsai, *Proceedings, 3rd International Symposium on Cosmological and particle astrophysics (CosPA 2006): Taipei, Taiwan, November 15-17, 2006*, Mod. Phys. Lett. **A22**, 2121 (2007), arXiv:hep-ph/0701156 [hep-ph]

[192] A. Djouadi, A. Falkowski, Y. Mambrini, and J. Quevillon, Eur. Phys. J. **C73**, 2455 (2013), arXiv:1205.3169 [hep-ph]

[193] N. Craig, H. K. Lou, M. McCullough, and A. Thalapillil, JHEP **02**, 127 (2016), arXiv:1412.0258 [hep-ph]

[194] P. Ko and H. Yokoya, JHEP **08**, 109 (2016), arXiv:1603.04737 [hep-ph]

[195] H. Han, J. M. Yang, Y. Zhang, and S. Zheng, Phys. Lett. **B756**, 109 (2016), arXiv:1601.06232 [hep-ph]

[196] A. A. Petrov and W. Shepherd, Phys. Lett. **B730**, 178 (2014), arXiv:1311.1511 [hep-ph]

[197] L. Carpenter, A. DiFranzo, M. Mulhearn, C. Shimmin, S. Tulin, and D. Whiteson, Phys. Rev. **D89**, 075017 (2014), arXiv:1312.2592 [hep-ph]

[198] M. Benito, N. Bernal, N. Bozorgnia, F. Calore, and F. Iocco, JCAP **1702**, 007 (2017), [Erratum: JCAP1806,no.06,E01(2018)], arXiv:1612.02010 [hep-ph]

[199] A. Tan *et al.* (PandaX-II), Phys. Rev. Lett. **117**, 121303 (2016), arXiv:1607.07400 [hep-ex]

[200] G. B. Gelmini and P. Gondolo, Phys. Rev. **D74**, 023510 (2006), arXiv:hep-ph/0602230 [hep-ph]

[201] J. M. Cline, K. Kainulainen, P. Scott, and C. Weniger, Phys. Rev. **D88**, 055025 (2013), [Erratum: Phys. Rev.D92,no.3,039906(2015)], arXiv:1306.4710 [hep-ph]

[202] F. S. Queiroz and K. Sinha, Phys. Lett. **B735**, 69 (2014), arXiv:1404.1400 [hep-ph]

[203] L. Feng, S. Profumo, and L. Ubaldi, JHEP **03**, 045 (2015), arXiv:1412.1105 [hep-ph]

[204] H. Wu and S. Zheng, JHEP **03**, 142 (2017), arXiv:1610.06292 [hep-ph]

[205] E. Aprile *et al.* (XENON), JCAP **1604**, 027 (2016), arXiv:1512.07501 [physics.ins-det]

[206] D. S. Akerib *et al.* (LZ), (2015), arXiv:1509.02910 [physics.ins-det]

[207] K. Ishiwata, Phys. Lett. **B710**, 134 (2012), arXiv:1112.2696 [hep-ph]

[208] A. Abada, D. Ghaffor, and S. Nasri, Phys. Rev. **D83**, 095021 (2011), arXiv:1101.0365 [hep-ph]

[209] K. P. Modak, D. Majumdar, and S. Rakshit, JCAP **1503**, 011 (2015), arXiv:1312.7488 [hep-ph]

[210] I. Brivio, M. B. Gavela, L. Merlo, K. Mimasu, J. M. No, R. del Rey, and V. Sanz, JHEP **04**, 141 (2016), arXiv:1511.01099 [hep-ph]

[211] N. Fonseca, R. Zukanovich Funchal, A. Lessa, and L. Lopez-Honorez, JHEP **06**, 154 (2015), arXiv:1501.05957 [hep-ph]

[212] T. Cohen, J. Kearney, A. Pierce, and D. Tucker-Smith, Phys. Rev. **D85**, 075003 (2012), arXiv:1109.2604 [hep-ph]

[213] C. Cheung and D. Sanford, JCAP **1402**, 011 (2014), arXiv:1311.5896 [hep-ph]

[214] F. Giacchino, A. Ibarra, L. Lopez Honorez, M. H. G. Tytgat, and S. Wild, JCAP **1602**, 002 (2016), arXiv:1511.04452 [hep-ph]

[215] S. Baek, P. Ko, and P. Wu, JHEP **10**, 117 (2016), arXiv:1606.00072 [hep-ph]

[216] G. Belanger and J.-C. Park, JCAP **1203**, 038 (2012), arXiv:1112.4491 [hep-ph]

[217] A. Biswas, D. Majumdar, A. Sil, and P. Bhattacharjee, JCAP **1312**, 049 (2013), arXiv:1301.3668 [hep-ph]

[218] S. Bhattacharya, P. Poulose, and P. Ghosh, JCAP **1704**, 043 (2017), arXiv:1607.08461 [hep-ph]

[219] A. Drozd, B. Grzadkowski, and J. Wudka, JHEP **04**, 006 (2012), [Erratum: JHEP11,130(2014)], arXiv:1112.2582 [hep-ph]

[220] I. M. Hierro, S. F. King, and S. Rigolin, Phys. Lett. **B769**, 121 (2017), arXiv:1609.02872 [hep-ph]

[221] K. Kawana, PTEP **2015**, 023B04 (2015), arXiv:1411.2097 [hep-ph]

[222] JHEP **02**, 045 (2017), arXiv:1606.01258 [hep-ph]

[223] Eur. Phys. J. **C77**, 397 (2017), arXiv:1607.02373 [hep-ph]

[224] S. Bhattacharya, S. Jana, and S. Nandi, Phys. Rev. **D95**, 055003 (2017), arXiv:1609.03274 [hep-ph]

[225] O. Fischer and J. J. van der Bij, Mod. Phys. Lett. **A26**, 2039 (2011)

[226] G. Arcadi, C. Gross, O. Lebedev, S. Pokorski, and T. Toma, Phys. Lett. **B769**, 129 (2017), arXiv:1611.09675 [hep-ph]

[227] K. Ghorbani and H. Ghorbani, Phys. Rev. **D93**, 055012 (2016), arXiv:1501.00206 [hep-ph]

[228] M. Pospelov, A. Ritz, and M. B. Voloshin, Phys. Lett. **B662**, 53 (2008), arXiv:0711.4866 [hep-ph]

[229] JCAP **1806**, 031 (2018), arXiv:1711.10957 [hep-ph]

[230] K. Kannike, Eur. Phys. J. **C76**, 324 (2016), [Erratum: Eur. Phys. J.C78,no.5,355(2018)], arXiv:1603.02680 [hep-ph]

[231] G. Aad *et al.* (ATLAS), JHEP **01**, 172 (2016), arXiv:1508.07869 [hep-ex]

[232] G. Aad *et al.* (ATLAS, CMS), JHEP **08**, 045 (2016), arXiv:1606.02266 [hep-ex]

[233] C. Collaboration (CMS), (2016)

[234] A. Belyaev, N. D. Christensen, and A. Pukhov, Comput. Phys. Commun. **184**, 1729 (2013), arXiv:1207.6082 [hep-ph]

[235] J. M. Alarcon, J. Martin Camalich, and J. A. Oller, Phys. Rev. **D85**, 051503 (2012), arXiv:1110.3797 [hep-ph]

[236] J. M. Alarcon, L. S. Geng, J. Martin Camalich, and J. A. Oller, Phys. Lett. **B730**, 342 (2014), arXiv:1209.2870 [hep-ph]

[237] L. Alvarez-Ruso, T. Ledwig, J. Martin Camalich, and M. J. Vicente-Vacas, Phys. Rev. **D88**, 054507 (2013), arXiv:1304.0483 [hep-ph]

[238] R. D. Young, *Proceedings, 30th International Symposium on Lattice Field Theory (Lattice 2012): Cairns, Australia, June 24-29, 2012*, PoS **LATTICE2012**, 014 (2012), arXiv:1301.1765 [hep-lat]

[239] A. Abdel-Rehim, C. Alexandrou, M. Constantinou, K. Hadjiyiannakou, K. Jansen, C. Kallidonis, G. Koutsou, and A. Vaquero Aviles-Casco (ETM), Phys. Rev. Lett. **116**, 252001 (2016), arXiv:1601.01624 [hep-lat]

[240] M. Duerr, F. Kahlhoefer, K. Schmidt-Hoberg, T. Schwetz, and S. Vogl, JHEP **09**, 042 (2016), arXiv:1606.07609 [hep-ph]

[241] G. Belanger, F. Boudjema, A. Pukhov, and A. Semenov, Comput. Phys. Commun. **185**, 960 (2014), arXiv:1305.0237 [hep-ph]

[242] Comput. Phys. Commun. **192**, 322 (2015), arXiv:1407.6129 [hep-ph]

[243] M. L. Ahnen *et al.* (MAGIC, Fermi-LAT), JCAP **1602**, 039 (2016), arXiv:1601.06590 [astro-ph.HE]

[244] M. Ackermann *et al.* (Fermi-LAT), Phys. Rev. **D91**, 122002 (2015), arXiv:1506.00013 [astro-ph.HE]

[245] J. F. Navarro, E. Hayashi, C. Power, A. Jenkins, C. S. Frenk, S. D. M. White, V. Springel, J. Stadel, and T. R. Quinn, Mon. Not. Roy. Astron. Soc. **349**, 1039 (2004), arXiv:astro-ph/0311231 [astro-ph]

[246] J. Einasto, Tartu. Astro. Obs. Publ., Vol. 36, p. 414-441

[247] J. F. Navarro, C. S. Frenk, and S. D. M. White, Astrophys. J. **462**, 563 (1996), arXiv:astro-ph/9508025 [astro-ph]

[248] J. F. Navarro, C. S. Frenk, and S. D. M. White, Astrophys. J. **490**, 493 (1997), arXiv:astro-ph/9611107 [astro-ph]

[249] D. Feldman, Z. Liu, and P. Nath, Phys. Rev. **D79**, 063509 (2009), arXiv:0810.5762 [hep-ph]

[250] M. Ibe, H. Murayama, and T. T. Yanagida, Phys. Rev. **D79**, 095009 (2009), arXiv:0812.0072 [hep-ph]

[251] W.-L. Guo and Y.-L. Wu, Phys. Rev. **D79**, 055012 (2009), arXiv:0901.1450 [hep-ph]

[252] D. Albornoz Vasquez, G. Belanger, and C. Boehm, Phys. Rev. **D84**, 095008 (2011), arXiv:1107.1614 [hep-ph]

[253] A. Chatterjee, D. Das, B. Mukhopadhyaya, and S. K. Rai, JCAP **1407**, 023 (2014), arXiv:1401.2527 [hep-ph]

[254] W. B. Atwood, A. A. Abdo, M. Ackermann, W. Althouse, B. Anderson, M. Axelsson et al., Astrophysical Journal 697 (June, 2009) 1071–1102

[255] V. Vitale and A. Morselli (Fermi-LAT), in *Fermi gamma-ray space telescope. Proceedings, 2nd Fermi Symposium, Washington, USA, November 2-5, 2009* (2009) arXiv:0912.3828 [astro-ph.HE]

[256] F. Calore, I. Cholis, and C. Weniger, JCAP **1503**, 038 (2015), arXiv:1409.0042 [astro-ph.CO]

[257] B. Zhou, Y.-F. Liang, X. Huang, X. Li, Y.-Z. Fan, L. Feng, and J. Chang, Phys. Rev. **D91**, 123010 (2015), arXiv:1406.6948 [astro-ph.HE]

[258] A. Boyarsky, D. Malyshev, and O. Ruchayskiy, Phys. Lett. **B705**, 165 (2011), arXiv:1012.5839 [hep-ph]

[259] M. Ackermann *et al.* (Fermi-LAT), Astrophys. J. **840**, 43 (2017), arXiv:1704.03910 [astro-ph.HE]

[260] M. Ackermann *et al.* (Fermi-LAT), Astrophys. J. **750**, 3 (2012), arXiv:1202.4039 [astro-ph.HE]

[261] JCAP **1712**, 040 (2017), arXiv:1709.10429 [hep-ph]

[262] A. McCann, Astrophys. J. **804**, 86 (2015), arXiv:1412.2422 [astro-ph.HE]

[263] N. Mirabal, Mon. Not. Roy. Astron. Soc. **436**, 2461 (2013), arXiv:1309.3428 [astro-ph.HE]

[264] J. Petrovi?, P. D. Serpico, and G. Zaharijas, JCAP **1502**, 023 (2015), arXiv:1411.2980 [astro-ph.HE]

[265] I. Cholis, D. Hooper, and T. Linden, JCAP **1506**, 043 (2015), arXiv:1407.5625 [astro-ph.HE]

[266] O. Macias, C. Gordon, R. M. Crocker, B. Coleman, D. Paterson, S. Horiuchi, and M. Pohl, Nat. Astron. **2**, 387 (2018), arXiv:1611.06644 [astro-ph.HE]

[267] R. M. O'Leary, M. D. Kistler, M. Kerr, and J. Dexter, (2015), arXiv:1504.02477 [astro-ph.HE]

[268] Q. Yuan and B. Zhang, JHEAp **3-4**, 1 (2014), arXiv:1404.2318 [astro-ph.HE]

[269] D. Gaggero, M. Taoso, A. Urbano, M. Valli, and P. Ullio, JCAP **1512**, 056 (2015), arXiv:1507.06129 [astro-ph.HE]

[270] T. A. Porter, G. Johannesson, and I. V. Moskalenko, Astrophys. J. **846**, 67 (2017), arXiv:1708.00816 [astro-ph.HE]

[271] E. Storm, C. Weniger, and F. Calore, JCAP **1708**, 022 (2017), arXiv:1705.04065 [astro-ph.HE]

[272] M. Ajello *et al.* (Fermi-LAT), Submitted to: Astrophys. J. (2017), arXiv:1705.00009 [astro-ph.HE]

[273] C. Eckner *et al.*, Astrophys. J. **862**, 79 (2018), arXiv:1711.05127 [astro-ph.HE]

[274] R. Bartels, E. Storm, C. Weniger, and F. Calore, Nat. Astron. **2**, 819 (2018), arXiv:1711.04778 [astro-ph.HE]

[275] JCAP **1805**, 058 (2018), arXiv:1708.06706 [astro-ph.HE]

[276] T. Linden, N. L. Rodd, B. R. Safdi, and T. R. Slatyer, Phys. Rev. **D94**, 103013 (2016), arXiv:1604.01026 [astro-ph.HE]

[277] D. Hooper and G. Mohlabeng, JCAP **1603**, 049 (2016), arXiv:1512.04966 [astro-ph.HE]

[278] D. Hooper and T. Linden, JCAP **1608**, 018 (2016), arXiv:1606.09250 [astro-ph.HE]

[279] D. Haggard, C. Heinke, D. Hooper, and T. Linden, JCAP **1705**, 056 (2017), arXiv:1701.02726 [astro-ph.HE]

[280] N. Okada and O. Seto, Phys. Rev. **D89**, 043525 (2014), arXiv:1310.5991 [hep-ph]

[281] A. Dutta Banik and D. Majumdar, Phys. Lett. **B743**, 420 (2015), arXiv:1408.5795 [hep-ph]

[282] P. Agrawal, B. Batell, P. J. Fox, and R. Harnik, JCAP **1505**, 011 (2015), arXiv:1411.2592 [hep-ph]

[283] D. Hooper, Phys. Rev. **D91**, 035025 (2015), arXiv:1411.4079 [hep-ph]

[284] A. Martin, J. Shelton, and J. Unwin, Phys. Rev. **D90**, 103513 (2014), arXiv:1405.0272 [hep-ph]

[285] P. Ko and Y. Tang, JCAP **1501**, 023 (2015), arXiv:1407.5492 [hep-ph]

[286] T. Mondal and T. Basak, Phys. Lett. **B744**, 208 (2015), arXiv:1405.4877 [hep-ph]

[287] L. Wang and X.-F. Han, Phys. Lett. **B739**, 416 (2014), arXiv:1406.3598 [hep-ph]

[288] M. Abdullah, A. DiFranzo, A. Rajaraman, T. M. P. Tait, P. Tanedo, and A. M. Wijangco, Phys. Rev. **D90**, 035004 (2014), arXiv:1404.6528 [hep-ph]

[289] D. G. Cerdeno, M. Peiro, and S. Robles, Phys. Rev. **D91**, 123530 (2015), arXiv:1501.01296 [hep-ph]

[290] J. M. Cline, G. Dupuis, Z. Liu, and W. Xue, Phys. Rev. **D91**, 115010 (2015), arXiv:1503.08213 [hep-ph]

[291] J.-C. Park, J. Kim, and S. C. Park, Phys. Lett. **B752**, 59 (2016), arXiv:1505.04620 [hep-ph]

[292] C.-H. Chen and T. Nomura, Phys. Lett. **B746**, 351 (2015), arXiv:1501.07413 [hep-ph]

[293] Y. G. Kim, K. Y. Lee, C. B. Park, and S. Shin, Phys. Rev. **D93**, 075023 (2016), arXiv:1601.05089 [hep-ph]

[294] S. Horiuchi, O. Macias, D. Restrepo, A. Rivera, O. Zapata, and H. Silverwood, JCAP **1603**, 048 (2016), arXiv:1602.04788 [hep-ph]

[295] M. Escudero, D. Hooper, and S. J. Witte, JCAP **1702**, 038 (2017), arXiv:1612.06462 [hep-ph]

[296] A. Dutta Banik, M. Pandey, D. Majumdar, and A. Biswas, Eur. Phys. J. **C77**, 657 (2017), arXiv:1612.08621 [hep-ph]

[297] P. Tunney, J. M. No, and M. Fairbairn, Phys. Rev. **D96**, 095020 (2017), arXiv:1705.09670 [hep-ph]

[298] M. Escudero, S. J. Witte, and D. Hooper, JCAP **1711**, 042 (2017), arXiv:1709.07002 [hep-ph]

[299] C. Amole *et al.* (PICO), Phys. Rev. Lett. **118**, 251301 (2017), arXiv:1702.07666 [astro-ph.CO]

[300] E. Aprile *et al.* (XENON), Phys. Rev. Lett. **119**, 181301 (2017), arXiv:1705.06655 [astro-ph.CO]

[301] M. Ackermann *et al.* (Fermi-LAT), Astrophys. J. **793**, 64 (2014), arXiv:1407.7905 [astro-ph.HE]

[302] R. Andrae, T. Schulze-Hartung, P. Melchior. Dos and don'ts of reduced chi-squared,

[303] T. Bringmann *et al.* (The GAMBIT Dark Matter Workgroup), Eur. Phys. J. **C77**, 831 (2017), arXiv:1705.07920 [hep-ph]

[304] W. A. Rolke, A. M. Lopez, and J. Conrad, Nucl. Instrum. Meth. **A551**, 493 (2005), arXiv:physics/0403059 [physics]

[305] P. Langacker, R. W. Robinett, and J. L. Rosner, Phys. Rev. **D30**, 1470 (1984)

[306] P. Langacker, Rev. Mod. Phys. **81**, 1199 (2009), arXiv:0801.1345 [hep-ph]

[307] P. Fileviez Perez and M. B. Wise, Phys. Rev. **D82**, 011901 (2010), [Erratum: Phys. Rev.D82,079901(2010)], arXiv:1002.1754 [hep-ph]

[308] M. T. Frandsen, F. Kahlhoefer, S. Sarkar, and K. Schmidt-Hoberg, JHEP **09**, 128 (2011), arXiv:1107.2118 [hep-ph]

[309] M. Duerr, P. Fileviez Perez, and M. B. Wise, Phys. Rev. Lett. **110**, 231801 (2013), arXiv:1304.0576 [hep-ph]

[310] M. Duerr and P. Fileviez Perez, Phys. Lett. **B732**, 101 (2014), arXiv:1309.3970 [hep-ph]

[311] A. Alves, S. Profumo, and F. S. Queiroz, JHEP **04**, 063 (2014), arXiv:1312.5281 [hep-ph]

[312] G. Arcadi, Y. Mambrini, M. H. G. Tytgat, and B. Zaldivar, JHEP **03**, 134 (2014), arXiv:1401.0221 [hep-ph]

[313] O. Lebedev and Y. Mambrini, Phys. Lett. **B734**, 350 (2014), arXiv:1403.4837 [hep-ph]

[314] M. Duerr and P. Fileviez Perez, Phys. Rev. **D91**, 095001 (2015), arXiv:1409.8165 [hep-ph]

[315] P. Fileviez Perez, Phys. Rept. **597**, 1 (2015), arXiv:1501.01886 [hep-ph]

[316] M. Duerr, P. Fileviez Perez, and J. Smirnov, Phys. Rev. **D93**, 023509 (2016), arXiv:1508.01425 [hep-ph]

[317] F. Kahlhoefer, K. Schmidt-Hoberg, T. Schwetz, and S. Vogl, JHEP **02**, 016 (2016), arXiv:1510.02110 [hep-ph]

[318] T. Jacques, A. Katz, E. Morgante, D. Racco, M. Rameez, and A. Riotto, JHEP **10**, 071 (2016), arXiv:1605.06513 [hep-ph]

[319] M. Fairbairn, J. Heal, F. Kahlhoefer, and P. Tunney, JHEP **09**, 018 (2016), arXiv:1605.07940 [hep-ph]

[320] G. Arcadi, M. D. Campos, M. Lindner, A. Masiero, and F. S. Queiroz, Phys. Rev. **D97**, 043009 (2018), arXiv:1708.00890 [hep-ph]

[321] P. Fileviez Perez, S. Ohmer, and H. H. Patel, Phys. Lett. **B735**, 283 (2014), arXiv:1403.8029 [hep-ph]

[322] S. Ohmer and H. H. Patel, Phys. Rev. **D92**, 055020 (2015), arXiv:1506.00954 [hep-ph]

[323] A. Ismail, W.-Y. Keung, K.-H. Tsao, and J. Unwin, Nucl. Phys. **B918**, 220 (2017), arXiv:1609.02188 [hep-ph]

[324] N. Okada, S. Okada, and D. Raut, Phys. Lett. **B780**, 422 (2018), arXiv:1712.05290 [hep-ph]

[325] N. Okada and S. Okada, Phys. Rev. **D95**, 035025 (2017), arXiv:1611.02672 [hep-ph]

[326] T. Bandyopadhyay, G. Bhattacharyya, D. Das, and A. Raychaudhuri, Phys. Rev. **D98**, 035027 (2018), arXiv:1803.07989 [hep-ph]

[327] J. Ellis, M. Fairbairn, and P. Tunney, JHEP **08**, 053 (2017), arXiv:1704.03850 [hep-ph]

[328] S. Caron, J. A. Casas, J. Quilis, and R. Ruiz de Austri, JHEP **12**, 126 (2018), arXiv:1807.07921 [hep-ph]

[329] A. Pais, Phys. Rev. **D8**, 1844 (1973)

[330] S. Rajpoot, Int. J. Theor. Phys. **27**, 689 (1988)

[331] R. Foot, G. C. Joshi, and H. Lew, Phys. Rev. **D40**, 2487 (1989)

[332] C. D. Carone and H. Murayama, Phys. Rev. **D52**, 484 (1995), arXiv:hep-ph/9501220 [hep-ph]

[333] H. Georgi and S. L. Glashow, Phys. Lett. **B387**, 341 (1996), arXiv:hep-ph/9607202 [hep-ph]

[334] T. R. Dulaney, P. Fileviez Perez, and M. B. Wise, Phys. Rev. **D83**, 023520 (2011), arXiv:1005.0617 [hep-ph]

[335] P. Fileviez Perez and M. B. Wise, JHEP **08**, 068 (2011), arXiv:1106.0343 [hep-ph]

[336] Phys. Rev. **D88**, 115009 (2013), arXiv:1310.7052 [hep-ph]

[337] Phys. Lett. **B731**, 232 (2014), arXiv:1311.6472 [hep-ph]

[338] B. Batell, P. deNiverville, D. McKeen, M. Pospelov, and A. Ritz, Phys. Rev. **D90**, 115014 (2014), arXiv:1405.7049 [hep-ph]

[339] M. Baak and R. Kogler, in *Proceedings, 48th Rencontres de Moriond on Electroweak Interactions and Unified Theories: La Thuile, Italy, March 2-9, 2013* (2013) pp. 349–358, [,45(2013)], arXiv:1306.0571 [hep-ph]

[340] T. A. collaboration (ATLAS), (2017)

[341] T. A. collaboration (ATLAS), (2016)

[342] M. Aaboud *et al.* (ATLAS), Phys. Rev. **D96**, 052004 (2017), arXiv:1703.09127 [hep-ex]

[343] M. Aaboud *et al.* (ATLAS), Phys. Rev. Lett. **121**, 081801 (2018), arXiv:1804.03496 [hep-ex]

[344] M. Aaboud *et al.* (ATLAS), Phys. Rev. **D98**, 032016 (2018), arXiv:1805.09299 [hep-ex]

[345] M. Aaboud *et al.* (ATLAS), Phys. Lett. **B788**, 316 (2019), arXiv:1801.08769 [hep-ex]

[346] J. Alitti *et al.* (UA2), Nucl. Phys. **B400**, 3 (1993)

[347] T. Aaltonen *et al.* (CDF), Phys. Rev. **D79**, 112002 (2009), arXiv:0812.4036 [hep-ex]

[348] D. Barducci, G. Belanger, J. Bernon, F. Boudjema, J. Da Silva, S. Kraml, U. Laa, and A. Pukhov, Comput. Phys. Commun. **222**, 327 (2018), arXiv:1606.03834 [hep-ph]

[349] G. Aad *et al.* (ATLAS), Eur. Phys. J. **C75**, 299 (2015), [Erratum: Eur. Phys. J.C75,no.9,408(2015)], arXiv:1502.01518 [hep-ex]

[350] Comput. Phys. Commun. **185**, 2250 (2014), arXiv:1310.1921 [hep-ph]

[351] I. H. P. L. B. . . .-. M. Chanowitz, M. Furman,

[352] M. E. Peskin and D. V. Schroeder, *An Introduction to quantum field theory* (Addison-Wesley, Reading, USA, 1995)

[353] P. Abreu *et al.* (DELPHI), Z. Phys. **C65**, 603 (1995)